Transferability of Regional Climate Models over different climatic domains

Emiola Olabode Gbobaniyi

Thesis Presented for the Degree of

DOCTOR OF PHILOSOPHY

In the Department of Environmental and Geographical Science

UNIVERSITY OF CAPE TOWN

August 2010

Dedicated to the loving memory of
Mariam Modupe Gbobaniyi

Transferability of regional climate models over different climatic domains

Emiola O. Gbobaniyi

Department of Environmental and Geographical Science, University of Cape Town, Private Bag X3, Rondebosch 7701, South Africa

ABSTRACT

In the continuing quest to improve climate model predictions to meet the increasing demand for knowledge on the regional effects of global climate change, it is pertinent to increase our understanding of how the underlying processes of climate are represented in the models we use to make these predictions. Concerted efforts in model evaluations and intercomparison have provided numerous insights into various model biases which plague current state-of-the-art regional climate models (RCMs). Model evaluation and assessment is crucial to model development and understanding how physical processes are represented in models is necessary for improving model parameterizations. This thesis explored model transferability as a new approach for systematic process-based intercomparison of RCMs. It investigated an untested transferability hypothesis which states that "for non-monsoon regions experiencing weak synoptic scale forcing, the height of the cloud base is correlated with the daytime surface fluxes". An initial transferability experiment was conducted over Cabauw, the Netherlands (51.97°N, 4.93°E) to assess the models' skill in resolving the diurnal and seasonal cycles and to investigate the simulated connections between surface and hydrometeorological variables over a non-monsoon station. The ability of models to resolve these cycles correctly is a good metric of their predictive capabilities. The data used for the study comprises three-hourly surface observations for the period October 2002 – December 2004 from the Coordinated Enhanced Observing Period (CEOP) measuring campaigns of the Global Energy and Water Cycle Experiment (GEWEX) and three-year simulations (2002 -2004) from five RCMs (CLM, GEMLAM, MRCC, RCA3 and RSM).

In simulating seasonal and diurnal cycles of CBH and surface variables, the European models (CLM and RCA3) demonstrate a clear home advantage over the North American models (GEMLAM, MRCC and RSM). Principal component analysis revealed that the models couple the cloud base height with surface fluxes as in observations

and that this coupling is not sensitive to changes in wind speed. This study found that summer daytime loadings gave the strongest couplings of variables. Three major processes were identified over Cabauw. First and most dominant is the surface energy process which couples sensible and latent heat with net radiation. The second process is thermodynamic, coupling temperature and surface moisture (specific humidity), and the third is a dynamic process which couples pressure and wind speed. A model intercomparison was then carried out across the six midlatitude domains to test the validity of the Cabauw findings. In observations, CBH is well coupled with the surface fluxes over Cabauw, Bondville, Lamont and BERMS, but coupled only with temperature over Lindenberg and Tongyu. All the models (except GEMLAM) simulated a good coupling with surface fluxes at all stations. In GEMLAM, there is no coupling between CBH and surface fluxes at any station. In less homogenous domains of the study, a very slight decrease in the strength of coupling is seen in most of the models, under strong large scale forcing. This would suggest that the coupling between cloud base height and surface fluxes in the models is possibly more influenced by radiative forcing than by synoptic controls. This second study confirmed the findings at Cabauw that the simulated cloud base is correlated with surface energy fluxes and the sign of the correlations in the models is as in observations. This finding is important for the modeling community as it establishes the fact that the models are actually simulating the direction of influence of surface fluxes and possibly, soil water variability, on cloud processes.

The entire analysis provides a robust framework for assessing the applicability of models in widely varying climatic domains and for validating them against climate observations. The varied couplings identified in the study and their complex feedbacks of processes present a major validation challenge for models that employ interchangeable parameterization schemes for the different physical processes. Since these feedbacks are likely to change each time a module is changed, their combination needs careful evaluation.

ACKNOWLEDGMENTS

I am forever grateful to God Almighty, who makes all things beautiful in His time.

I would like to thank many people for their support and assistance during the course of this work. I am most grateful to my supervisor, Bruce Hewitson, for giving me the unique opportunity of investigating this pioneering topic; and to my co-supervisor, Babatunde Abiodun who guided me through the long and ardous path to success. Mark Tadross is thanked for invaluable input and criticism. I am very indebted to my mentor, Prof. Ekundayo E. Balogun, for giving me the opportunity to come to South Africa to broaden my horizons. I am grateful to the entire staff and students in the Climate Systems Analysis Group and the EGS department, which has been my home away from home for the duration of this research, for creating a harmonious atmosphere to work in. In particular, Nana Browne who was always ready to look through my manuscripts despite having a lot of her own to deal with, Frank Eckhart who always had a listening ear, and Sharon Barnard for helping to keep the financial 'lifeline' intact.

I thank Jonas Bhend and Beate Geyer of the GKSS for their support while conducting part of my research at their centre. Appreciation goes to Markus Quante of the GKSS for providing the Cabauw ceilometer data. The National Research Foundation and Deutscher Akademischer Austausch Dienst (DAAD) are credited for financial support of my PhD programme and the research visit to Germany. I am grateful to the Associateship Programme of the Abdus Salam International Centre for Theoretical Physics (ICTP) for giving me the opportunity and benefits of being a junior associate.

To Rafiu Raji, Sisanda Ntshinga, and Kunle Joseph, thank you for your friendship, assistance, enthusiastic belief that I could do this, and ever constant support. Anita Ciric, thank you for the love, kindness and support shown throughout the course of this work. To Erica Sarnataro, thank you for proof reading when my eyes could no longer tell a comma apart from a stop. Grazie tante!

And to my family, I am grateful for your unending love, support and prayers. Bami and Deji, thank you for being such strong little men and waiting for daddy!

CONTENTS

Chapter 1

Introduction

1.1 The basis

In the continuing quest to improve climate model predictions to meet the increasing demand for knowledge on the regional effects of global climate change, it is pertinent to increase our understanding of how models handle the underlying processes of climate. In other words, how are these processes represented in the models we use for predictions? Concerted efforts in model evaluation and intercomparison e.g. (Takle et al., 1999; Tjernström et al., 2005; Rinke et al., 2006; Christensen et al., 2007; Déqué et al., 2007) have provided numerous insights into various model biases which plague current state-of-the-art regional climate models (RCMs). Model transferability experiments are a new way of exploring these biases which are often the consequence of region-specific tuning in model parameterizations (Takle et al., 2007). Exposing model biases and the factors responsible for them serve to increase understanding and lead to better implementations of important parameterizations in models, ultimately giving us more reliable tools of the trade.

This thesis thus seeks to address these issues with a focus on investigating model representation of specific surface processes such as the interaction of the surface energy fluxes with cloud base height. The diurnal and seasonal cycles of these interactions and of other state meteorological variables are important indices for diagnosing deficiencies in model physics (Betts et al., 1997; Dai and Trenberth, 2004). This study builds on the lessons learned from numerous regional climate model intercomparison projects by providing a new and insightful way of assessing model performance and exploring model biases under various climate conditions. The following section gives a comprehensive review of major model intercomparison projects carried out for the purposes of model evaluation and assessment by different modeling groups across the globe over a wide range of climatic regimes. Thereafter, the key lessons learned from these activities are summarized.

1.2 Model intercomparison projects (MIPs)

The Atmospheric Model Intercomparison Project (AMIP) began back in 1990 as a standard experimental protocol for global atmospheric general circulation models (AGCMs). Its objectives were to provide a community-based infrastructure to facilitate climate model diagnosis, validation, intercomparison, documentation and data access (Gates, 1992). The AMIP programme, which involved the international climate modeling community, allowed scientists to analyze AGCMs in a systematic manner designed to contribute to model improvement. The AMIP experiment involved constraining an AGCM by realistic sea surface temperature and sea ice from 1979 to near present, with a comprehensive set of fields saved for diagnostic research. This model configuration enabled scientists to focus on the atmospheric model, which of course is coupled to the land surface, without the accompanying complexity of ocean-atmosphere feedbacks in the climate system. Following the success of AMIP, the regional climate modeling community began series of coordinated model intercomparison projects (MIPs) over different climate regions. These projects were designed to explore the strengths and weaknesses of simulating specific regional climates at subcontinental scales. The various MIPs are described in the following paragraphs.

1.2.1 Arctic Regional Climate Model Intercomparison (ArcMIP)

The Arctic Regional Climate Model Intercomparison Project (ArcMIP) is an international intercomparison of eight regional model simulations in the Arctic conducted using a common forcing dataset. ArcMIP focused on the period September 1997 – September 1998, which coincides with the Surface Heat Budget of the Arctic Ocean (SHEBA) project period. The rationale for selecting this period is that high quality data are available from SHEBA, the Atmospheric Radiation Measurement (ARM) Barrow site, aircraft observations and several remote sensing satellites. Also, wide-ranging data are available from the Mackenzie GEWEX Study (MAGS), a series of large-scale hydrological and related atmospheric and land-atmosphere measurements conducted within the Mackenzie Basin in Canada. In their work which quantified the scatter among these models and therefore the magnitude of disagreement and unrelia-

bility of current Arctic RCM simulations, Rinke et al. (2006) reported that the ensemble model mean reproduces the driving reanalysis (European Centre for Medium-Range Weather Forecasts ERA40) quite well when constrained by a small domain. A few models have severe biases that contribute substantially to the bias in the ensemble mean, although some models perform better than the ensemble mean or median. Even using a constrained experimental design (small integration domain, specified lower boundary condition for ocean and sea ice) and specified horizontal boundary conditions from data analyses, there is a considerable scatter among the different RCMs. In general, the largest across-model scatter is found in the 2 m temperature over land, in the surface radiation fluxes, and in the cloud cover which implies a reduced confidence level for these variables. These are likely due to different radiation cloud and land-surface schemes employed in the models. Both performance biases and inter-model differences are largest at very low height levels and near the surface. Here, individual physical model parameterizations come into play and the land-surface and boundary layer parameterizations, radiative transfer and cloud treatment become of primary importance. Using the SHEBA point measurements, Køltzow et al. (2003) showed that model biases in the incoming and upward shortwave radiative fluxes at the surface in summer can be reduced by using a more sophisticated surface albedo scheme. Wyser and Jones (2005) showed that a more sophisticated cloud scheme significantly improves the annual cycle of cloud cover in their model.

Tjernström et al. (2005) reported that the models capture well much of the resolved scale meteorology. However, there are biases in near-surface wind speeds that are consistent with surface stress and which lead to incorrect sea ice drift. Errors in surface fluxes are often up to or larger than the net heat flux itself. While some of the models show good skill in some of the radiation flux components, none of them have good, or consistent, skill in all components. The simulated turbulent heat fluxes have very little similarity, if any at all, to observations. While the long-term errors in turbulent heat flux tend to compensate, this compensation is not an attempt to obtain correct fluxes but more probably a result of wind stress tuning. The simulated downward shortwave radiation suggests that cloud amounts are reasonably accurate. A positive correlation exists between cloud water and specific moisture bias in all models, which indicates inconsistencies. The structural similarity between the cloud

liquid-water profiles and the temperature-bias profiles in summer is an issue that deserves more study. There are very good reasons to assume that some of the errors in the boundary layer arise from elsewhere in the model. Most of the systematic errors are different in the lowest kilometer rather than aloft, but they hardly disappear with altitude, despite applying the same lateral boundary conditions to all models. No single model stands out as being superior in all situations. In summary, these results lead the authors to conclude that there are uncertainties in current modeling of Arctic climate processes that may be reduced by improving important process descriptions in climate models.

1.2.2 North American Monsoon Model Assessment Project (NAMAP)

The international North American Monsoon Experiment (NAME) was organized to improve understanding and prediction skill of warm-season precipitation fluctuations in the monsoonal region of southwest North America. Investigators carried out enhanced observations at the core of the North American Monsoon System (NAMS) during the NAME field campaign in summer 2004. The NAME Model Assessment Project (NAMAP) was designed to evaluate the state of the art of warm season climate modeling before the field campaign (Gutzler et al., 2005). In NAMAP, six groups independently carried out numerical simulations of a single summer across southwestern North America. The most fundamental distinction in model characteristics is between the four regional models and the two global models. The RCMs are strongly forced by time-varying analyzed fields around the lateral boundaries of their computational domain. The GCMs are not subjected to any lateral atmospheric forcing but forced only by prescribed lower boundary conditions. The RCMs are therefore more tightly constrained by the constant influence of “perfect” large-scale dynamical features at the lateral boundaries. The NAMAP simulations were carried out with significantly different configurations. Five simulations are continuous runs beginning with springtime initial conditions, while one is a succession of daily reinitialized 24–36 hour forecasts. The latter simulation was not notably closer to observations than the free-running simulations, indicating that model drift is not the foremost reason for evident deficiencies in the simulations.

Although this project lacks a tightly constrained framework on lateral boundary conditions usually employed in most intercomparisons, its evaluation of the monsoon of the southwest United States and northwest Mexico using four RCMs and two GCMs provides invaluable insights on model behaviour for an important climatic feature. The North American monsoon interacts strongly with coastal terrains and provides both latitudinal and orographic contrasts for comparison with other continental monsoon systems. Gutzler et al. (2005) reported that all four NAMAP RCMs reproduced the observed July 1990 maximum precipitation, whereas the two GCMs reproduced peak precipitation in August. The monthly mean resolution of the NAMAP output makes it impossible to quantify the time lag accurately, but the onset date is well defined with the existing observational precipitation data set so there is no doubt that the delayed onset is an actual anomaly in the global model simulations. All four RCMs maintained their diurnal cycle phase before, during and after the monsoon maximum, and three had their hourly amplitudes proportionally reduced after the observed July peak. One model behaved differently however, partitioning all of the difference between July and August rain into the nocturnal component. The substantial differences in nocturnal precipitation suggest that systematic propagation of convective systems is occurring to varying degrees in the model simulations, and that different model physics and dynamical schemes come up with various ways of resolving precipitation. This issue as well as that of late afternoon convective peak needs to be addressed in models. The models diverge on the interaction of convection with topography and this is more pronounced for regions of intense convection in areas with complex terrains. The authors asserted that simulation of intense convective precipitation in regions of extremely complicated terrain poses a unique challenge to dynamical models, and suggested that improvements in convective parameterizations are an indispensable prerequisite to enhancing climate prediction skill in the NAME domain.

1.2.3 Project to Intercompare Regional Climate Simulations (PIRCS)

The Project to Intercompare Regional Climate Simulations (PIRCS) was developed to evaluate the strengths and weaknesses of regional climate models and their component procedures through systematic comparative simulations. PIRCS also provides a framework for improving mesoscale climate models both individually and as a group

and has grown with strong community involvement (Gutowski et al., 1998; Takle et al., 1999). The initial series of PIRCS experiments examined extreme events of two to three month duration (the 1988 drought and the flood of 1993) over the central United States (Takle et al., 1999). The drought phase allowed for the simulation of a period with minimal model dependence on convective parameterization, whereas the intense rainfall period offered a contrast, allowing for the investigation of the impacts of widespread convection over the same region. Takle et al. (1999) reported that all models reproduced the succession of wet and dry days when the flow is driven by large scale motion, but mesoscale and convective precipitation tended to be captured more stochastically in the models with less precise agreement in temporal and spatial patterns than for the synoptically organized events. Most models captured the nocturnal precipitation maximum in the United States Midwest despite the fact that this feature was absent in the climatology of the forcing reanalysis. Also, most model simulations placed the precipitation maximum during the 1993 flood event northeast of its actual location with a lower total rainfall amount than was observed. The authors concluded that although there are some common strengths and deficiencies among the models, no single model stands out as best in all comparisons, rather each model displays individual strengths and deficiencies.

1.2.4 Regional Climate Model Intercomparison Project for Asia (RMIP)

In contrast to other monsoonal climates, East Asia has high terrain to the west and ocean to the south and east making it a challenging region to model. The Regional Climate Model Intercomparison Project (RMIP) for Asia was established in 1999 to improve further RCM simulations of East Asian climate by evaluating their strengths and weaknesses in a common framework. The specific objectives of RMIP are to assess the current status of East Asian regional climate simulation, provide a scientific basis for further RCM improvement, and to provide scenarios of East Asian regional climate change in the 21st century based on an ensemble of RCMs nested within a GCM. In the initial RMIP phase, nine RCMs simulated an 18-month period (March 1997 - August 1998) that covers a full annual cycle, the East Asian drought and heat waves during summer 1997, and flooding in Korea, Japan, and the Yangtze and Songhua river valleys of China, during summer 1998. Fu et al., (2005) reported that models

usually displayed a cool bias with lower magnitude at lower altitudes and largest over arid regions of northern China. Individual model biases range from ± 1º to ± 6ºC, which very much exceeds the ensemble average bias. This inconsistency, the authors noted, suggests the need for further systematic evaluation of RCM performance over different regions and across more models, before making any general conclusions. The models tend to produce too much precipitation at high latitudes but generally simulate the annual cycle of precipitation well over China, Japan and Korea, except in the western arid and semi-arid regions. The nine RCM ensemble averages for temperature and precipitation perform better than any individual model, a result which suggests that there is value in using an ensemble of RCMs when projecting future climate to get a mean change and range of possible changes. Most models captured wet and dry extreme events, including, to some extent, a belt of heavy rain over the Yangtze valley and its associated 850 hPa low-level jet.

1.2.5 Baltic Sea Experiment (BALTEX)

The major objective of BALTEX (the BALtic sea EXperiment) is to explore and quantify the energy and water cycles of the Baltic region (Bengtsson, 1995). BALTEX gave rise to the Numerical Studies of the Energy and Water Cycle in the Baltic region (NEWBALTIC) I and II, two studies which intercompared simulations of components of the hydrological cycle produced by RCMs applied to the Baltic Sea area. This domain exhibits the strong seasonal changes representative of midlatitude and sub-Arctic climates. From a land surface modeling study in hydrology and meteorology, Graham and Bergström (2000, 2001) concluded that meteorological models should maintain their multifaceted approach for modeling soil temperature but incorporate a simpler, yet physically consistent, hydrological approach for modeling snow processes and soil water transport. One common problem in all models studied is compensating errors in their snow routines. This, the authors opined, might block further development, as improvement in one process description may be interpreted misleadingly as a failure if a compensating error is not concurrently analyzed. More attention must be paid to internal process validation in models. Hamelbeck et al. (2001) report that total convective heat flux is a useful sub grid scale quantity for unifying model physics across RCMs. Jacob et al. (2001) compared results from eight

RCMs for a three-month period and found that the models diverge significantly in radiative properties, cloud cover, average precipitation, and runoff even though they captured synoptic events quite well. In contrast to earlier findings (e.g. Christensen et al., 1997) no systematic low summer precipitation bias was found in this study.

The reason for this is mainly attributed to the fact that the key mechanism leading to a low summer precipitation bias (positive feedback leading to a decline in land surface evaporation, precipitation and soil moisture content) does not play a major role in the Baltic Sea area. Although the evaporation-precipitation feedback was not explicitly quantified, the highest portion of the precipitation in the area probably originates from the Atlantic Ocean and Baltic Sea, thus reducing the impact of the land surface feedback. This was also suggested by Koster et al. (2000).Van Meijgaard et al. (2001) compared RCM cloud simulation with measurements by ceilometers, infrared radiometers, and satellite observations. They reported that RCMs systematically overestimate cloud amount below 900 hPa and compensate by simulating less than that observed at 800 hPa. They attributed this behaviour to underestimated planetary boundary layer height. The models exhibit similar cloud properties but diverge considerably in their cloud radiative fluxes.

1.2.6 Prediction of Regional Scenarios and Uncertainties for Defining European Climate Change Risks and Effects (PRUDENCE)

The Prediction of Regional Scenarios and Uncertainties for Defining European Climate Change Risks and Effects (PRUDENCE, Christensen, 2005) focuses on improving projections of future climate change. PRUDENCE aims at a number of objectives which include a series of high resolution climate change scenarios for Europe for 2071 - 2100, an assessment of uncertainties of European regional climate models, and an assessment of risks caused by climate change for Europe. Other objectives include the application of RCM results to a number of climate impact studies, an assessment of implications of climate change for socio-economic and political decision making and a broad dissemination of PRUDENCE results. Various European climate modeling institutes used RCMs to create the high resolution simulations which are then used to assess changes in the frequency and magnitude of extreme

weather events. Further still, the variability and level of confidence in these scenarios is analyzed as a function of uncertainties in model formulation. Jacob et al. (2007) reported that regional models reproduce the circulation patterns of the driving GCM well. Nevertheless, in many regions there are significant differences between the GCM and RCM surface temperature and precipitation simulations for some RCMs. There is no clear association of differences with regions but some models have region and season independent tendencies to deviate in terms of temperature or precipitation. This is in agreement with Déqué et al. (2005) who reported that individual regional models present a larger spread than the difference between GCMs and RCMs. The systematic error in temperature is less than half the climate change for the A2 (end of the 21st century) climate scenario. The sources of uncertainty for global models, in decreasing order, are from model to scenario (B2 versus A2), sea surface temperature forcing, and sampling. For regional models, the order is from scenario to boundary forcing (GCM), model, and sampling. Sea surface temperature (SST) forcing and model to model variability are the principal sources of uncertainty in precipitation for both global and regional models, and this is followed by scenario and sampling error. Christensen et al. (2007) concluded that impact studies in PRUDENCE that compared various methods of scenario development and application provide convincing examples that show that application of RCM-based scenarios can have significant advantages over AOGCM based scenarios in many impact studies. On the other hand, they also indicate that RCMs do not yet provide a universal solution, and some of the impact studies highlight potential limitations of relying solely on RCM-based information. Overall, PRUDENCE represents the first comprehensive, continental-scale intercomparison and evaluation of high resolution climate models and their applications.

1.2.7 International Research Institute/Applied Research Centers (IRI/ARC) Projects

Roads et al. (2003) examined the subtropical climates through an intercomparison of four regional model simulations in a region with steep topographic features under the influence of Atlantic SSTs, El Niño-Southern Oscillation (ENSO) events and the South American monsoon. The models captured the seasonal cycle of precipitation as well as the precipitation maximum associated with the monsoon. The precipitation

totals were however less than those observed. All models had extreme variability near the Andes with less predictability on the leeward than the windward side. The models performed better in summer and winter than in the transition seasons.

1.2.8 Other continuing intercomparison projects

Other recent and emerging model intercomparison projects (MIPs) include the La Plata Basin Project (PLATIN) in the Rio de La Plata basin in Argentina and Uruguay, the African Monsoon Multidisciplinary Analysis (AMMA) in West Africa, the Quantification of Uncertainties in Regional Climate Change and Climate Change Simulations (QUIRCS) in central Europe, and Assessments of Inputs and Adaptations to Climate Change (AIACC) in southern Africa. The Structured Grid Model Intercomparison Project (SGMIP) compares results of stretched grid models, which offer advantages for simulating regional climates by allowing full interaction with coarsely resolved regions outside the region of interest. SGMIP results so far have focused on overall accuracy of the method and have not intercompared model validity on specific climate features.

The COordinated Regional climate Downscaling Experiment (CORDEX) is a World Climate Research Programme (WCRP) sponsored program to organize an international coordinated framework to provide an improved generation of regional climate change projections worldwide for input into impact and adaptation studies within the Intergovernmental Panel on Climate Change 5th Assessment Report (AR5) timeline and beyond. CORDEX will produce an ensemble of multiple dynamical and statistical downscaling models considering multiple forcing GCMs from the CMIP5 archive. Multiple common domains covering most land areas in the World have been selected (with initial focus on AFRICA). These regions take advantage of some of the existing regional projects already discussed above. Although CORDEX is not an intercomparison project in the strict sense, the wealth of data it will provide from various models applied over different domains will no doubt prove useful for model intercomparison purposes.

1.3 Lessons learned from model intercomparison projects (MIPs)

All the previously discussed model intercomparison studies and a few other recent ones (see Takle et al., 2007) provide vast insights toward the advancement of model evaluation and development. These studies have shown that RCM simulations on domains well constrained by analyzed boundary conditions offer an opportunity for assessing and improving parameterizations in higher resolution models (e.g. Déqué et al., 2007). With such constraints, parameterizations can be developed while being shielded from error propagation from remote regions. Takle et al. (2007) reported that as more and different regional climate model intercomparisons are being documented, some clear patterns have emerged from the results. Probably the most common conclusion from these studies is that no single model outperforms others in accuracy in all variables being simulated, a fact that seems to also equally hold for GCMs (e.g. Sanderson et al., 2008; Knutti, 2009; Knutti et al., 2010).

While a model might exhibit remarkable accuracy in one variable for a region, it may be very unreliable for other variables in the same domain or for the same variable in another domain. One might argue however that this, to some degree, can only be on appearances, given the inherent inter-dependency of variables when one considers the dynamics across timescales. Another central outcome of the model intercomparisons is that the ensemble means of regional models are often closer to observations than any individual model (e.g. Takle et al., 1999; Fu et al., 2005; Tjernström et al., 2005). These ensemble means, however, fail to reproduce the magnitude of extreme events. Many of the regional model intercomparisons discussed have concluded that model physics (e.g. convection schemes, boundary layer physics) contributed more than the numerical solution (e.g. spectral versus grid) to divergence in model results and between model results and observations (e.g. Déqué et al., 2005; Jacob et al., 2007). Particular features in specific regions can provide opportunities to study model processes in a more involved way. The diurnal pattern of components of the hydrological cycle is an example of this. In the PIRCS study, the nighttime summer precipitation maximum over the U.S. Midwest allowed the investigation of the moisture convergence processes that feed these nocturnal storms in the models (Takle et al., 1999). The models produced nighttime maxima of moisture convergence and both convec-

tive and stratiform precipitation, a remarkable feat as these features were absent in the driving reanalysis boundary conditions. This confirms the value added by a set of regional models applied over a region for the season simulated.

1.4 Model transferability

From the above discussions, it is evident that much has been learned through individual regional climate model intercomparisons where several RCMs were applied over a single domain of interest. However, a major limitation of these studies is that there is no uniformity across the different MIP frameworks, for example, in the choice of lateral boundary forcing for the models and in the use of observations. This lack of uniformity limits the ability of the community of regional modelers to draw far reaching conclusions regarding understanding of the hydrological and energy cycles on a global scale. Takle et al. (2007) proposed "transferability experiments" as a next step in regional climate model development. In a transferability experiment, a single model is applied to multiple domains with the model options kept fixed for all domains simulated. This allows for the assessment of model skill outside of a model's primary domain of development and application (home domain).

A transferability intercomparison involves several models in a coordinated set of transferability experiments where, as much as possible, all experiments use the same configuration (lateral boundary conditions, domain size and resolution) on a prescribed suite of domains for periods where high temporal resolution observations are available. Such a transferability intercomparison requires the archiving of results in a highly standardized and well-coordinated manner. Simulations for the first transferability intercomparison project (the Inter-Continental Scale Experiments Transferability study, ICTS) were started in 2005 by the Transferability Working Group (TWG), under the auspices of the GEWEX (Global Energy and Water Cycle Experiment) Hydrometeorology Panel (GHP). The ICTS simulates a five-year period (2000-2004) which includes all the Coordinated Enhanced Observing Period (CEOP) Phase I observations for all the GEWEX Continental Scale Experiment (CSE) regions (Takle et al., 2007). Locations of the CEOP reference sites were taken into consideration in defining the domains of the transferability experiments. All models

participating in the transferability experiments have all their configurations and parameterizations well documented, and all the experiment domains were simulated without changing these parameters. All the models were driven by the same reanalysis data and archiving of model output was well-coordinated with strict quality control to ensure accuracy for common analysis (see http://www.gkss.de/icts/).

1.5 Transferability hypotheses

Such systematic intercomparison across models and domains offer unique opportunities for exposing individual and collective biases in regional models. Transferability intercomparisons, by focusing attention on selected climatological processes and regions of interest, can explore and evaluate the spatial and temporal differences in model predictability (Takle et al., 2007). A way of achieving this is by testing the validity of specific hypotheses which allow for the assessment of generality in regional models. Takle et al. (2007) proposed four such non-exclusive hypotheses as follows:

Models show no superior performance on their domains of origin as evaluated by their accuracy in reproducing the diurnal cycles of key surface hydrometeorological variables.

For all climatic regions and periods having convective precipitation during both day and night, alternative parameter settings in convective schemes at a specific resolution result in changes of intensity and diurnal phasing of precipitation that are correlated.

No single domain provides climatic conditions for developing and tuning a regional climate model that result in measurably better regional climate model performance on all climate domains in the transferability domain ensemble.

For all non-monsoon climatic regions experiencing weak large scale forcing, daytime surface fluxes are correlated with the height of cloud base.

The hypotheses above are for the most part yet to be tested. These hypotheses are tied to key processes and/or regions and their validation will provide insights into how models reproduce these processes over a given domain of interest. In a preliminary test of the first hypothesis, Takle et al. (2007) evaluated the diurnal cycles of surface

energy fluxes using five models for the CEOP enhanced observing period (1 July 2001 - 30 September 2001). Three-hourly model results were compared with CEOP observations from three CSE reference sites [Cabauw (51.970N, 4.930E, The Netherlands, Europe), Bondville (40.010N, 88.290W, USA, North America) and Pantanal (19.560S, 57.010W, Brazil, South America)]. Their findings suggest a "weak" home domain advantage for regional models. They also found that most models capture the daytime peaks of sensible and latent heat flux, even though the peak times are different across the observation sites. Models overestimated the variability of latent heat flux for the warmer climate site (Pantanal) and underestimated it for the cooler climate sites (Bondville and Cabauw), but the opposite is the case with sensible heat flux. Pantanal, the only tropical site of the three, showed the highest divergence between models' comparisons with observations. Of the three sites, Pantanal is the most 'foreign' (farthest from domain of design and application) to these models which were developed in and primarily applied over mid and high latitudes. Rockel et al. (2005) report that precipitation totals for reference sites surrounded by shallow orography exhibit the lowest variations for both observations and model output, whereas the opposite is true in regions of high orography or heterogeneous surfaces.

1.6 Research objectives

From the discussions above, it is clear that regional model transferability studies can provide a useful means of model assessment and evaluation, which is an important part of model development. While it is true that model skill is partly limited by our level of understanding of the workings of the climate system, it is important that our present understanding of climate processes be adequately translated in the models we construct to simulate these processes. Assessing models to ascertain how they reproduce known features of climate is key to improving the reliability and predictive accuracy of these models. This thesis thus aims to facilitate current understanding in model representation of observed physical processes. This task, in its entirety, is far beyond the scope of this or any other thesis for that matter. Specifically, the investigations in this thesis are focused on model representation of the relationship between cloud base height and the surface energy fluxes.

The primary aim is thus to investigate the fourth transferability hypothesis which states "for non-monsoon regions experiencing weak synoptic scale forcing, the height of the cloud base is correlated with the daytime surface fluxes." (Takle et al., 2007). To support this aim the following questions are the primary objectives of the thesis:

Do models couple cloud base with surface energy fluxes as seen in observations (Betts, 2004) and do they reproduce the observed diurnal and seasonal variations in the direction and magnitude of cloud base-surface energy flux couplings?

What influences do weak and strong synoptic forcings have on the coupling of cloud base height with surface fluxes in models?

What differences exist in the coupling of surface fluxes and cloud base height in monsoon and non-monsoon domains?

Are there specific areas of commonalties or divergence in models, in other words, do the models in this study exhibit common weaknesses or strengths and on which aspects do they diverge?

Can we verify that regional models exhibit a 'home advantage' which gives them better predictive capabilities in their domain of development and application as suggested in the preliminary results of Takle et al. (2007)?

To investigate these issues, model output location time series from five regional climate models are compared with surface observations from three enhanced observing periods of the Coordinated Enhanced Observing Period programme of GEWEX. The investigations employed the use of statistical tools for analyses and details of these are provided in Chapter III.

1.7 Thesis outline

This thesis is composed of six chapters. Following the introductory chapter which presents an overview of model intercomparison projects and pioneering works on regional climate model transferability from its origin to its present status vis-à-vis this study, Chapter II gives a summary of the climate system and climate modeling. Chap-

ter III discusses the models, methods and data used in this research and also gives a description of the various domains and sites of the study. Chapter IV lays a foundation for the model transferability question this thesis seeks to answer by investigating the simulated connections between surface and hydrometeorological variables over a non-monsoon station. Using five regional models, the hypothesis under investigation is evaluated using the model intercomparison convention. This approach serves as a platform for model validation while also providing an insight into the performance of each model used in the study. Chapter V expands on this foundation and investigates the transferability of these RCMs by assessing their performance over different climate domains across twelve CEOP reference sites around the globe. Chapter VI summarizes and synthesizes the outcomes of these experiments and provides an outlook for future research.

Chapter 2

Climate Modeling

2.1 Introduction

This chapter provides an overview of the history of climate modeling as a background to the central theme of regional climate model evaluation and assessment. It introduces the climate system and its components, which in essence (and limitedly so) is what climate models aspire to reproduce. A background is provided on the hierarchy of climate models and the various applications of global and regional climate models highlighted.

2.2 Earth's climate system

Climate in a narrow sense is a statistical description, in terms of the mean and variability, of relevant quantities (usually surface variables such as temperature, precipitation, and wind) over a period of time ranging from months to thousands or millions of years. The classical period, as defined by the World Meteorological Organization, is 30 years. Climate in a wider sense is the state, including a statistical description, of the climate system. The study of the Earth's climate system is rooted in the desire to understand the processes that determine the state of the climate along with the possible ways in which this state may have changed in the past or may change in the future. The Earth's climate is composed of a number of components which include but are not limited to the atmosphere, oceans, cryosphere, and the biosphere (see Figure 2.1). These components are non-linear systems in their own right and their evolution is governed by various physical, chemical, and biological processes which are spatially non-local (Kiehl and Ramanathan, 2006). Each component exhibits different response timescales and thermodynamic properties (Bard, 2002). Natural climate variability arises from variability within each of the components of the climate system, and also from the interactions between them. For example, the large heat capacity and thermal isolation of the deep ocean provides the climate sys-

tem with a long-term "memory", resulting in a spectrum of internal variability which extends to millennial timescales (Bigg and Wadley, 2001). The complex, nonlinear nature of the Earth system gives rise to different modes of variability like stochastic resonances and rapid transitions between regimes (Rial et al., 2004). An example of the former is the El Niño-Southern Oscillation (ENSO, Philander, 1990; Tziperman et al., 1994), which represents a mode of internal variability of the coupled atmosphere-ocean system. The Dansgaard-Oeschger and Heinrich events which mark the Earth's glacial climate (Bond and Lotti, 1995; Bard, 2002) are examples of the latter. Climate variability can also be induced by factors external to the climate system. Volcanic eruptions may result in cooling trends lasting several years, while changes in solar output may cause decadal to centennial-scale variability (Ramaswamy et al., 2001; Robertson et al., 2001). Pseudo-cyclic variations in the Earth's orbital parameters, on timescales of 10^4 to 10^5 years, give rise to the glacial cycles (e.g. Berger and Loutre, 2004) whereas plate tectonic processes become significant on timescales of 10^6 years and longer, as do the changes in and orbital path of the sun through the Milky Way Galaxy (Pavlov et al., 2005; Sloan, 2006).

The high level of nonlinear complexity means the Earth system, though deterministic, is chaotic and not completely predictable (Lorenz et al., 1996; Hansen et al., 1997b). However, this does not imply a totally unpredictable system for if this were the case, climate modeling would not be possible. A couple of factors are responsible for the predictability of the Earth's system. One is that the system is driven externally through insolation from the sun, thereby receiving a forcing that is pseudo-regular on a varied range of timescales. The seasonal cycle is the principal forcing that the Earth experiences, and is very regular. The other factor is the existence of specific modes of variability such as the already mentioned ENSO. Because these signals are quasi-periodic, they are predictable to some degree of accuracy (Kiehl and Ramanathan, 2006). The representation of the Earth system thus requires statistical as well as deterministic approaches. All climate models are deterministic. Some incorporate stochasticity in their parameterizations (and one might argue, in their numerics) but their underlying formulation is dynamical and deterministic. However, modeling the climate system is concerned with understanding and simulating the behaviour (dynamics) of the coupled system such that the simulation is representative of the real

world in terms of the statistics of the system, rather than with predicting the exact time and location of a specific small-scale event. In other words, knowing the mean and variance of the climate system is the best we can do. We cannot predict the exact trajectory of the system beyond a week or so in advance, we can only predict the statistics. This ends up essentially being climatology plus a forced response. The fact that the two (climatology and forced response) are separable is a fortunate apparent property of the climate system that does not at all follow obviously from such a complicated chaotic system.

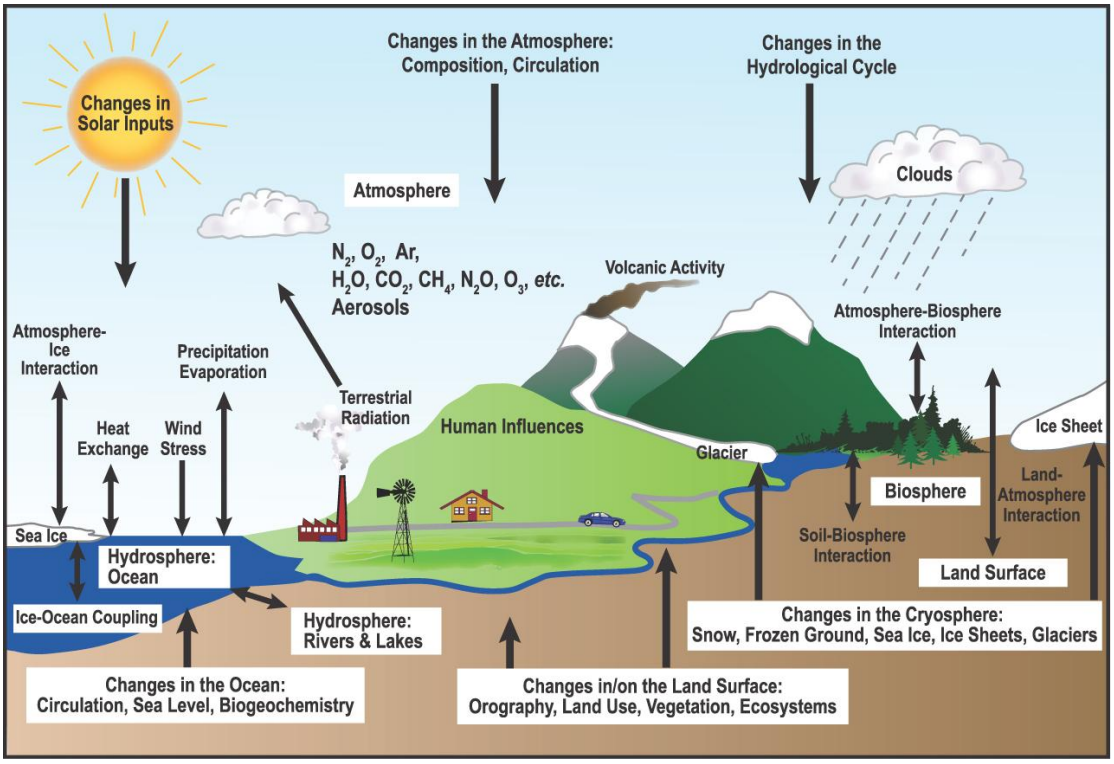

Figure 2.1: Schematic view of the components of the global climate system, including their processes and interactions [taken from IPCC, 2007].

The present and future state of Earth's climate must account for another forcing factor due to human industrial activity (Hansen et al., 1998; Mitchell et al., 2001; Hansen et al., 2005). This is generally attributed to a gradual buildup of greenhouse gases and trace constituents, although it has been suggested that land-use changes began to exert an influence upon global climate as far back as 8,000 years ago (Ruddiman, 2003).

The impact of these anthropogenic changes to the energy budget of the Earth is quite significant (Houghton et al., 2001), considerably dominating that due to natural forcing, at the global interannual scale (IPCC, Solomon et al., 2007). An understanding of the full range of natural climate variability is necessary if recent climatic changes (e.g. Mann and Jones, 2003; Jones and Mann, 2004) are to be attributed to human influence, and also in order to anticipate the full range of climate states that might be encountered in the future. Given the potential for significant anthropogenic climate change during the coming decades (e.g. Cubasch et al., 2001; Knutti et al., 2002; Kattsov et al., 2007; Tebaldi and Knutti, 2010; Trenberth and Fasullo, 2010), understanding the Earth's climate system and the ability to predict the climate poses one of the most challenging scientific questions of our time.

2.3 Climate Modeling

Climate models are essential tools for assessing, evaluating and predicting the changes that have happened, are happening and are likely to happen in the Earth's climate as well as the implications of these changes. Climate models are mathematical representations of the numerous discrete processes that shape global and regional climate. The relationships between these processes can be calculated using fundamental principles of physics or simplifications of this, as opposed to empirically driven relationships (Harvey et al., 1997). Models solve the equations of the atmosphere and oceans approximately by breaking their domains up into volumetric grids, or boxes, each of which is assigned an average value for properties like velocity, temperature and humidity. In a model, the size of the box is the spatial resolution and the smaller the box, the higher the resolution. A common assumption is that the realism of climate simulations will improve as the resolution increases. In practice, computing limitations do not allow models of high enough resolution to resolve important sub-grid processes. A few examples of phenomena occurring over length scales smaller than those of the most highly resolved models, and that cannot be ignored, include cloud formation and cloud interactions with atmospheric radiation; sulphate aerosol dynamics and light scattering; ocean plumes and boundary layers; sub-grid turbulent eddies in both the atmosphere and oceans; atmosphere/biosphere exchanges of mass, energy

and momentum; terrestrial biosphere growth, decay and species interactions; and marine biosphere ecosystem dynamics.

Differences between the scale of these processes and computationally-achievable grid scales in global models pose a well-known problem in Earth system science. To account for sub-grid climate processes, the approach has been to use empirical or semi-empirical relations to approximate net (or area-averaged) effects at the resolution scale of the model. This is usually referred to as parameterization. It is important to stress that all climate system models contain empirical parameterizations and that no model derives its results entirely from first principles. The primary difference between simple and complex models is the hierarchical level at which the empiricism enters (Harvey et al., 1997).

2.3.1 Governing equations

The mathematical equations that describe the motions of the atmosphere and on which climate models are based are known as the governing equations. As described in Kalnay and Cai (2003), Bjerknes (1904) stated for the first time that there is a complete set of seven equations with seven unknowns that governs the dynamical evolution of the atmosphere:

Newton's (three equations for the three velocity components) second law or conservation of momentum;

The continuity (conservation of mass) equation;

The equation of state for ideal gases;

The first law of thermodynamics;

A conservation equation for water mass (continuity equation for atmospheric water vapour).

Newton's second law (or conservation of momentum) on the rotating frame of the Earth is written as:

$$\frac{d\boldsymbol{v}}{dt} = -\alpha\nabla p - \nabla\emptyset + \mathbf{F} - 2\Omega \text{ x } \mathbf{v} \qquad (1.1)$$

where **v** is the relative velocity of a parcel of air, α is the specific volume (the inverse of the density ρ), p is the pressure, $\emptyset$ is the geopotential, **F** is the frictional force and Ω is the angular velocity.

The continuity equation (in flux form) is written as:

$$\frac{\partial \rho}{\partial t} = -\nabla \cdot (\rho\, \mathbf{v}) \qquad (1.2)$$

The equation of state for perfect gases is written as:

$$p\alpha = RT \qquad (1.3)$$

Here, the atmosphere is assumed to be a perfect gas with absolute pressure p, specific volume α and absolute temperature T where R is the universal gas constant.

The thermodynamic energy (or conservation of energy) equation is given by:

$$Q = C_p \frac{dT}{dt} - \alpha \frac{dp}{dt} \qquad (1.4)$$

Where Q is the heat applied to an air parcel per unit mass and C_p is the coefficient of specific heat at constant pressure.

Lastly, the equation (in flux form) for conservation of atmospheric water vapour is given by:

$$\frac{\partial pq}{\partial t} = -\nabla \cdot \rho \mathbf{v} q + \rho\,(E - C) \qquad (1.5)$$

The right hand side gives the convergence of flux of the mixing ratio q, with moisture sources evaporation E and moisture sink condensation C.

The physical components of climate models are based on the above equations. These equations require the addition of appropriate boundary conditions at the bottom and top of the atmosphere (for derivations see: Haltiner and Williams, 1980; James, 1994;

Kalnay and Cai, 2003). In summary, calculations of thermal energy involve detailed analysis of the vertical radiative transfer of shortwave and longwave radiation, and the modes of transport (moist and dry, convective and turbulent). There are two components of the water vapour equation, as its production and 'destruction' needs to be included in the prediction equation for it. Thus, evapotranspiration from the Earth' surface acts as a source and condensation or precipitation as a sink (Dickinson, 1986). Conservation of mass implies the continuity of atmospheric circulation. The numerical solution of the model equations is carried out on a prescribed spatial grid, or at a prescribed spatial resolution. Dynamic motions and processes smaller than the specified grid cannot be spatially resolved, and must be implicitly added in the model. These sub-grid processes need to be parameterized in terms of the large scale resolved fields.

2.3.2 Climate model development and application

Climate modeling involves the development of models from basic principles, the comparison of models with observations, and the use of models to improve understanding by answering fundamental scientific questions (Henderson-Sellers and McGuffie, 1987). Modelers develop processes for the atmosphere, ocean, land or cryosphere. Such development is guided by observational data which can be from satellite platforms or terrestrial observations or a combination of these sources (e.g. Graves et al., 1993). Thus, model processes are developed hand in hand with physical understanding or observations (Randall et al., 1996). However, it is possible (given there is no programming error) that the data or understanding on which the development is based is faulty or limited in some way. In such a case, the modeled process is flawed or incomplete to some extent. This is the prime reason model simulations must be consistently evaluated against a wide range of authentic observations (Kiehl and Ramanathan, 2006).

Application of models in research can take at least three forms. Firstly, climate models may be used to gain understanding of basic processes in the Earth system, for example climate forcing, feedbacks, and response (e.g. Hansen et al., 1997a; McGuffie and Henderson-Sellers, 2001; Meehl et al., 2003). Secondly, models can be

used to test hypotheses about the workings of the climate system, for example, the role of clouds in the partitioning of net radiation (e.g. Betts, 2004; Abiodun et al., 2008). Thirdly, models can be used to predict the state of future climate (e.g. Kattenberg et al., 1996; Timmermann et al., 1999; Cubasch et al., 2001; Allen and Ingram, 2002; Beniston et al., 2007).

2.4 Hierarchy of climate models

A hierarchy of models exists to address the wide range of scientific questions identified above (Harvey, 2000). The hierarchal order of models is usually based on the number of spatial dimensions explicitly modeled. The simplest climate models are zero-dimension energy balance models, which represent globally annually averaged conditions (Henderson-Sellers and McGuffie, 1987; Kiehl and Ramanathan, 2006). Another formulation of zero-dimension climate model is the linearized time dependent coupled atmosphere-ocean system (Dickinson, 2000). These are useful for understanding what processes control the overall time scale of the entire climate system rather than the time scale of individual components in the climate system. One-dimensional models may include the vertical direction. Those one-dimensional models which include only the vertical balances between radiative and convective processes are referred to as radiative-convective models (Ramanathan and Coakley, 1978) and have been useful in studying the effects of increased trace gases on climate. Energy-balance models that exclude the vertical dimension but include a meridional direction are also one-dimensional (Meehl, 1984). These have been employed to consider sea-ice processes as amplifiers of climate change (Lian and Cess, 1977).

Two-dimensional climate models incorporate zonally averaged momentum, thermodynamic, and continuity equations which yield information on the meridional temperature and circulation (i.e. latitude versus pressure). The contributions from the zonal circulations (eddy terms) to the zonal mean are parametrically included (Kiehl and Ramanathan, 2006). These models are often used to study stratospheric circulations and chemical interactions. Another type of two dimensional model is the energy-balance model which has been extended to two-dimensions in latitude and longitude, where horizontal dynamics are assumed to be diffusive (North et al., 1983). These

models have been useful in studying a range of climate-change problems related to the distribution of changes in surface temperature (see North and Cahalan, 1981). Three-dimensional (or more appropriately, four-dimensional) models include the solution of the full three-dimensional equations of momentum, energy, and mass and integrate these forward in time. They are the most complete and complex form of climate models. These models were referred to as general circulation models and more recently called global climate models (GCMs). The different types of general circulation models are presented below.

2.4.1 General Circulation Models

GCMs are complex climate models and are essential scientific tools for understanding and predicting natural and human-caused changes in Earth's climate. These models are systems of differential equations derived from basic laws of physics, fluid motion, and chemistry formulated to be solved numerically. Essentially, the accuracy of climate models is limited by grid resolution and our ability to describe the complexities of atmospheric, oceanic, and chemical processes mathematically. Depending on the horizontal and vertical resolution some processes still need to be parameterized e.g. convective cells in the ocean and the atmosphere. These calculations require a lot of computer power which limits the length and number of the simulations (e.g. sensitivity tests and ensemble runs) that can be obtained in an adequate time. To reduce the computational effort, often atmosphere (e.g. Hall and Valdes, 1997) or ocean-only GCMs (AGCM or OGCM respectively) are utilized. Atmospheric GCMs (AGCMs) model the atmosphere and impose sea surface temperatures. Oceanic GCMs (OGCMs) model the ocean (with fluxes from the atmosphere imposed) and may or may not contain a sea ice model. A step towards a more complete coupled system between atmosphere and ocean are AGCMs with a slab or mixed layer ocean (e.g. Vettoretti and Peltier, 2004). In recent years more and more fully coupled Atmosphere-Ocean GCMs (AOGCMs) have been used in climate research (e.g. Cubasch et al., 1997; Montoya et al., 2000; Collins et al., 2002; Zorita et al., 2004). AOGCMs represent the pinnacle of complexity in climate models and internalize as many processes as possible. They may be coupled to models of other processes, such as the carbon cycle, so as to better model feedback effects.

While GCMs remain the most important tools at hand for modeling and assessing global climate change, they have a limitation in that the current resolution at which they are generally run is too coarse to resolve small-scale atmospheric dynamics such as the effects of orography or the interactions of the land surface and boundary layer (McGregor, 1997). This need for local scale information gives rise to downscaling of global climate output. Downscaling can either be statistical or dynamical with each method having subsets and unique merits and demerits. This thesis however focuses on dynamical downscaling and the following section describes this in more detail.

2.4.2 Regional Climate Models

The field of regional climate modeling evolved towards the end of the 1980s to bridge the gap in GCM applicability at finer spatial scales and provide regional climate information for impact assessment studies (Giorgi, 2006). This bridge is usually referred to as downscaling. Two general categories exist for downscaling techniques: process-based techniques focused on nested models, and empirical techniques using one form or another of transfer function between scales (Hewitson and Crane, 1996). This thesis focuses entirely on the earlier category i.e. dynamic nested models. The earliest use of regional climate models involved the nesting of a limited area model (LAM) within a GCM or within observation re-analyses (Dickinson et al., 1989; Giorgi, 1989). According to McGregor (1997), it is desirable that any GCM simulation should produce realistic intensities and frequencies for each type of major synoptic system. If an RCM is nested in such a global model, it should then be possible to produce a realistic detailed climatology at a local scale. This possibility holds at least for midlatitude domains where boundary forcing largely determine the behaviour of the RCM (Vukicevic and Paegle, 1989) although successful applications have also been made over tropical domains where local small-scale physics are even more important. RCMs have thus been employed to dynamically downscale GCM simulations and further extended to make seasonal climate change predictions with the aim of obtaining useful climate information on the regional scale. In achieving these objectives RCMs have become an indispensable tool and a core part of the climate assessment or prediction system (Wang et al., 2004) where these models serve to bridge the divide between GCMs and other modeling components such as hydrological models that re-

quire regional climate information (e.g. Leung et al., 1996; Miller and Kim, 1996). Numerous studies have demonstrated the ability of regional climate modeling to improve simulation at regional scales especially in areas where the spatial distribution of climate variables is controlled by forcing due to complex orography (e.g. Giorgi, 1990; Jones et al., 1995; Walsh and McGregor, 1995; Wang et al., 2000).

A model of a given system is expected to, among other things, improve understanding of the system so modeled. Regional climate modeling has proven to be useful in this regard, improving our understanding of climate processes such as cumulus convection, land-atmosphere feedbacks, cloud-radiation forcing, boundary layer processes and climate change processes (e.g. Pan and Wu, 1995; Dudek et al., 1996; Paegle et al., 1996; Schär et al., 1999; Barros and Hwu, 2002; Sen et al., 2004a; Sen et al., 2004b; Wang et al., 2004; Tadross et al., 2006; Abiodun et al., 2008). The land surface has a strong influence on climate at both global and local scales through the exchange of heat, moisture and momentum (e.g. Pielke and Avissar, 1990; Betts, 2004). Even as it exerts such a forcing, the land surface is in turn affected by feedbacks from the atmosphere. The result of all this is a very complex land-atmosphere interaction and accurate representation of the involved processes in climate models is critical to the realistic simulation of global and regional heat and hydrological cycles (Wang et al., 2004). Some of these processes in effect occur at scales too small for regional models to resolve or too complex to be rendered into forms solvable by exact numerical computation. Parameterizations that describe the underlying physical behaviour of these processes are consequently used to represent them in models. RCMs are applied on domains typically up to the size of continents or large regions on continents.

2.4.3 Generality of RCMs

As they are usually applied over sub-global domains, RCMs can isolate the noisy influences of processes occurring in faraway domains while focusing attention on processes in the region of interest. Higher resolution of regional models reduces the extent of grid cell averaging, thus highlighting the role of fine-scale regional features like fronts and mesoscale convective complexes. It stands to reason that regional models, being based on the fundamental laws of physics, should be applicable any-

where on the globe. However, the prominence of physical processes represented in models by the use of parameterizations may differ from one domain to another. A simulation for a tropical domain, for example, would not require intricate details about the physical processes in frozen soils, and in the same vein, a simulation over the Arctic region would not benefit much from parameterizations of vegetation classes and soil hydraulics. Thus, model development for different regions by most climate modeling groups have focused mainly on accurate representation of the range of climatic processes native to their specific regions of interest. This has resulted in a range of highly 'tuned' regional models and the loss of generality across RCMs. It is such loss of generality in models that might, among other things, lead to regional models exhibiting a home advantage. In Chapters IV and V, we investigate the effects of this loss of generality and seek to identify areas of commonalty and divergence in model simulations. It is also important to note that while RCMs grew out of numerical weather prediction models (NWP), the former attempts to solve a boundary-value problem while the latter deals with an initial value problem. Thus, the generality or transferability associated with NWPs cannot be automatically expected of RCMs.

Chapter 3

Models, data and methods

3.1 Introduction

This chapter provides a detailed description of the models, data and methods used in this study. It begins with a concise description of the five models used followed by a brief description of the Inter CSE Transferability Study (ICTS) domains and each reference station used in the study. A summary of the ICTS coordinated simulations is then provided, the format of data yielded from these experiments described, and their delimitations discussed. Finally, a description of the statistical methods used in the core analyses is provided.

3.2 ICTS regional climate models

Seven RCMs currently participate in the ICTS; however, at the time of this study, only five of these RCMs have both completed their simulations and provided Model Output Location Time Series (MOLTS) data to the central archive. This study makes use of these five RCMs (see Table 3.1). A concise description of the numerics and physics of the models is presented below.

3.2.1 Climate version of the Lokal Model (CLM)

The non-hydrostatic regional climate model CLM was developed by colleagues from the Institute for Coastal Research (GKSS), The Potsdam Institute for Climate Impact Research (PIK) and Brandenburgische Technische Universität (BTU) Cottbus as a climate version of the Local Model (LM) version 3.1 (now COSMO model), originally developed by the German Weather Service. Model version 3.4.6 was used for the ICTS simulations. Regarding dynamics, model variables are staggered on an Arakawa-C/Lorenz grid with scalars (temperature, pressure and humidity variables) defined at the centre of a grid box and the normal velocity components defined on the corresponding box faces. Model equations are solved by second order horizontal and

vertical differencing. Hybrid terrain-following height coordinates are used with horizontally explicit, vertically implicit (HE-VI) time-splitting integration. For the ICTS simulations, the Davies-relaxation formulation is employed for the treatment of lateral boundary conditions (Davies, 1976) along with the spectral nudging option (Von Storch et al., 2000). A time step of 300 s is used for the ICTS simulations with boundary values provided by the global-model (GME) at hourly intervals. Model Physics includes Grid scale precipitation with parameterized cloud microphysics. The Kain-Fritsch convection scheme (Kain and Fritsch, 1993) was applied for all CSE domains (see section 3.3) except GAME domain, where the Tiedtke (1989) mass flux convection scheme was used. The model used a level 3.5 vertical diffusion scheme which includes a laminar boundary layer. A Two-stream radiation scheme after Ritter and Geleyn (1992), with full cloud-radiation feedback, is used for short- and longwave fluxes. For land surfaces, CLM employs the DWD soil model TERRA3D after Jacobsen and Heise (1982). Grid specifications consist of a limited area rotated latitude-longitude grid (rotation chosen differently for different ICTS domains), of 0.5° horizontal resolution and 32 vertical levels. A detailed description of the model can be found in Steppeler et al., (2003), Rockel et al. (2008) and Rockel and Geyer (2008).

3.2.2 Global Environmental Multiscale-Limited Area Model (GEM-LAM)

The University of Quebec at Montreal (Canada) uses the Global Environmental Multiscale-Limited Area Model (GEM-LAM). The GEMLAM ICTS simulations were done with the GEM Model version: v.3.3.1. Model formulation is based on hydrostatic primitive equations with discretizations in space and time. Space descritization employs 3-D finite differences on an Arakawa-C staggered grid in the horizontal, and on an Arakawa-A grid in the vertical (Côté, 1997) with no motion across top and bottom surfaces. Descritization in time uses semi-implicit semi-Lagrangian (3-D) two time-level time discretization scheme (Côté et al., 1998a; Côté et al., 1998b). This scheme is designed to avoid the highly-restrictive time step limitation which would be imposed by the use of a more conventional Eulerian scheme. A time step of 1800 s is used for all ICTS simulations. Prognostic variables are T (temperature), $\ln(p_{surface})$ (natural logarithm of the surface pressure), U (east-west wind component), V (north-south wind component) and q (liquid water content). Horizontal diffusion is used only

on the momentum variables and a stratospheric sponge layer is present to prevent spurious heat increase at the top of the model. Model physics parameterizations are as follows: Correlated-K solar and terrestrial radiations scheme (Li and Barker, 2005) for radiative transfer, deep and shallow moist convective processes after Kain and Fritsch (1990), large-scale (stratiform) precipitation uses the Sundqvist condensation scheme (Sundqvist et al., 1989). Parameterizations relating to sub-gridscale orography include gravity-wave drag (McFarlane, 1987) and low-level orographic blocking (Lott and Miller, 1997). GEMLAM uses the Interactions among Soil, Biosphere and Atmosphere (ISBA) land-surface scheme (Bélair et al., 2003) which includes prognostic variables for surface and soil temperatures, snow depth, and soil volumetric water contents.

GEMLAM has a limited area latitude-longitude grid, with optional computational poles rotated with respect to geographic poles (rotation chosen differently for different ICTS domains), at 0.5° horizontal resolution, with 53 hybrid levels, topmost level at 10 hPa. Soil cover basic data set is from the USGS. For all ICTS simulations, sea-surface temperature and sea-ice surface boundary conditions were interpolated from the AMIP2 (Atmospheric Model Intercomparison Project v2) observed, 1º×1º monthly mean values, as obtained online from the Lawrence-Livermore National Laboratory (LLNL) Program for Climate Model Diagnosis and Intercomparison (PCMDI). A full description of the model can be found in Côté et al. (1998b).

3.2.3 Canadian Regional Climate Model (CRCM)

The Consortium on Regional Climatology and Adaptation to Climate Change (OURANOS) uses an updated version of the first-generation Canadian Regional Climate Model CRCM-I (Laprise et al., 1998). This limited-area nested model, developed at the University of Quebec at Montreal, uses a dynamical kernel (Laprise et al., 1997). This model version 4.1.0 is the same model as the older version, but with allowance for the Southern Hemisphere. CRCM numerics compose of fully elastic non-hydrostatic equations with the following discretization in time: non-centered semi-implicit semi-Lagrangian three-time-level marching scheme with a weak running time filter, and in space: Arakawa C-type grid (with staggering in the horizontal

as well as in the vertical). Vertical resolution is variable with a Gal-Chen scaled-height terrain-following coordinate (Gal-Chen and Somerville, 1975). There is no motion across top and bottom surfaces, and horizontal diffusion is used on prognostic variables. A time step of 900 s is used for all ICTS simulations. Physics package is as follows; Solar radiation (Puckrin et al., 2004); Terrestrial radiation (Morcrette, 1984); Bechtold-Kain-Fritsch scheme for deep and shallow convection (Bechtold et al., 2001); Large-scale condensation parameterized by a simple super saturation-based condensation scheme. Land surface uses the CLASS_v3.7 "Canadian LAnd Surface Scheme" (Verseghy et al., 1993). Cloud formulation is relative humidity and stability dependent (Lorant et al., 2002), and vertical diffusion follows Monin-Oboukhov, K-theory (Jiao and Caya, 2006). The model horizontal grid is uniform in a polar stereographic projection at 60° North or South. The resolution is chosen to be between 42 and 45 km in the center of each domain, with 29 vertical levels, top at 30 km (~10hPa). There is no spectral nesting, but pilot temperature is applied at the top level. Lateral sponges (usually 10 grid points) are applied to all meteorological fields and to topography. There are three soil layers (depths: 0.1 m, 0.25 m and 3.75 m). Land-cover data is based on the Global Land Cover (GLC 2000) initiative (Eva et al., 2004; Mayaux et al., 2004). Initial deep soil parameters are obtained from a Canadian Centre for Climate Modeling and Analysis (CCCma) General Circulation Model III simulation. Basic references for the model are Caya and Laprise (1999) and Plummer et al. (2006). CRCM is hereafter referred to by its French acronym, MRCC.

3.2.4 Rossby Centre Atmospheric regional climate model (RCA3)

The Swedish Meteorological and Hydrological Institute (SMHI) developed the Rossby Centre Atmosphere model. RCA is the atmospheric and land surface component of RCAO, the Rossby Centre Coupled Regional Climate Model. The most recent version of RCA at the time of study is RCA3 from 2004 (Kjellström, 2005). RCA was originally developed from the high resolution weather prediction model HIRLAM (Källén, 1996; Undén et al., 2002). While basically retaining the dynamical core of the model, the physical parameterization schemes have been replaced or further developed to allow an accurate operation in climate mode. After the initial adaptation and definition of the model, a second version, RCA2, was developed which is de-

scribed in detail by Jones et al. (2004a). RCA3 builds mainly on RCA2 but includes some substantial modifications. RCA3 is a hydrostatic grid point model using a terrain-following vertical coordinate system. The model uses a 2 time level semi-lagrangian, semi-implicit dynamical core with 6th order horizontal diffusion. The vertical mixing as described by the turbulence scheme in RCA3 is based on a prognostic turbulent kinetic energy scheme with a diagnostic length scale (Cuxart et al., 2000) modified to give a smoother transition between stable and unstable conditions (Lenderink and De Rooy, 2000; Lenderink and Holtslag, 2004). A 30-minute time step was used for the ICTS simulations. Model physics consists of a radiation scheme originally developed by Savijärvi (1990) and Sass (1994), modified to include CO_2 absorption by Räisänen et al. (2000). The scheme is computationally fast with only one wavelength band for short wave and long wave respectively. RCA3 introduces a new land-surface scheme. The land portion in each grid point is sub-divided into three tiles with three surface types: forest, open land or snow. A further specification is made for the forest tile to cope with forest canopy, forest floor soil and snow on forest floor. Each tile is thus basically differently treated so that the final grid value is received as a weighted mean of all fluxes in the tiles according to their fractional coverage. More details (e.g. the coupling to soil moisture changes) are given by Kjellström et al. (2005) and Samuelsson et al. (2006). In RCA3 a prognostic process-oriented cloud parameterization is applied following Rasch and Kristjánsson (1998a). Convective clouds and convective processes are described using the approach of Kain and Fritsch (1990). The treatment of shallow convective clouds has been radically changed in RCA3 and is described in detail by Jones and Sanchez (2002) and Albrecht (1981). The RCA3 radiation scheme is based on the original formulation by Savijärvi (1990) but slightly modified by Räisänen et al. (2000). To compensate for some deficiencies of the plane-parallel homogeneous cloud approach (not truly representative of real clouds, especially concerning the case of broken or inhomogeneous clouds) some modifications were introduced according to Cahalan et al. (1994).

RCA3 uses a rotated area grid with South Pole at longitude = 0.0°, latitude = -90.0°. 50 km horizontal resolution is used for the ICTS simulations with 24 hybrid vertical layers in the atmosphere. There are 5 soil layers for temperature (no-flux boundary condition at 3 m) and 2 layers for soil moisture (maximum depth 3.2 m) Soil cover

basic dataset is provided by USGS. Boundary forcing is from ECMWF reanalyses (2° by 2°), every 6 hours. Sea surface temperature (SST) is also from ECMWF (2° by 2°) monthly data. Basic references for the model are Undén et al. (2002), Kjellström et al. (2005) and Jones et al. (2004b).

3.2.5 Experimental Climate Prediction Center (ECPC) Regional Spectral Model (RSM)

The United States Experimental Climate Prediction Centre developed the Regional Spectral Model (RSM). The basic RSM formulation is a primitive equation system, consisting of the momentum equation, hydrostatic equation, thermo-dynamic equation and mass continuity equation. The dependent variables are the zonal and meridional component of winds, virtual temperature, specific humidity and log of surface pressure. The model utilizes a terrain following sigma coordinate system. The primitive equation system assumes that the horizontal scale is less than the vertical scale (which leads to hydrostatic assumption). This limits the refinement of the horizontal resolution of the model to about 10 km. The basic concept of RSM is to apply sine and cosine series to the deviation of the full forecast field from global base field or perturbations (Juang and Kanamitsu, 1994). Semi-implicit time integration for ln (pressure), divergence and temperature are performed on the perturbations in spectral space. A three time level time discretization scheme (leaf-frog) is also used with Asselin's time filter. A time step of 60 - 120 s is used for ICTS simulations. 4^{th}-order horizontal diffusion is used on prognostic variables. Model physics package include short- and long-wave radiation (Chou, 1992; Chou and Lee, 1996; Chou and Suarez, 1996) with diurnal variation and diagnostic cloud (Slingo, 1987); Simplified Arakawa-Schubert cumulus convection (after Grell, 1993) from Pan and Wu (1995) was used for the ICTS Simulations. Large-scale condensation is obtained by LRGSCL, a fortran subroutine implemented by Hong and Pan (1996) which calculates grid-scale precipitation for one leapfrog time-step; The boundary layer physics employs a non-local diffusion concept after Troen and Mahrt (1986). This scheme is strongly coupled to the surface layer physics. In the scheme the turbulent diffusivity coefficients are calculated from a prescribed profile shape as a function of boundary layer height and scale parameters derived from similarity requirements (Hong and Pan, 1996).

Table 3.1: An overview of the five Inter Continental Transferability Study (ICTS) Regional Climate Models (RCMs) used in the study

Mode	Institute	Dynamics	Lateral boundary	Radiation	Land-surface	Turbulence	Microphysics	Convection	Large-Scale Precipitation
CLM	GKSS Germany	**non-hydrostatic** flow in a moist atmosphere without any scale approximations (Steppeler et al., 2003)	Davies relaxation method (Davies, 1976)	SW and LW radiation. Two-stream radiation scheme (Ritter and Geleyn, 1992)	DWD soil model TERRA3D (Schrodin and Heise, 2001)	Mellor and Yamada hierarchy level 2.0 (Muller, 1981)	Kessler (1979), Lin et al. (1983)	Kain-Fritsch (Kain and Fritsch, 1990) Mass flux scheme	Modified warm rain scheme, (Kessler, 1969)
GEMLAM	RPN/MSC and University of Quebec, Canada	**hydrostatic** primitive equation using implicit two time leve semi-Lagrangian scheme in time and 3D finite elements in space (Côté et al., 1998b)	Davies relaxation method (Davies, 1976)	cccmarad radiative transfer scheme (Li and Barker, 2005)	Interactions between Soil-Biosphere-Atmosphere (ISBA) land surface scheme (Bélair et al., 2003)	moist turbulent kinetic energy scheme, Moist-KE (Mailhot et al., 2006)	Fully explicit micro-physical condensation scheme (Kong and Yau, 1997)	Kain-Fritsch (Kain and Fritsch, 1990) Mass flux scheme	Consun condensation, (Sundqvist et al., 1989)
MRCC	OURANOS, Canada	**non-hydrostatic,** fully elastic Euler equations (Laprise et al., 1997)	Davies (1976) refined by Yakimiw and Robert (1990)	SW radiation (Puckrin et al., 2004). LW radiation (Morcrette, 1984)	Canadian Land Surface Scheme (CLASS) (Verseghy, 1991; Verseghy et al., 1993)	Vertical diffusion following Morin-Oboukhov, K-theory (Jiao and Caya, 2006)	Relative humidity and stability dependant cloud formation (Lorant et al., 2002)	Kain-Fritsch (Kain and Fritsch, 1990) Mass flux scheme	Modified cloud scheme (Lorant et al., 2002)
RCA3	Rossby Centre, SMHI, Sweden	**hydrostatic** grid point model (Kjellström, 2005)	Davies relaxation method (Davies, 1976)	SW radiation (Savijärvi, 1990), LW radiation (Rogers, 1977; Stephens, 1984; Savijärvi, 1990)	Modified HIRLAM land surface scheme (Kjellström, 2005; Samuelsson et al., 2006)	prognostic turbulent kinetic energy combined with a diagnostic length scale (Cuxart et al., 2000)	(Jones and Sanchez, 2002)	Kain-Fritsch (Kain and Fritsch, 1990) Mass flux scheme	Rasch-Kristjánsson scheme. (Rasch and Kristjánsson, 1998b)
RSM	Experimental Climate Prediction Center, USA	**hydrostatic** spectral model perturbed using primitive equations in sigma coordinates (Juang and Kanamitsu, 1994)	Explicit relaxation scheme after Juang et al. (1997)	SW radiation (Chou, 1992), LW radiation, (Chou and Suarez, 1994)	Updated four-layer soil model Noah (Mitchell et al., 2004)	Non-local vertical diffusion package (Hong and Pan, 1996)	(Juang and Kanamitsu, 1994)	Simplified Arakawa-Schubert formerly by Grell (1993)version from Pan and Wu (1995)	LRGSCL routine, calculates grid scale precipitation for one leap-frog time-step. Pan Hua-Lu (1990)

Above the mixed layer, the local diffusion approach is applied to account for free atmospheric diffusion. RSM uses an updated four-layer version 3.7 Noah land surface model *LSM* (Mitchell et al., 2004). For the ICTS simulations, the grid is on a Mercator projection true at Equator with 50 km horizontal resolution and 28 sigma layers of atmosphere. Two soil layers (top layer 10 cm, bottom layer 190 cm) with soil cover data obtained from the USGS dataset. Boundary forcing on the atmosphere is from NCEP2 reanalyses, every 6 hours. SST from AMIP2 1°x1°data, monthly interpolated to daily. Lateral boundary relaxation method used is after Juang et al. (1997). A full description of the model can be found in Juang and Kanamitsu (1994).

3.3 Domains of the ICTS

Seven computation areas (domains) were defined in the ICTS (Figure 3.1). Each of the domains is derived from a Continental Scale Experiment in GEWEX. Several aspects were considered in defining the domains. For instance the model boundaries should not cut through mountain ridges and typical features for a region should be included in the model domain. Furthermore the domain should be large enough to minimize the influence of the driving model. In addition several test simulations were performed to find the optimal domain. In order to minimize these tests the choice of the domain size is based on the experience of other simulation studies already performed on these domains. A requirement in ICTS was to use the same model settings for each domain. Only the number of grid points and the rotated North Pole are different for each domain (see Table 3.2). Participants in the ICTS interpolated the results of their simulations onto a common geographical grid and common domains (Table 3.3).

Table 3.2: Model configuration for the different domains of the original CSE (adapted from Rockel and Geyer, 2008)

domain	**number of grid points (including relaxation zone ~ 8 grid points)**	**lon/lat of the rotated North Pole**
Africa	131 x 131	0. 0/ 90.0
Asia	201 x 147	-70. /60.0
Australia	127 x 127	135.0 / 65.0
Europe	105 x 111	-170.0 / 32.5
North America 1	137 x 125	80.0 / 55.0
North America 2	115 x 105	70.0 / 28.0
South America	149 x 181	-60.0 / 68.0

Table 3.3: Definition of common grid domains of the ICTS. Grid mesh is 0.5° CSE (adapted from Rockel and Geyer, 2008)

domain	acronym	number of grid points	lon/lat of lower left corner
Africa	AF01	95 x 95	-22. 0 / -20.0
Asia	AS01	202 x 106	45.5 / 0.5
Australia	AU01	132 x 81	100.5 / -45.0
Europe	EU01	139 x 84	-24.5 / 32.0
North America 1	NA01	143 x 89	-135.0 / 10.5
North America 2	NA02	190 x 73	-171.0 / 43.5
South America	SA01	126 x 143	-91.0 / -57.0

The boxes in Figure 3.1 show the outlines of these domains. A brief description of each of the seven Continental Scale Experiment domains is given below.

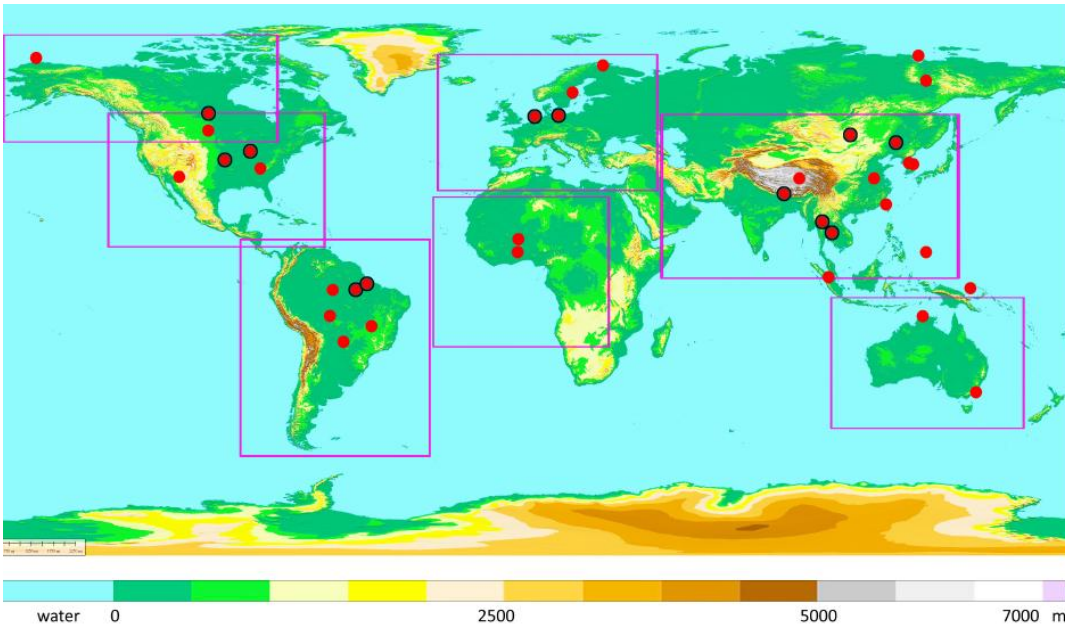

Figure 3.1: Seven Domains used for ICTS simulations (boxed). Red dots denote CEOP reference sites, stations used in this study are ringed in black (adapted from Takle et al., 2007).

The domain for Africa (AF01) is based on the African Monsoon Multidisciplinary Analysis (AMMA) region in Africa which is based on a map in the AMMA implementation plan. The Asian domain (AS01) covers the GEWEX Asian Monsoon Experiment (GAME) region, expanded to cover the Himalayan CEOP reference sites. The domain for Australia (AU01) covers the Murray-Darling-Basin Water Budget Project (MDB) area and was based on a previous case study that was part of the GEWEX Cloud System Study (GCSS; Ryan et al., 2000). The domain over Europe (EU01) includes the BALTEX catchment area, as defined by the study area that CLM

focused on for the European Union (EU) Prediction of Regional scenarios and Uncertainties for Defining European Climate change risks and Effects project PRUDENCE (Christensen, 2005; Christensen and Christensen, 2007). The first North American domain (NA01) is covered by the Mackenzie GEWEX Study (MAGS) region. The second North American domain (NA02) covers the GEWEX Americas Prediction Project (GAPP) and was defined by the Project for Intercomparison of Regional Climate Simulations, PIRCS (Takle et al., 1999). The final domain, over South America (SA01) is from the Large-Scale Biosphere–Atmosphere Experiment in Amazonia (LBA) and the La Plata Basin (LPB) region, which was used for a previous South America model intercomparison (Roads et al., 2003). All these domains cover regions having high land-atmosphere coupling strength as identified by Koster et al. (2004).

3.4 The Coordinated Energy and Water Cycle Observations Project (CEOP) reference sites

Model validation data are obtained from the CEOP global data sets including in-situ observations from reference sites (see Table 3.4), which fall within the GEWEX continental scale experiments (CSE). These data were collected during the first and second phases of CEOP between 2000 and 2004. Observational datasets for the reference sites are not available for the full duration of the RCM simulations. Therefore, model output analyses placed emphasis on the periods with observational data. In this section, the CEOP project is described briefly followed by a description of the reference sites used in this study. The Coordinated Energy and Water Cycle Observations Project (CEOP) is an amalgamation of the World Climate Research Programme (WCRP) Global Energy and Water-cycle Experiment (GEWEX) Hydrometeorology Panel (GHP) and the ‘Coordinated Enhanced Observing Period' (‘CEOP’), which was an element of WCRP initiated by GEWEX. One of the main objectives of CEOP is the provision of consistent research quality data of the Earth's energy budget and water cycle and their variability on interannual to decadal timescales, for use in climate system analysis and model development and evaluation; and to improve the predictive capability for key water and energy cycle variables (Bosilovich and Lawford, 2002).

Table 3.4: CEOP reference sites (at the time of the first CEOP Phase I campaigns).

Number	Reference Site Name	Longitude	Latitude
01	Lindenberg	52.200N	14.120E
02	Cabauw	51.970N	4.930E
03	Sodankylä	67.370N	26.650E
04	Norunda	60.080N	17.480E
05	Oueme	9.500N	2.000E
06	Niamey	13.500N	2.500E
07	ARM Southern Great Plains	36.610N	97.490W
08	Bondville	40.010N	88.290W
09	Fort Peck	48.310N	105.100W
10	Oak Ridge	35.960N	84.290W
11	Mt Bigelow	32.420N	110.730W
12	BERMS (Old Black Spruce)	54.000N	105.000W
13	Eastern Siberian Tundra	71.617N	128.750E
14	Eastern Siberian Tiaga	62.000N	129.667E
15	Mongolia	46.283N	107.298E
16	Tibet	32.000N	91.899E
17	Tibet-Gaize	32.300N	84.080E
18	Yangtze River	32.000N	116.000E
19	Inner Mongolia	44.417N	122.867E
20	Northern South ChinaSea-Southern Japan	24.967N	121.181E
21	Himalayas	27.959N	86.813E
22	Korean Haenam	37.440N	127.900E
23	Korean Peninsula	37.550N	126.570E
24	Chao-Phraya River	17.160N	99.870E
25	Chao-Phraya River-Phitsanulok	16.850N	100.480E
26	Chao-Phraya River-Lampang	18.40N	99.470E
27	Chao-Phraya River Kog-ma	18.810N	98.900E
28	North-EastThailand	14.466N	102.379E
29	Western Pacific Ocean	7.050N	134.270E
30	Western Pacific Ocean-Aimeliik	8.460N	138.480E
31	Equatorial Island	0.200S	100.320E
32	Rondonia	10.080S	61.930W
33	Manaus	2.610S	60.210W
34	Santarem	3.020S	54.970W
35	Caxiuana	1.710S	51.510W
36	Pantanal	19.560S	57.010W
37	Brasilia	15.930S	47.920W
38	Tumbarumba	36.660S	148.150E
39	ARM North Slope of Alaska (Barrow)	71.320N	156.620W
40	ARM Tropical Western Pacific (Manus)	2.058S	147.425E
41	ARM Tropical Western Pacific (Darwin)	12.425S	130.891E

The Enhanced Observing Periods of 2002 - 2004 (EOP 2/3) provided hourly observation of surface meteorological variables and energy fluxes from October 1, 2002 through December 31, 2004. Nine basic variables from the CEOP dataset are used in this study. These variables fall into two categories: surface meteorological and radiative data (i.e., 2 m air temperature, pressure, specific humidity, wind speed, downward and upward longwave radiation, downward and upward shortwave radiation) and surface energy flux data (i.e. net radiation, sensible and latent heat fluxes) which are used to validate the model predictions. Twelve CEOP reference sites were used in the model validation process. These sites and their respective vegatation types and station elevation are presented in Table 3.5.

Although twelve sites were used in the model validation process discussed in chapter four, only six sites from CEOP Enhanced Observation Periods (EOP2 and EOP3) met the data requirements of our principal component analysis. The six sites (Cabauw, Lindenberg, Bondville, Lamont, BERMS and Tongyu) are located in five countries across three continents. These six CEOP reference sites fall into three broad climate types and four different vegetation covers. A brief description of each of the six sites is given below.

3.4.1 Cabauw (grassland)

The Cabauw tower site is located in the central region of The Netherlands. The surroundings are flat and consist of meadows which are used for grazing and for the production of hay (Beljaars and Bosveld, 1997). The grass at the measuring field is kept at a height of approximately 8 cm by frequent mowing. The vegetation cover at Cabauw is close to 100% all year. Cabauw is one of the sites of the Baltic Sea Experiment (BALTEX) and has been demonstrated to be a useful case study for midlatitude homogeneous grasslands within the Project for Intercomparison of Land-Surface Parameterization Schemes (PILPS) framework (Henderson-Sellers et al., 1995; Chen et al., 1997).

3.4.2 Lindenberg (mixed forest and grassland)

Lindenberg is located in the east of Germany and also forms a member site of BALTEX. The climate type of Lindenberg is the same as Cabauw, with heterogeneous land use dominated by a mixture of forest (43%) and agricultural farmland (45%) with a number of small and medium-sized lakes (7%) (Beyrich and Adam, 2004). The Lindenberg data for CEOP EOP-1 include the near surface measurements carried out at GM Falkenberg, which represent only the farmland (low vegetation, grassland) part of the area.

3.4.3 Bondville (cropland)

Bondville is located in central Illinois, USA and is both a member site of the GEWEX America Prediction Project (GAPP) and a member of the AmeriFlux network. The climate of Bondville is temperate continental and the vegetation type in the summer of 2001 was predominantly corn. Although the MODIS land classification shows the land cover at Bondville is homogeneous, the MODIS pixel over this site is actually a mixture of corn and soybean since there is a companion site at Bondville which is located 400 m north of the major site and is planted with opposite crop in corn/soybean rotation. It is the only representative agricultural site from the six CEOP sites used here.

3.4.4 Lamont (Southern Great Plains)

The Lamont Southern Great Plains (SGP) site was the first field measurement site established by DOE's Atmospheric Radiation Measurement (ARM) Program. Scientists are using the information obtained from the SGP to improve cloud and radiative models and parameterizations and, thereby, the performance of atmospheric general circulation models used for climate research. Lamont was chosen as the first ARM field measurement site for several reasons including its relatively homogeneous geography and easy accessibility, wide variability of climate cloud type and surface flux properties, and large seasonal variation in temperature and specific humidity. It also already had a large, existing network of weather and climate research and instrumentation. The SGP site consists of in situ and remote-sensing instrument clusters arrayed

across approximately 55,000 square miles (143,000 km^2) in north-central Oklahoma. The Lamont site is arguably the largest and most extensive climate research field site in the world.

3.4.5 BERMS (cold forest)

The Canadian study area of the Boreal Ecosystem Research and Monitoring Sites (BERMS) in CEOP consist of three individual stations with vegetation covers of Old Aspen, Old Jack Pine and Old Black Spruce respectively. Old Aspen is deciduous while the other two are needle leaf forests found in cold midlatitude climates typical of BERMS. The in-situ tower flux measurements from the Old Black Spruce station during CEOP EOP-3/4 were used in our study.

3.4.6 Tongyu

The Tongyu observation site consists of two stations that are maintained by the Institute of Physics of Jinlin province, Chinese Academy of Sciences. The stations are 5 km apart and located at Tongyu, Northeastern China (44.416 N, 123.867 E, elevation 184 m), on a flat Songliao plain. The area is semi-arid with a mean annual precipitation of 388 mm in Tongyu County, about 30 km northeast of the site. Precipitation totals are highly variable from year to year. Approximately 80% of precipitation occurs between May and September. The mean annual air temperature in Tongyu County is 5.70 °C. There is one grassland station and one cropland station. Only the cropland station data was used in this study. The main crops within 1 km of the measurement location are corn and sunflower, which achieve a height of 2 m during the growing season. The ground is partly bare in the winter. Soils are described as sandy, salty alkaline, black humus, or meadow soil. Meteorological measurements are made from a 20 m tower. Radiation measurements are made at 3 m height, 20 m away from the tower.

Table 3.4: Brief overview of stations used in the study.

S/N	Station	Latitude	Longitude	Country (Continent)	Climate	Station height (asl)	Short Description
1	Lindenberg	52.200N	14.120E	Germany (Europe)	Mixed Forest and Grassland	101 m	Heterogeneous land use dominated by a mixture of forest (43%) and agricultural farmland (45%) with a number of small and medium-sized lakes (7%) (Beyrich and Adam 2004)
2	Cabauw	51.970N	4.930E	Netherlands (Europe)	Grassland	4 m	Flat surroundings with meadows for grazing and for the production of hay. Vegetation cover is about to 100% all year (Beljaars and Bosveld 1997).
3	Bondville	40.010N	88.290W	USA (N. America)	Temperate Continental	216 m	Agricultural site. MODIS pixel shows mixture of corn and soy-bean.
4	Lamont	36.610N	97.490W	USA (N. America)	Southern Great Plains	314 m	Relatively homogeneous geography and wide variability of climate cloud type and surface flux properties. Large seasonal variation in temperature and specific humidity.
5	BERMS (Old Black Spruce)	54.000N	105.000W	Canada (N. America)	Cold Mid-latitude	628 m	Vegetation is needle leaf forest
6	Tongyu	44.417N	122.867E	China (Asia)	Semi-arid	184 m	A cropland station: corn and sunflower, which achieve a height of 2 m during the growing season. The ground is partly bare in the winter. Soils are described as sandy, salty alkaline, black humus, or meadow soil.
7	Mongolia	46.283N	107.298E	Mongolia (Asia)	Grassland	1409 m	Mongolian plateau in the southern region of Ulaanbaatar. Seasonal land cover changes include greening from April to September and dead grassland from October to March.
8	Himalayas	27.959 N	86.813 E	India (Asia)	Alpine	5050 m	Dominant land cover here is restricted to small areas of alpine meadow. The area is characterized by patches of low brushes dominated by rhododendron.
9	Chao Praya River	17.160 N	99.870 E	Thailand (Asia)	Tropical Monsoon	241 m	38 year old Teak plantation.
10	North East Thailand	14.466 N	102.379 E	Thailand (Asia)	Tropical Monsoon	311 m	Surrounded by cassava field. The height of the Cassava changes with the growing season, while the maximum height is around the 250cm; in dry season there is no vegetation. Soil Characteristics: Uniform acrisols up to 7m depth
11	Manaus	2.610 S	60.210 W	Brazil (S. America)	Evergreen Forest	130 m	Located within 100 km of the Manaus city in evergreen secondary and primary forest, pastures derived from primary forest conversion, logged forest, pastoral areas, and inundated areas. Soils are relatively nutrient-poor, sandy.
12	Santarem	3.020 S	54.970 W	Brazil (S. America)	Para Forest	130 m	The site is located in the Tapajós National Forest (Flona Tapajós), which contains nearly 600,000 ha of protected old growth evergreen forest and is located 50 km south of Santarém. These soils are acidic, have a low base saturation and have high clay content.

3.5 ICTS coordinated simulations setup

In the ICTS simulations, each model is required to use the same setup on all domains i.e. no tuning or changing of parameterizations between regions. Each model thus used a configuration that gives the most satisfactory results over its 'home' domain (and thus taken to be its default setup) to simulate the other ICTS domains. Initial and boundary data for the models were taken from the NCEP (National Centers for Environmental Prediction) reanalysis II data set (Kanamitsu et al., 2002). This data is available for 00, 06, 12, and 18 UTC each day on a Gaussian grid with a horizontal resolution of 1.875 in the meridional. Spectral nudging of U and V wind components (where applicable) above 850 hPa, with grid nudging at lateral sponges (usually 8 grid points affected) were applied to all prognostic fields.

A 50 km horizontal model resolution was used by all the ICTS models and simulations were carried out for the period of July 1999 to December 2004, covering all three Coordinated Enhanced Observation Period (CEOP) campaigns (Bosilovich and Lawford, 2002; Yang et al., 2007). The first six months of the simulations serve as spin-up time for the models. External forcings are the same for all ICTS simulations. These include green house gas concentrations, assumed constant (CO_2 360 ppm); Aerosols assumed constant for rural, urban, desert areas and sea (Louis et al., 1981) and solar constant taken to be 1.368 kWm^{-3}.

3.6 Observed and model data

The Climate Environmental Retrieval and Archive (CERA) database of the World Data Centre for Climate archives the Model Output Location Time Series (MOLTS) generated for all CEOP reference sites from the coordinated ICTS simulations. MOLTS are three-hourly station data, covering the four-year coordinated simulation period (2000 to 2004). Only surface observed data from the 3rd and 4th CEOP campaigns (October 1, 2002 - December 31, 2004) are used to validate the model results. For this study, we used net radiation (net shortwave and net longwave), heat fluxes (latent and sensible), temperature (at 2 m), surface pressure, wind speed (at 10 m), specific humidity (at 2 m) and soil moisture.

3.6.1 Derived variable: Cloud Base Height (CBH)

The first study, discussed in the next chapter, is a transferability experiment over Cabauw. Although CBH measurements are available for Cabauw, we use the Lifting Condensation Level (LCL) as CBH for two reasons: (1) to have consistently derived CBH data for the RCM simulations and the station observations as the models did not provide CBH directly; (2) other stations used later in the transferability intercomparison study (Chapter V) do not have ceilometer data. We use the Lifted Parcel Theory (LPT, Manzato and Morgan, 2003), a standard method for evaluating the instability of a sounding, to compute CBH from the surface variables (i.e. temperature, pressure and specific humidity). In implementing the method, we choose an initial surface parcel to represent the moist and warm air that will create the cloud, let us assume that this parcel has initial pressure, temperature and dew point temperature (p_0, T_0,T_{d0}). We lift the parcel to a higher level, along a dry adiabat, such that the new values of p, T, T_d will conserve the potential temperature and the initial mixing ratio, until the parcel becomes saturated. This level is called Lifting Condensation Level (Manzato and Morgan, 2003), and it is a good estimate for CBH. However, to demonstrate the usefulness and some deficiencies of the LPT method, we compare the calculated CBH and the ceilometer measurement from Cabauw (Fig. 3.2). The method generally underestimates CBH, for two reasons. First, we use the air parcel within 2 m surface layer to calculate the CBHs; in reality, the parcels that form the clouds could come

from a deeper layer or other locations. The 2 m air parcel could be moister than the actual and produce a lower CBH. Second, the LPT method does not account for entrainment process; it assumes that the lifted parcel remains homogeneous until it reaches the LCL (Manzato and Morgan, 2006). This is not always the case in the atmosphere, where the entrainment process mixes the moist surface parcels (that form cloud) with the dry air aloft as the parcels rise. Thus, with the entrainment process the parcel may be drier and produce a higher CBH. Nevertheless, the level of agreement between derived and observed CBH is good enough for the present study, viewing the computed CBH as a lower bound for cloud base height. Hereafter, the calculated CBH from the observed data is the observed CBH, and the calculated CBH from the models data is the simulated CBH.

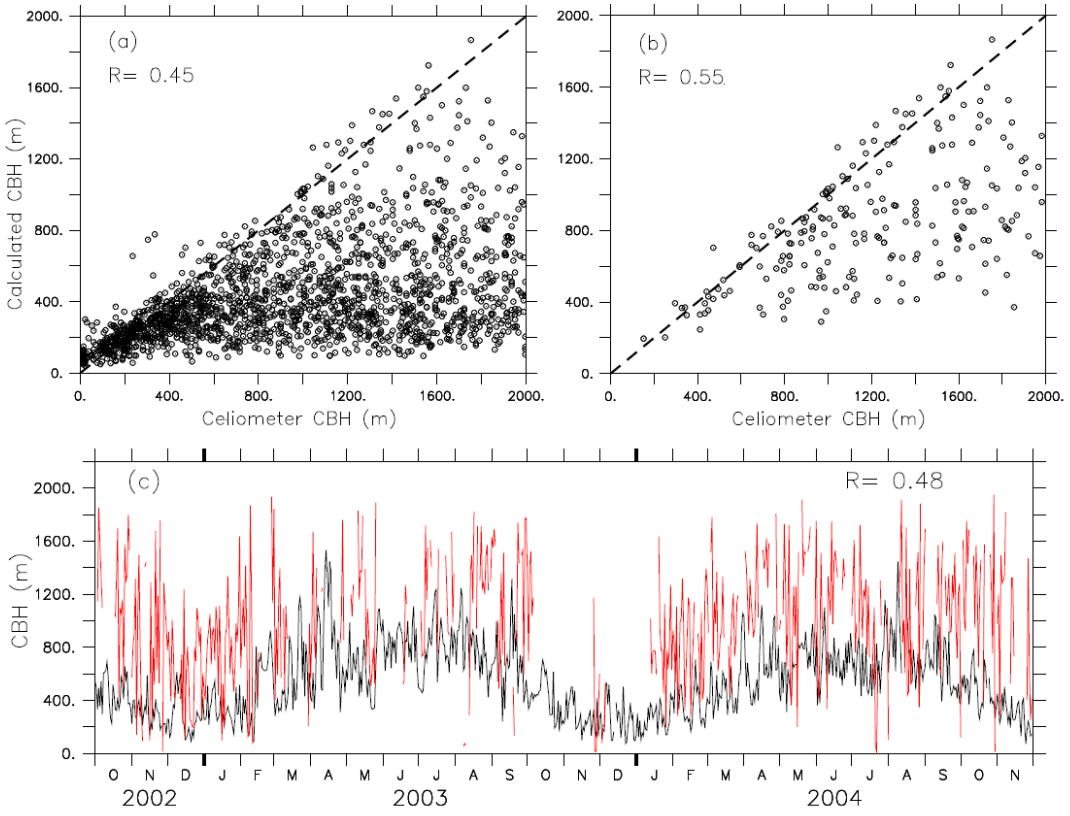

Figure 3.2: Comparison of calculated (using lifted parcel method) and measured (using ceilometer) cloud base height (CBH) over Cabauw, in (a) 3-hourly full-period, (b) summer daytime and (c) daily averaged datasets. The correlation coefficient for each case is shown. In panel (c), the black line shows the calculated CBH and the red line shows the measured.

3.7 Statistical analyses

Two types of statistical analyses were used in this study: Spearman correlation coefficient (which gives a measure of the strength of the 'linear' relationship between two quantitative variables), and principal component analysis (PCA). First, the correlations investigated the relationship between CBH and the surface variables in observations and models. The variables were then subjected to a principal component analysis. PCA is a well known statistical technique frequently used in meteorology and climatology. It was introduced by Pearson (1901), and consequently a mathematical basis was developed for it by Hotelling (1933). PCA allows common modes of variability to be identified between variables (Richman, 1986; Jolliffe, 1990) and therefore the reduction of a large number of interrelated variables to a few principal components that capture much of the variance of the original data set (Hair et al., 1998). We apply PCA on summer daytime three-hourly surface values of R_{net} (net radiation), T2M (temperature), QV (surface, 2 m specific humidity), PS (surface, 2 m pressure), SHF (sensible heat flux), LHF (latent heat flux), CBH (cloud base height), WSP (10 m wind speed) taken from 1 October 2002 to 31 December 2004 at six stations (Lindenberg, Cabauw, Bondville, Lamont, BERMS and Tongyu). We treat observed and model datasets separately, normalized the variables as each has different units and scale of magnitude and used varimax rotation to optimize the variance of the analysis. The summer daytime data is then separated into weak-wind (WSP < 3 m/s) and strong-wind (WSP > 3 m/s) cases to represent weak and strong large scale forcing situations respectively. These subsets provide input for investigating the conditions earlier stated in the hypothesis.

In each analysis, we retained only those principal components which fulfilled the Kaiser criterion. According to Kaiser (1958), when a correlation matrix is factorized, it is pointless to retain components that explain less variance than the original standardized variables. Therefore, principal components with eigenvalues equal or less than 1.0 are excluded from the analysis. However, this criterion in itself is not sufficient as it is possible to get eigenvalues greater than 1.0 with random numbers. We therefore, in addition, imposed the Cattell scree test (Cattell, 1966). The Catell scree test is a visual device which graphs the eigenvalues with the component number. We find

where the graph appears to behave randomly (scree or elbow) and identify the line representing this scree. The number of components to retain corresponds to the number of eigenvalues preceding this scree.

Taylor diagrams (Taylor, 2001) provide a way of graphically summarizing how closely a pattern (or a set of patterns) matches observations. The similarities or differences between patterns are quantified in terms of their correlation, their root-mean-square difference and the amplitude of their variations (represented by their standard deviations). Taylor diagrams are useful for investigating multiple aspects of complex models or in evaluating the relative skill of several different models. We compare simulated seasonal and diurnal cycles of surface meteorological variables with observations at station level and discuss the correlations and standard deviations between these values using Taylor diagrams.

Chapter 4

A transferability experiment

4.1 Introduction

Cloud base height (CBH) is a prominent factor in determining the infrared radiative properties of clouds, a major component of the climate system and an element of climate change. CBH presents the largest uncertainty in predicting global and regional climate change with climate models, because it influences the accurate timing and magnitudes of greenhouse gas-induced warming (Cess et al., 1989; Allmen and Kegelmeyer, 1996). In addition, CBH with wind speed and direction at cloud level play an important role in air safety (Janeiro et al., 2009); for instance, low level clouds with high wind speed at low altitudes influence the safety of aircraft in the vicinity of airports. However, despite its importance, how CBH interacts locally with surface processes (like the energy budget and hydrological cycle) is not well known and remains unexplored, because the interaction is complex. Nevertheless, it is important for regional climate models, the basic tools for regional climate research, to realistically represent this interaction.

In this chapter, we use the transferability concept and data (observations and RCM simulations) to study the interaction between CBH and surface fluxes over Cabauw. This experiment examines a transferability hypothesis "that for all non-monsoonal climatic regions experiencing weak large-scale forcing, daytime surface fluxes are correlated with the height of the cloud base" (Takle et al., 2007). Betts (2004) found a strong correlation between CBH and surface fluxes in observations from different sites. Here we investigate if the hypothesis is true in the models, by studying the coupling between CBH and surface fluxes (including other meteorological variables) under various atmospheric conditions in five RCM simulations over Cabauw (51.9N, 4.5E), a non-monsoon CEOP reference station. It is expected that the magnitude and direction of the simulated couplings should give insights into the causes of model biases and deficiencies in the relevant parameterizations.

4.2 Diurnal and seasonal cycles of atmospheric variables

It is essential to validate model simulations with observations before looking at the coupling of the variables in order to assess individual model skills or biases. Validation focuses on how well the models reproduce the observed annual mean, diurnal cycles and standard deviation of the variables, and also considers the correlation between simulated and observed data. Table 4.1 and Figures 4.1 – 4.3 present the results of the validation.

All models produce realistic simulations of R_N over Cabauw, but with some errors. The observed annual mean R_N for the 2-year (2002 - 2003) period is 56.5 Wm^{-2} (Table 4.1); CLM, GEMLAM, MRCC and RCA3 underestimate it by about 10.9 Wm^{-2} (19.3%), 1.2 Wm^{-2} (2.1%), 14.0 Wm^{-2} (24.8%) and 11.0 Wm^{-2} (19.4%) respectively, but RSM overestimates it by 17.3 Wm^{-2} (31.6%). They all replicate the seasonal and diurnal cycles of R_N, except for the differences in amplitudes (Figures 4.1a and d). In agreement with the observed, the simulated annual maximum R_N occurs in the summer months (June – August) and the minimum in winter months (November – February) (Figure 4.1a); the daily maximum occurs during the day (between 14 -16 LST) and the minimum at nighttime (Figure 4.1d). RSM, which produces the largest errors in R_N, overestimates the annual maximum R_N by 40 Wm^{-2} (34.3%) and the summer daytime maximum by about 80 Wm^{-2} (22.8%), because it uses lower albedo (0.06) than the observed values (0.2). In other models, the albedo is much closer to the observed. As expected, the differences in albedo produce highest error in R_N in summer daytime when the incoming shortwave radiation is at its peak. In addition, RSM produces the highest standard deviation, which is higher than the observed by a factor of 1.2 (Figure 4.1g); the standard deviations of other models are almost the same as observed. However, CLM produces the smallest correlation coefficient ($r = 0.8$) with the observed, while the other models have a correlation of about 0.85. Overall, all the models simulate reliable annual mean seasonal cycles, diurnal variations, and standard deviations of R_N with high correlation coefficients when compared with observations over Cabauw. In partitioning the R_N into SHF and LHF, both the observed and simulations agree that more energy goes for latent heating than for sensible heating over Cabauw, but with different partitioning (Bowen) ratios (Table 4.1).

The annual mean LHF (SHF) is about 41.3 Wm^{-2} (1.7 Wm^{-2}) in observed; 55.0 Wm^{-2} (-9.8 Wm^{-2}) in CLM; 46.1 Wm^{-2} (11.7 Wm^{-2}) in GEMLAM; 37.8 Wm^{-2} (-5.2 Wm^{-2}) in MRCC; 47.5 Wm^{-2} (-5.2 Wm^{-2}) RCA3; and 58.4 Wm^{-2} (0.2 Wm^{-2}) in RSM.

Table 4. 1: Observation and simulation errors in the annual mean Net Radiation (R_N), Sensible Heat Flux (SHF), Latent Heat Flux (LHF), Soil Moisture (SM), Surface Temperature (T_S), Specific Humidity (Q_V), surface pressure (P_S), wind speed (WSP), Cloud Base Height (CBH), albedo and summer daytime evaporation fraction over Cabauw. The highest error in each variable is in bold.

		Errors *(simulated minus observed)*				
Variables	**Observed**	**CLM**	**GEMLAM**	**MRCC**	**RCA3**	**RSM**
R_{net} (Wm^{-2})	56.5	-10.9	-1.2	-14.0	-11.0	**17.3**
SHF(Wm^{-2})	1.7	**-11.6**	10.0	3.4	-7.0	-1.6
LHF (Wm^{-2})	41.3	13.7	4.8	-3.5	6.2	**17.1**
SM (m)	0.6	0.1	-0.2	**-0.6**	-0.3	-0.1
Temp (^oC)	10.2	0.7	1.1	**-1.4**	0.3	0.4
QV(Wm^{-2})	6.7	**0.8**	0.1	0.3	0.1	0.4
PS (mb)	1016.0	0.0	-0.8	**-3.5**	1.5	-2.0
WSP (ms^{-1})	4.1	0.5	0.7	**1.9**	-0.6	0.9
CBH (m)	536.8	-114.6	87.1	**-187.5**	51.6	-33.7
Albedo	0.22	-0.07	-0.03	-0.02	0.04	**-0.14**
Evaporation fraction*	0.70	0.00	**-0.18**	0.00	0.03	0.05

**summer daytime*

The simulated seasonal and diurnal cycles of LHF and SHF are similar to the observed, except for the errors in the amplitudes. As in R_N, RSM still produces the largest error in simulating LHF and SHF; it underestimates the annual minimum LHF (16 Wm^{-2} in January) by 88%, overestimates the annual maximum (60 Wm^{-2} in June) by 133%, and the summer daytime maximum (180 Wm^{-2}) by about 44%. This can be attributed to the albedo error discussed earlier. Consistent with this, RSM overestimates the daytime SHF (80 Wm^{-2} at 1400) by about 100%. GEMLAM is another outlier in simulating LHF and SHF. In daytime summer, it underestimates LHF by 20 Wm^{-2} (14%) and overestimates SHF by 70 Wm^{-2} (87%), making its Bowen ratio (0.99) greater than the observed (0.44) by a factor of 2.25. The errors of other models are within ±10 Wm^2 and their Bowen ratios are very close to the observed (Table 4.1). Nevertheless, the simulated LHF and SHF from all models show high correlation with the observed. For SHF, GEMLAM produces the worst correlation (r = 0.65), while other models have the similar values (about 0.75). For LHF, CLM simulation has the best correlation coefficient (0.85), and other models have the same value (about 0.75).

Generally, the simulated standard deviations for SHF and LHF are worse than those of R_N. RSM produces the highest standard deviations for in SHF and LHF, which are 2.0 and 1.6 of the observed values respectively (Figure 4.1).

The models perform poorly in simulating soil moisture, which plays a key role in the partitioning of R_N into sensible and latent heating. Although, the observed soil moisture does not show any significant diurnal variation, it has a well defined seasonal cycle that is opposite to that of LHF, i.e. maximum in winter and minimum in summer. This suggests that latent heating (i.e. evaporation) depletes soil moisture more in summer than in winter by about 0.3 m (water depth). However, none of the models reproduce this summer-winter soil moisture difference. Ironically, GEMLAM, which grossly underestimates the amplitude of the LHF, reproduces the closest winter-summer soil moisture differences; but it always underestimates soil moisture by 0.3 m. MRCC produces the worst soil moisture by simulating a constant value of 0.06 m for all the months, yet it is one of the best models in simulating the seasonal cycles of R_N, LHF and SHF over the station (Figure 4.1). In the correlation coefficients, RSM ($r = 0.6$) and MRCC ($r = 0.0$) are outliers; other models have the same value ($r = 0.9$). The simulated standard deviations of all the models are less than 0.6 of the observed; here, GEMLAM is the best (NSD = 0.58) and MRCC is the worst (NSD = 0.01).

Despite the poor performances of the models in simulating the soil moisture index (SMI), the level of agreement between the simulated and observed T_S (and to some extent Q_V) is quite good (Figure 4.2). Only GEMLAM and MRCC produce what is apparently different from the observed. In summer, GEMLAM overestimates the temperature by 2 ^oC and underestimates the specific humidity by 2.0 g/kg. This is consistent with the model's error in simulating the Bowen ratio, as discussed earlier. Paradoxically, MRCC that simulates too little soil moisture overestimates specific humidity (by 3.0 g/kg) during the summer daytime and underestimates temperature (by 2.0 ^oC) in the morning hours; in winter it underestimates both temperature and moisture, yet it remains one of the best models in simulating the diurnal and seasonal cycles of the surface fluxes.

The simulated seasonal and diurnal cycle of P_S and WSP are in good agreement with the observed (Figure 4.3). WSP shows a well defined seasonal cycle, but P_S does not. In the seasonal cycle, WSP attains a maximum in winter and a minimum in summer; in contrast P_S attains double maximums during the transition between summer and winter period (in March and September) and a minimum in October. This is consistent between the observed and simulated, though with different magnitudes. In general, RCA3 overestimates P_S by about 2 mb, MRCC underestimates it by 3 mb, and the errors of other models fall between +2 and -3 mb. All the models, except RCA3, overestimate WSP; MRCC overestimates it by about 4 m s^{-1}, while RCA3 underestimates it by about 1 m s^{-1}. However the correlation between the simulated and observed is higher in P_S ($r \geq 0.9$) than in the WSP ($r = 0.65$). The simulated normalized standard deviations of P_S are very close to the observed, clustering around 1.2 of the observed. The simulated normalized standard deviations of WSP in CLM, RSM and GEMLAM are also close to the observed (NSD = 1.2), while those of RCA3 (NSD = 0.7) and MRCC (NSD = 1.4) are outliers. Nevertheless, all the models capture the variations and the amplitudes of P_S and WSP reasonably well.

The observed and simulated CBH are in a good agreement. In the annual cycle, the maximum CBH occurs in summer and the minimum in winter; while in the diurnal cycle, the maximum is during the day and the minimum at night. This is somewhat consistent with the ceilometer data, but values of the ceilometer data are much higher. With CBH, GEMLAM produces the highest error, overestimating it in summer by about 250 m and underestimating it in winter by about 300 m, while other models generally underestimate it. The correlation coefficients ($r > 0.6$) between the observed and simulated are generally good. In the standard deviation of MRCC (NSD = 1.2) is an outlier, while other models cluster around 0.7 of the observed value.

In summary, the models perform differently in simulating different variables over Cabauw. CLM and RCA3 capture all the variables very well, but they underestimate soil moisture (by 0.2 m and 0.4 m, respectively) in summer months. GEMLAM gives a very good simulation of R_N, but overestimates sensible heat flux (by 80 Wm^2), surface temperature (by about 2 ^oC) and cloud base height (by about 600 m) in summer months, and underestimates the soil moisture (by 0.2 m) and specific humidity (by

0.2 gkg^{-1}). MRCC simulates the surface fluxes very well, but produces very low soil moisture (0.06, constant through the year), underestimates surface temperature, CBH and T_S, and overestimates Q_V and WSP. RSM overestimates the surface fluxes because of high albedo, underestimates soil moisture, but captures the remaining variables very well.

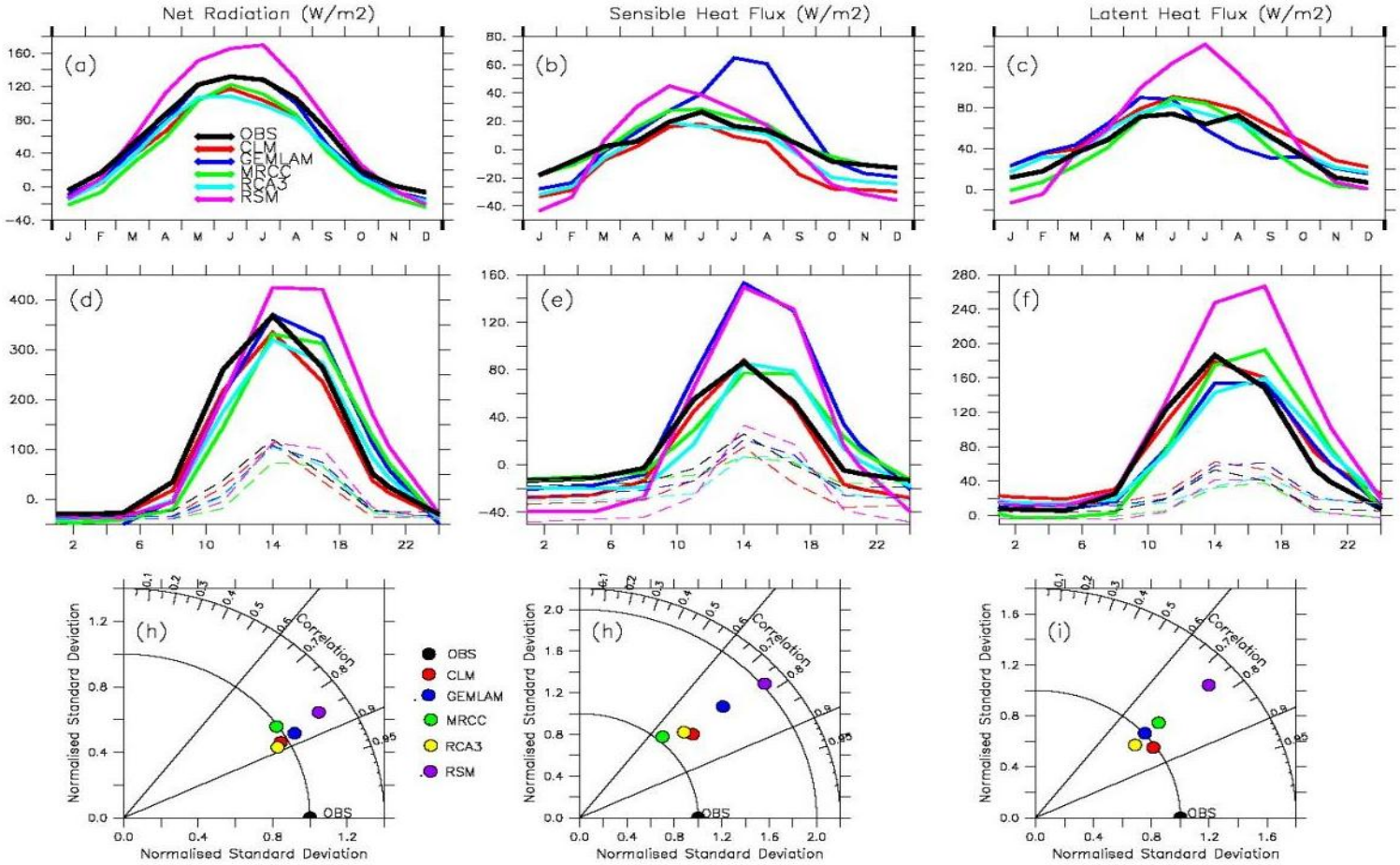

Figure 4.1: Comparison of simulated and observed net total radiation (RN; left panels), sensible heat flux (SHF; middle panels) and latent heat flux (LHF; right panels), using their seasonal variations (upper panels), diurnal variations (middle panels) and Taylor diagrams (lower panels). In the middle panels, thick continuous lines show the summer plots, while thin dashed lines show the winter plots

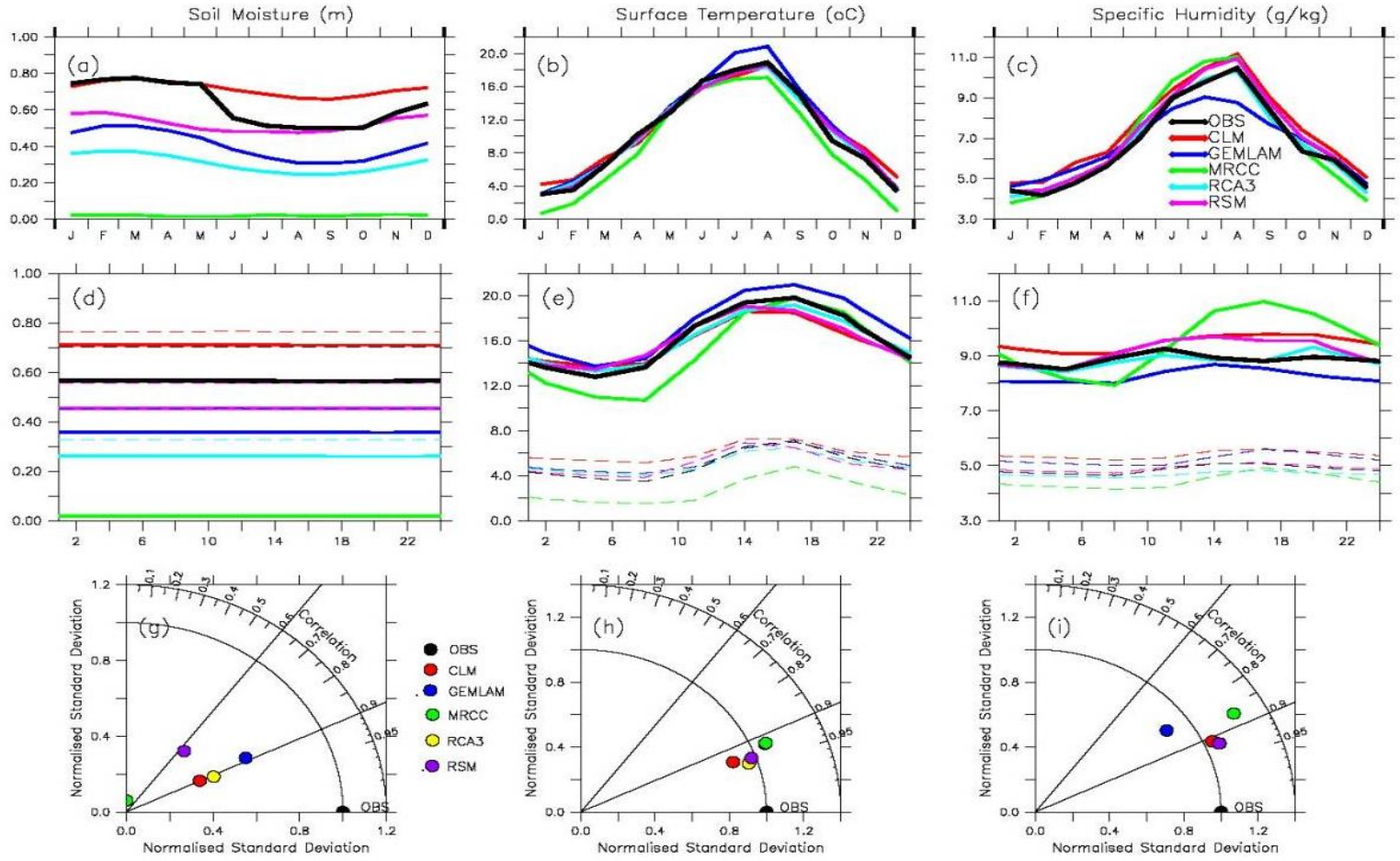

Figure 4.2: Same as figure 4.1, but for soil moisture (SM; left panels), surface temperature (TS; middle panels) and specific humidity at surface (QV; right panels). In panel (i), the plot of RSM completely overlaps that of RCA3 plots.

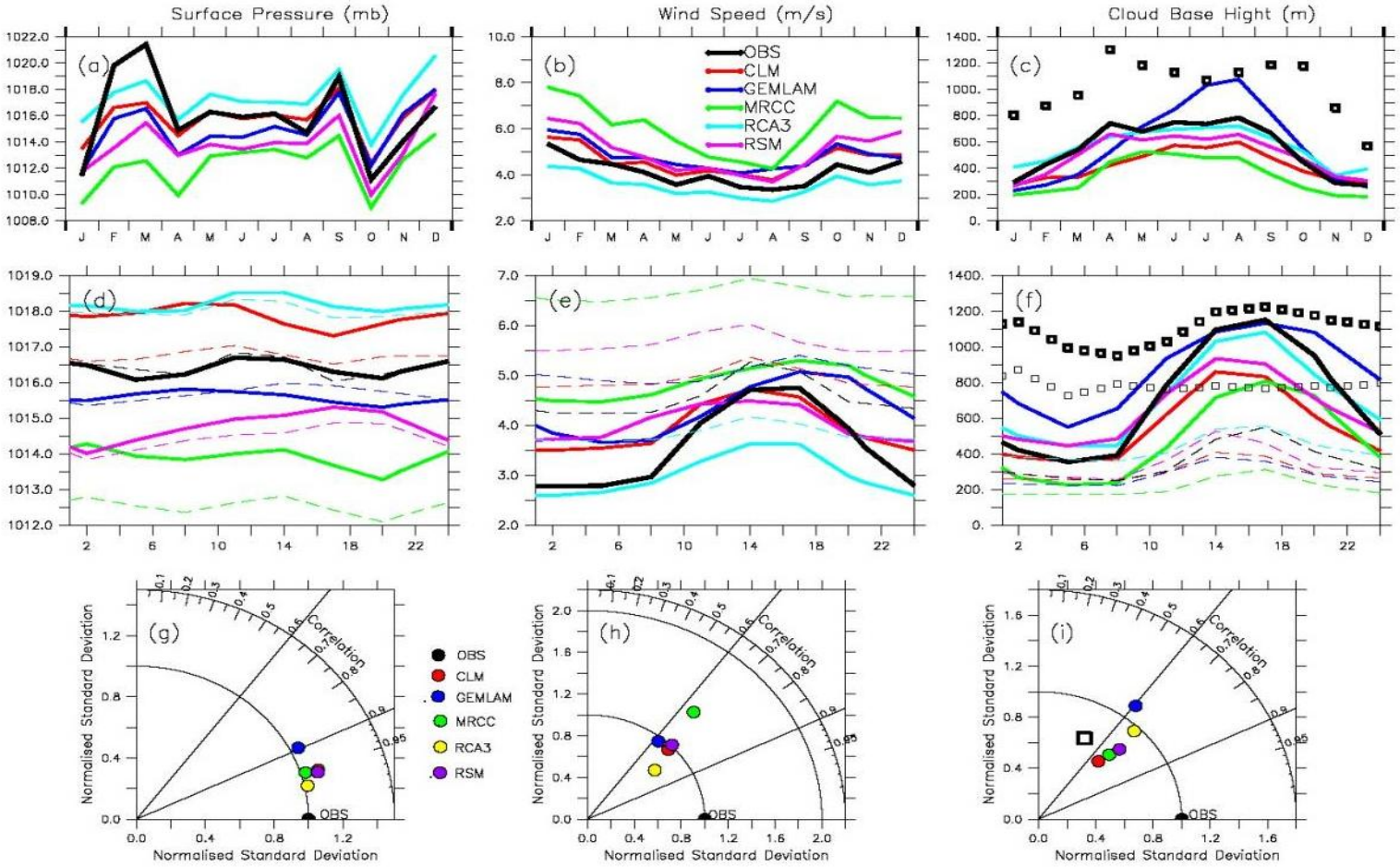

Figure 4. 3: Same as Figure 4.1, but for surface pressure (PS; left panels), wind speed (WSP; middle panels) and cloud base height (CBH; right panels). The squares plots in the right panels show the measured CBH from ceilometer data; in panel (f), the thick squares are for summer data and thin squares for the winter

4.3 Coupling processes

Here we discuss the PCA results on the coupling of atmospheric processes, with emphasis on the coupling of CBH with other surface variables. We first look at the couplings in the full datasets before considering the couplings in the data subsets that investigate the impacts of seasonal, diurnal and synoptic wind variation on the couplings.

4.3.1 Coupling in the full EOP data

In the PCA loadings of the full data, only three principal components (out of nine) have eigenvalues greater than 1, in both observed and simulated data (Table 4.2a). We should note here that the eigenvalues are well separated and that the largeness of the sample size (> 6,500 samples) greatly reduces the instance of effective degeneracy (see North et al., 1982) in the principal components. The three principal components (hereafter PF1, PF2, and PF3) jointly explain 80.05%, 79.82%, 76.94%, 77.92%, 72.48%, and 80.71% of the total variance in the observed, CLM, GEMLAM, MRCC, RCA3 and RSM respectively. In the observed loadings, PF1 alone explains about 39% of the total variance and shows a high loading for R_N (0.96), SHF (0.88), LHF (0.94), and CBH (0.78). This suggests a strong coupling between CBH and these surface fluxes. In other words, the surface energy balance process has strongest influence on variations in CBH, or vice versa. PF2 alone explains 26% of the total variance and shows a high loading for T (0.82), Q (0.92) and SMI (-0.81); this represents the relationship between surface temperature and moisture. The loading of CBH (0.17) on PF2 is very low, suggesting that the relationship has little influence on the CBH in this case. PF3, which accounts for about 15% of the total variance, shows a high loading in PS (-0.78) and VABS (0.83), describing the relationship between surface pressure and 10 m wind speed. Similarly, the loading of CBH (0.05) on PF3 is very small.

The above therefore suggests that, in the observed data, variations in the surface energy balance significantly affect the CBH. The situation is the same in the models; the energy balance is strongly coupled with CBH in all the models. The loading of CBH in PF1 is strongest in CLM (0.86) and weakest in RCA3 (0.52) and GEMLAM (0.51).

Surprisingly, RSM that performs worst in simulating the heat fluxes captures the loading of CBH (0.81) on PF1 closest what obtains in observations. In addition, the loading of CBH in temperature-moisture processes (PF2) is negligible in all the models, except in GEMLAM, where it is 0.62. Note that it is the same model that produces the highest SHF, temperature and CBH (Figure 4.1). Moreover, the simulated coupling of CBH with the pressure-wind process (PF3) is also negligible, strongest in GEMLAM (-0.16) and weakest in RCA3 (0.02). Interestingly, in both observatons and models, soil moisture is well coupled with the surface temperature- moisture relationship (PF2), except in MRCC, where it is coupled with surface pressure-wind speed relationship. Recall that MRCC produces the worst soil moisture.

A Fourier analysis of all model data (periodogram not shown) reveals that the time series of PF1 has two peaks indicating a diurnal and annual cycle. Hence, the coupling of CBH with surface energy process exhibits seasonal and diurnal peaks because of the variation in insolation reaching the Earth's surface. The PCA analysis of the daily dataset, where the influence of the diurnal cycle is removed, showed that the above relationships still hold, but the loadings are weaker (Table 4.2b); in addition only two principal components are retained in MRCC and RSM, where the temperature-moisture process joins the surface energy balance process. However, the 3-hourly dataset is used for the rest of the discussion in this study.

4.3.2 Summer and winter couplings

Furthermore, we compare the PCA loadings of summer (MJJAS) and winter (NDJFM). The summer loadings (Table 4.3a) are similar to the full data loadings. The three principal components (PF1, PF2 and PF3) still describe the surface energy balance, temperature–moisture relationship and pressure-wind association, respectively. However, the total variance represented by surface energy processes (PF1) increases by about 8%, 8%, -2%, 11%, 36% and 6% in observed, CLM, GEMLAM, MRCC, RCA3 and RSM respectively; while that represented by the temperature-moisture process (PF2) decreases by 24%, 13%, 18%, 11% 27% and 30% in observed, CLM, GEMLAM, MRCC, RCA3 and RSM respectively. The variance represented by the pressure-wind relationship (PF3) remains almost the same, except in GEMLAM,

where it drops by about 12%. In addition, GEMLAM now has a fourth principal component which represents only specific humidity, while PF2 in GEMLAM describes a temperature- soil moisture relationship. For both observed and models, the loadings of temperature increases in the surface energy process (PF1), but decreases in the temperature-moisture process (PF2). In summary, the coupling of CBH with surface energy fluxes in the observed and modeled summer datasets are comparable in magnitude with the observed and modeled full dataset, except in GEMLAM where the CBH is strongly coupled with soil moisture and temperature.

The winter loadings (Table 4.3b) are different from those of summer. First, in both observations and models, the proportion of total variance explained by each of the three principal components is closer, ranging between about 20% and 35%. This implies that variation in the three processes (surface energy balance, temperature-moisture relationship and pressure-wind relationship) have almost equal influence. Second, R_N loadings are stronger in temperature-moisture and pressure-wind relationships but weaker in surface energy balance when compared with the summer case. Third, there is no general agreement among observed and models on which of the three processes control CBH. For instance, CBH has a strong coupling with LHF and R_N in observed, CLM and MRCC; a strong coupling with only LHF in GEMLAM, and a moderately strong coupling with surface moisture in RCA3. In the winter situation, only MRCC reproduces the coupling between CBH and surface energy as in the observed.

Hence, we can conclude that the variation of CBH with the surface energy budget variables is stronger in summer than winter. Here, all the five models capture the coupling very well in summer, except GEMLAM; but in winter, MRCC produces the best coupling and RCA3 the worst coupling, when compared with the observed. The rest of the discussion now focuses on the summer case.

4.3.3 Summer daytime and nighttime couplings

We further divide the summer case into daytime and nighttime cases to investigate the influence of insolation on the coupling. Tables 4.4a and b present the loadings for daytime and nighttime periods respectively. The summer daytime loadings reveal cer-

tain differences to the overall summer loadings. While in general the three principal components still explain the earlier mentioned physical processes, there are changes in the variances they capture. As in summer loadings (Table 4.3a), the three principal components still explain about 70%, or more, of the total variance in the daytime data (Table 4.4a). However, total variance explained by the surface energy balance (PF1) drops (by about 20%, 7%, 12% 11% and 9% in observed, CLM, MRCC, RCA3 and RSM respectively), while that explained by the temperature-moisture relationship (PF2) increases (by about 2%, 3%, 2%, 0.1% and 2% in observed, CLM, RCA3 and RSM respectively). GEMLAM remains an outlier in the coupling. It still retains four principal components in the summer daytime analysis: PF1 now shows high loadings for CBH (0.87), Temperature (0.87) and SMI (-0.77); PF2 groups the surface fluxes; PF3 still represents the pressure-wind relationship; and PF4 describes specific humidity. In summary, the energy process (PF1) retains the highest explained variance in observations and most models. The drop in summer daytime PF1 variance increases the contribution of other processes (PF2 and PF3) and their coupling with CBH. For instance, although CBH is still coupled with the surface energy process (PF1), it is also moderately coupled with the pressure-wind process (PF3) in observations. All models, except GEMLAM (which couples CBH with temperature and soil moisture), reproduce the observed coupling of CBH with the surface energy balance, but none of them reproduces the moderate coupling between CBH and the pressure-wind process.

The nighttime loadings (Table 4.4b) are different from those of daytime. Here, the pressure-wind relationship breaks down and CBH becomes coupled to wind speed and the surface fluxes (mainly SHF) in observations. The temperature-moisture relationship persists while net radiation and latent heat flux emerge as the dominant variables for PF3. CLM, MRCC and RSM each come up with four principal components all showing different couplings. In general, the total variances explained by the first principal components decrease and those explained by the other principal components increase moderately. The total variances explained by each of the principal components are of comparable magnitude, ranging between 20% and 30% as in the winter case. The observed nighttime loading of CBH in PF1 is 0.64 with CLM, GEMLAM, MRCC, RCA3 and RSM having loadings of 0.09, 0.10, 0.03, 0.35, and

0.32 respectively. Thus we see that as in the winter case, there is no general agreement between the models and observations on which processes influence CBH at nighttime.

In summary, we see that (1) the total variance explained by the energy process is higher in the daytime than in the nighttime; (2) the coupling of CBH with the surface fluxes is stronger in daytime than nighttime; (3) although most models show the nighttime coupling between surface fluxes and wind speed, they do not reproduce the observed moderate coupling these have with CBH. We therefore proceed with the summer daytime case to see the influence of synoptic wind.

4.3.4 The role of synoptic wind on summer daytime couplings

To investigate the influence of synoptic situations on the couplings identified for summer daytime, we further separate summer daytime into weak-wind (< 3.5 ms^{-1}) and strong-wind (> 3.5 ms^{-1}) situations, indicating weak and strong large scale forcings respectively, and compare their PCA loadings. The observed loadings for weak-wind summer daytime (Table 4.5a) are similar to those of summer daytime (Table 4.4a) with a slightly less strong coupling between CBH and the surface fluxes. All the models except MRCC reproduce this coupling in their respective PFs along with a very slight increase in total variance explained when compared with summer daytime loadings. MRCC however returned only two principal components, its PF1 merging both the surface energy process and the temperature-moisture process while its PF2 shows a moderate inverse coupling between surface pressure and soil moisture index. A comparison of weak-wind and strong-wind situations reveal that the coupling between CBH and the energy process (PF1) is slightly stronger in weak-wind situations. GEMLAM and RSM each return four principal components but only GEMLAM fails to reproduce the coupling between CBH and surface energy process. GEMLAM also fails to reproduce the temperature-moisture process in its second principal component as observed and simulated by the other models. There is no significant difference between the total variances explained by each of the three principal components over Cabauw for summer daytime strong and weak wind situations.

This low sensitivity to wind speed could be largely due to the fact that the station is situated in an open and flat arable land with homogeneous characteristics. Thus it

makes little difference whether a rising parcel of air originating in one part of the field reaches condensation over that same part or is moved along in the wind. This is characteristic of Cabauw and may be quite different for other stations situated in non-homogeneous domains or experiencing strong monsoonal climates.

Table 4.2: (a) 3 hourly and (b) daily data PCA loadings for the EOP-3/4 i.e. 10 October 2002 to 30 November 2004 for observed and models. (Significant values from 0.70 and above in red.)

a) Full Period (3-hourly)

Variable	OBSERVED			CLM			GEMLAM			MRCC			RCA3			RSM		
	PF1	PF 2	PF 3	PF1	PF 2	PF 3	PF1	PF 2	PF 3	PF1	PF 2	PF 3	PF1	PF 2	PF 3	PF1	PF 2	PF 3
NTR	**0.96**	0.12	0.04	**0.96**	0.11	0.00	**0.96**	0.16	-0.01	**0.92**	0.25	-0.03	**0.92**	0.23	0.07	**0.95**	0.18	-0.02
SHF	**0.88**	0.08	-0.16	**0.84**	0.06	0.31	**0.83**	0.26	-0.27	**0.89**	0.12	-0.24	**0.83**	0.17	-0.34	**0.87**	0.10	-0.30
LHF	**0.94**	0.15	0.17	**0.9**	0.11	-0.24	**0.90**	0.03	0.21	**0.88**	0.29	-0.05	**0.77**	0.28	0.38	**0.86**	0.30	0.00
LCL	**0.78**	0.17	0.05	**0.85**	0.26	0.06	0.51	0.62	-0.16	**0.80**	0.25	-0.16	0.52	-0.16	-0.10	**0.81**	0.27	0.02
T2M	0.48	**0.82**	0.09	0.44	**0.85**	0.04	0.41	**0.87**	0.06	0.46	**0.86**	-0.06	0.39	**0.86**	0.07	0.42	**0.87**	0.06
QV	0.15	**0.92**	0.05	0.21	**0.90**	0.03	0.19	**0.78**	0.22	0.28	**0.93**	-0.04	0.07	**0.92**	0.10	0.16	**0.93**	0.04
PS	0.15	-0.27	**-0.78**	0.12	-0.18	**0.75**	0.10	-0.15	**-0.80**	0.11	-0.17	**-0.76**	0.18	-0.22	**-0.71**	0.15	-0.22	**-0.77**
VABS	0.20	-0.21	**0.83**	0.09	-0.2	**-0.86**	0.07	-0.10	**0.81**	0.10	-0.33	**0.74**	0.09	-0.23	**0.83**	0.02	-0.31	**0.82**
SMI	-0.01	-0.81	0.04	0.04	-0.76	0.05	0.12	-0.80	0.10	-0.28	-0.05	0.62	0.05	-0.74	0.13	-0.22	-0.80	0.16
Tot. Var(%)	**38.84**	**26.17**	**15.04**	**38.18**	**25.35**	**16.29**	**32.46**	**27.81**	**16.61**	**38.17**	**21.94**	**17.81**	**28.76**	**26.92**	**16.59**	**36.92**	**29.06**	**15.31**

(b) Full Period (Daily)

Variable	OBSERVED			CLM			GEMLAM			MRCC		RCA3			RSM	
	PF1	PF 2	PF 3	PF1	PF 2	PF 3	PF1	PF 2	PF 3	PF1	PF 2	PF1	PF 2	PF 3	PF1	PF 2
NTR	**0.88**	0.24	0.22	**0.93**	0.14	0.21	0.46	**0.83**	0.24	**0.88**	0.35	0.68	0.18	0.60	**0.85**	0.31
SHF	0.60	0.15	0.61	0.61	0.05	0.66	0.58	0.39	0.58	0.65	0.64	0.36	**0.74**	0.41	0.53	**0.73**
LHF	**0.87**	0.18	-0.04	**0.89**	0.08	-0.25	0.05	**0.92**	-0.17	**0.85**	0.31	0.62	-0.35	0.55	**0.85**	0.20
LCL	**0.85**	0.08	0.10	**0.81**	0.23	0.18	**0.73**	0.36	0.23	0.66	0.42	-0.10	0.14	**0.79**	**0.73**	0.17
T2M	0.65	**0.70**	-0.07	0.63	**0.70**	0.08	**0.90**	0.38	-0.02	**0.95**	0.03	**0.94**	-0.01	0.20	**0.94**	-0.03
QV	0.43	**0.82**	-0.08	0.52	**0.75**	0.06	**0.80**	0.28	-0.20	**0.91**	-0.05	**0.94**	-0.05	-0.02	**0.86**	-0.07
PS	0.06	-0.28	**0.73**	-0.03	-0.13	**0.73**	-0.14	-0.05	**0.81**	-0.09	**0.77**	-0.23	**0.70**	0.11	-0.16	**0.77**
VABS	-0.01	-0.21	**-0.88**	-0.05	-0.18	**-0.89**	-0.15	0.02	**-0.83**	-0.21	-0.65	-0.17	**-0.88**	0.10	-0.25	**-0.79**
SMI	-0.02	**-0.88**	-0.09	0.04	**-0.85**	0.03	**-0.85**	0.27	-0.12	-0.22	-0.67	-0.70	-0.19	0.14	-0.75	-0.20
Tot. Var(%)	**35.74**	**24.21**	**19.44**	**37.42**	**21.19**	**21.14**	**36.61**	**23.63**	**20.89**	**0.88**	**0.35**	**0.68**	**0.18**	**0.60**	**0.85**	**0.31**

Table 4.3: (a) November-March (winter) and (b) April-September (summer) PCA loadings for the EOP-3/4 period for observed and models. (Significant values from 0.70 and above in red.)

(a) Winter (NDJFM)

Variable	OBSERVED			CLM			GEMLAM				MRCC			RCA3			RSM		
	PF1	PF 2	PF 3	PF1	PF 2	PF 3	PF1	PF 2	PF 3	PF4	PF1	PF 2	PF 3	PF1	PF 2	PF 3	PF1	PF 2	PF 3
NTR	**0.92**	0.14	-0.16	**0.82**	0.32	0.31	0.32	0.65	0.54	0.30	**0.80**	0.36	-0.10	0.07	0.02	**0.94**	**0.87**	0.21	0.03
SHF	**0.71**	0.02	-0.57	0.43	0.13	**0.78**	-0.04	0.23	**0.91**	0.12	0.68	-0.11	-0.56	-0.64	0.16	0.67	**0.76**	-0.01	-0.49
LHF	**0.91**	0.05	0.18	**0.92**	-0.02	-0.26	0.14	**0.86**	-0.01	0.32	**0.92**	-0.03	-0.19	0.69	0.10	0.49	**0.70**	0.01	-0.29
LCL	**0.75**	-0.19	0.15	**0.83**	-0.19	-0.04	-0.10	**0.84**	0.00	-0.32	**0.88**	0.02	0.16	0.07	0.51	0.14	**0.88**	0.04	0.18
T2M	0.45	**0.73**	0.36	0.17	**0.94**	-0.02	**0.89**	0.26	-0.02	-0.23	0.21	**0.95**	0.09	0.34	**-0.71**	0.47	0.29	**0.92**	0.07
QV	0.08	**0.87**	0.33	-0.05	**0.97**	-0.04	**0.96**	-0.01	-0.05	-0.13	0.06	**0.96**	0.06	0.30	**-0.86**	0.21	-0.04	**0.97**	0.01
PS	0.09	-0.17	-0.63	-0.03	-0.37	0.58	-0.56	0.14	0.41	-0.30	0.16	-0.20	-0.63	-0.55	0.34	0.03	0.19	-0.43	-0.53
VABS	0.20	0.05	**0.83**	0.29	0.04	**-0.82**	0.23	0.42	**-0.79**	0.16	0.11	-0.04	**0.90**	**0.88**	0.06	-0.02	0.07	0.08	**0.86**
SMI	0.25	-0.69	0.13	0.30	-0.40	0.14	-0.20	0.07	0.02	**0.84**	-0.30	0.49	0.42	0.06	0.58	0.13	-0.17	-0.40	0.51
Tot. Var(%)	**34.01**	**20.61**	**19.44**	**28.99**	**25.26**	**19.93**	**24.97**	**24.42**	**21.49**	**13.32**	**32.45**	**24.95**	**19.63**	**24.38**	**22.20**	**20.91**	**30.48**	**24.36**	**18.09**

(b) Summer (MJJAS)

Variable	OBSERVED			CLM			GEMLAM				MRCC			RCA3			RSM		
	PF1	PF 2	PF 3	PF1	PF 2	PF 3	PF1	PF 2	PF 3	PF4	PF1	PF 2	PF 3	PF1	PF 2	PF 3	PF1	PF 2	PF 3
NTR	**0.96**	0.01	0.04	**0.98**	0.03	0.05	**0.97**	0.12	0.01	0.07	**0.94**	0.19	0.00	**0.94**	0.09	0.15	**0.97**	0.12	0.00
SHF	**0.88**	-0.04	-0.06	**0.91**	0.01	-0.15	**0.84**	0.28	-0.09	0.07	**0.91**	0.07	-0.14	**0.91**	-0.04	-0.12	**0.92**	-0.01	0.17
LHF	**0.95**	-0.02	0.14	**0.91**	-0.01	0.23	**0.91**	-0.09	0.13	0.03	**0.90**	0.23	0.04	**0.79**	0.15	0.39	**0.90**	0.20	-0.13
LCL	**0.82**	0.14	0.03	**0.88**	0.18	-0.09	0.41	**0.80**	0.02	-0.23	**0.86**	0.16	-0.13	**0.87**	-0.02	-0.13	**0.82**	0.15	-0.07
T2M	0.59	**0.73**	0.11	0.54	**0.81**	-0.07	0.44	**0.79**	0.03	0.29	0.63	**0.72**	-0.03	0.59	**0.75**	-0.11	0.48	**0.85**	0.03
QV	-0.05	**0.89**	0.13	0.06	**0.92**	0.01	0.12	0.09	0.04	**0.96**	0.30	**0.90**	0.04	-0.07	**0.95**	0.00	0.02	**0.97**	0.08
PS	0.18	-0.14	**-0.87**	0.14	-0.07	**-0.81**	0.08	0.15	**-0.77**	-0.28	0.07	-0.01	**-0.77**	0.22	-0.35	**-0.73**	0.15	-0.20	**0.78**
VABS	0.35	-0.15	**0.76**	0.15	-0.17	**0.81**	0.10	0.07	**0.83**	-0.18	0.15	-0.42	**0.72**	0.20	-0.09	0.69	0.06	-0.15	**-0.79**
SMI	0.03	-0.62	0.12	0.09	-0.63	0.06	0.26	**-0.80**	0.11	-0.11	-0.22	0.33	0.64	-0.02	-0.36	0.55	-0.05	0.06	0.38
Tot. Var(%)	**42.11**	**19.71**	**15.46**	**41.4**	**21.9**	**15.78**	**32.79**	**22.72**	**14.63**	**13.27**	**42.44**	**19.39**	**17.38**	**39.2**	**19.59**	**17.04**	**38.99**	**20.18**	**16.12**

Table 4. 4: PCA loadings for (a) summer daytime and (b) summer nighttime, observed and models.(Significant values from 0.70 and above in red.)

(a) Daytime (Summer)

Variable	OBSERVED			CLM			GEMLAM				MRCC			RCA3			RSM		
	PF1	PF 2	PF 3	PF1	PF 2	PF 3	PF1	PF 2	PF 3	PF4	PF1	PF 2	PF 3	PF1	PF 2	PF 3	PF1	PF 2	PF 3
NTR	**0.96**	0.00	0.00	**0.97**	0.01	0.02	0.22	**0.94**	0.14	0.06	**0.93**	0.20	0.09	**0.92**	0.08	0.17	**0.96**	0.07	0.00
SHF	**0.86**	-0.09	-0.07	**0.89**	-0.03	0.20	0.53	0.61	0.13	0.04	**0.90**	0.02	0.25	**0.91**	-0.11	-0.07	**0.87**	-0.16	0.22
LHF	**0.93**	-0.02	-0.10	**0.87**	-0.06	-0.21	-0.18	**0.90**	-0.02	0.03	**0.84**	0.31	-0.04	0.62	0.32	0.53	**0.81**	0.28	-0.19
LCL	0.58	0.21	0.40	**0.81**	0.19	0.25	**0.87**	0.16	0.10	-0.22	**0.75**	0.22	0.31	**0.82**	-0.14	-0.34	**0.80**	0.07	0.10
T2M	0.33	**0.87**	0.20	0.50	**0.84**	0.14	**0.87**	0.20	0.11	0.28	0.55	**0.77**	0.10	0.51	**0.72**	-0.38	0.35	**0.90**	0.14
QV	-0.12	**0.86**	-0.13	0.03	**0.92**	-0.04	0.03	0.08	-0.01	**0.97**	0.23	**0.92**	-0.09	-0.18	**0.94**	-0.11	-0.12	**0.96**	0.07
PS	0.11	-0.20	**0.81**	0.19	-0.09	**0.81**	0.14	0.08	**0.77**	-0.27	0.12	0.06	**0.72**	0.32	-0.39	-0.59	0.17	-0.15	**0.79**
VABS	0.20	-0.18	**-0.79**	0.07	-0.28	**-0.77**	-0.05	-0.04	**-0.83**	-0.23	0.04	-0.54	-0.62	0.01	-0.20	0.56	-0.14	-0.32	**-0.74**
SMI	0.07	-0.54	0.00	0.14	-0.56	-0.12	**-0.77**	0.43	-0.06	-0.03	-0.20	0.15	**-0.71**	0.01	-0.16	**0.70**	-0.09	0.06	0.40
Tot. Var(%)	**33.82**	**21.36**	**16.79**	**38.36**	**22.15**	**16.00**	**27.82**	**25.95**	**14.81**	**13.23**	**37.41**	**21.71**	**17.77**	**34.70**	**19.52**	**19.29**	**35.31**	**21.97**	**16.19**

(b) Nighttime (Summer)

Variable	OBSERVED			CLM				GEMLAM			MRCC				RCA3			RSM			
	PF1	PF 2	PF 3	PF1	P2	PF 3	PF 4	PF1	PF 2	PF 3	PF1	PF2	PF 3	PF 4	PF1	PF 2	PF 3	PF1	PF2	PF 3	PF 4
NTR	-0.14	0.02	**0.97**	0.14	0.02	0.06	**0.94**	0.26	-0.25	**0.75**	0.13	0.44	0.16	**0.76**	0.16	0.32	0.66	-0.08	0.23	**0.90**	0.00
SHF	**-0.84**	0.05	0.42	-0.68	0.13	-0.20	0.62	-0.60	-0.30	0.64	-0.08	**0.81**	-0.32	0.26	**-0.91**	0.05	0.09	**-0.92**	0.00	0.27	-0.01
LHF	0.50	-0.11	**0.76**	**0.79**	-0.19	0.45	0.24	**0.86**	-0.11	0.15	0.07	-0.24	-0.01	**0.86**	**0.84**	0.04	0.21	**0.72**	0.06	0.57	0.07
LCL	0.64	0.24	-0.03	0.10	0.16	**0.83**	0.11	0.15	**0.72**	-0.40	0.24	**-0.78**	-0.19	0.32	0.35	0.16	-0.69	0.34	0.51	-0.13	-0.44
T2M	0.29	**0.91**	0.09	-0.08	**0.95**	0.22	0.07	0.12	**0.94**	0.14	**0.95**	-0.22	0.01	0.16	0.10	**0.96**	-0.10	0.06	**0.98**	0.13	-0.05
QV	0.00	**0.93**	0.13	-0.08	**0.97**	-0.02	0.05	0.00	0.46	**0.73**	**0.98**	0.03	0.06	0.03	-0.09	**0.91**	0.28	-0.12	**0.86**	0.22	0.15
PS	-0.51	-0.17	-0.20	-0.60	-0.22	0.49	-0.18	-0.55	0.04	-0.38	-0.05	0.05	**-0.77**	0.05	-0.42	-0.20	-0.52	-0.38	-0.05	-0.48	0.27
VABS	**0.85**	-0.11	0.19	**0.91**	-0.07	-0.03	-0.02	**0.87**	0.07	-0.13	-0.26	-0.43	**0.70**	0.19	**0.95**	-0.03	-0.01	**0.89**	0.01	0.23	-0.06
SMI	0.02	-0.53	0.21	-0.04	-0.49	-0.55	0.27	0.19	-0.65	0.03	0.22	0.42	0.65	0.11	0.10	-0.44	0.51	0.05	0.06	-0.10	**0.90**
Tot. Var(%)	**27.15**	**23.35**	**20.34**	**25.61**	**24.54**	**17.08**	**16.11**	**25.56**	**24.67**	**20.81**	**22.94**	**21.24**	**18.46**	**17.36**	**30.81**	**23.35**	**17.51**	**27.07**	**22.65**	**17.53**	**12.31**

Table 4. 5: PCA loadings for (a) summer weak-wind (WSP < 3ms^{-2}) and (b) summer strong-wind period ((WSP > 3ms^{-2}), observed and models.

(a) Weak-wind (Summer Daytime)

Variable	OBSERVED			CLM			GEMLAM			MRCC			RCA3			RSM		
	PF1	PF 2	PF 3	PF1	PF 2	PF 3	PF1	PF 2	PF 3	PF1	PF 2	PF 3	PF1	PF 2	PF 3	PF1	PF 2	PF 3
NTR	**0.96**	-0.01	0.00	**0.96**	0.10	-0.03	**0.98**	0.03	0.00	**0.86**	0.39		**0.93**	-0.06	0.07	**0.97**	0.11	0.09
SHF	**0.86**	-0.07	-0.16	**0.94**	0.00	-0.02	**0.75**	0.34	-0.19	**0.72**	0.55		**0.91**	-0.17	-0.13	**0.88**	-0.16	0.13
LHF	**0.96**	-0.04	0.05	**0.92**	0.14	0.02	**0.82**	-0.24	0.26	**0.91**	0.19		**0.79**	0.21	0.39	**0.88**	0.30	0.05
LCL	0.58	0.24	0.22	**0.79**	0.17	0.30	0.16	**0.89**	-0.01	**0.85**	0.14		**0.80**	-0.07	-0.47	**0.87**	0.00	-0.04
T2M	0.35	**0.85**	0.26	0.48	**0.84**	0.08	0.28	**0.84**	0.37	**0.91**	-0.31		0.52	**0.80**	-0.15	0.39	**0.87**	0.11
QV	-0.10	**0.83**	0.14	0.03	**0.94**	-0.16	0.20	-0.06	**0.72**	**0.73**	-0.56		-0.12	**0.92**	0.24	-0.12	**0.96**	0.11
PS	0.18	-0.07	**-0.78**	0.19	-0.18	**0.79**	0.19	0.03	**-0.75**	0.00	0.60		0.16	-0.17	-0.69	0.12	-0.34	0.69
VABS	0.10	0.09	0.49	-0.02	-0.25	-0.06	0.04	-0.24	0.17	-0.03	-0.09		0.09	-0.44	0.06	0.00	-0.19	-0.49
SMI	0.15	-0.61	0.49	0.12	-0.40	**-0.77**	0.27	**-0.79**	0.30	-0.02	-0.58		0.17	-0.25	**0.80**	0.04	0.16	**0.72**
Tot. Var(%)	**34.83**	**20.57**	**13.91**	**39.53**	**21.19**	**14.88**	**27.29**	**26.28**	**16.06**	**46.17**	**18.06**		**36.70**	**20.45**	**17.72**	**38.11**	**22.05**	**14.19**

(b) Strong-wind (Summer Daytime)

Variable	OBSERVED			CLM			GEMLAM				MRCC			RCA3			RSM			
	PF1	PF 2	PF 3	PF1	PF 2	PF 3	PF1	PF 2	PF 3	PF4	PF1	PF 2	PF 3	PF1	PF 2	PF 3	PF1	PF 2	PF3	PF 4
NTR	**0.96**	0.02	0.02	**0.97**	0.01	0.06	0.28	**0.92**	0.15	0.07	**0.94**	0.20	0.09	**0.94**	0.04	0.14	**0.97**	0.04	0.04	0.03
SHF	**0.87**	-0.07	-0.05	**0.88**	-0.02	0.25	0.58	0.56	0.14	0.08	**0.88**	0.04	0.30	**0.90**	-0.04	-0.21	**0.83**	-0.17	0.33	-0.08
LHF	**0.92**	0.01	-0.09	**0.86**	-0.08	-0.21	-0.15	**0.91**	0.03	0.00	**0.85**	0.29	-0.05	0.60	0.05	0.61	**0.84**	0.28	-0.23	0.13
LCL	0.57	0.19	0.48	**0.81**	0.19	0.28	**0.88**	0.14	0.11	-0.24	**0.71**	0.22	0.42	**0.75**	0.10	-0.45	**0.71**	0.07	0.24	-0.33
T2M	0.31	**0.87**	0.25	0.51	**0.83**	0.13	**0.88**	0.16	0.13	0.25	0.54	**0.77**	0.14	0.49	**0.82**	-0.16	0.31	**0.91**	0.15	-0.11
QV	-0.13	**0.86**	-0.14	0.04	**0.91**	-0.07	0.06	0.05	0.02	**0.96**	0.23	**0.92**	-0.13	-0.18	**0.86**	0.28	-0.12	**0.96**	-0.01	0.07
PS	0.12	-0.27	**0.78**	0.20	-0.09	**0.79**	0.18	0.06	**0.77**	-0.26	0.12	0.07	0.69	0.35	-0.24	-0.67	0.13	-0.12	**0.75**	0.24
VABS	0.26	-0.18	**-0.76**	0.02	-0.22	**-0.79**	-0.04	-0.10	**-0.79**	-0.28	0.00	-0.56	-0.54	-0.02	-0.14	0.52	-0.04	-0.29	**-0.81**	0.17
SMI	0.03	-0.56	0.03	0.19	-0.64	-0.13	**-0.75**	0.47	-0.05	-0.09	-0.16	0.10	**-0.75**	0.01	-0.63	0.45	-0.06	0.00	0.07	**0.93**
Tot. Var(%)	**33.79**	**21.63**	**16.60**	**38.30**	**22.43**	**16.40**	**28.71**	**25.48**	**14.45**	**13.43**	**36.37**	**21.61**	**18.25**	**33.46**	**20.93**	**18.43**	**33.12**	**21.82**	**16.28**	**12.19**

Figure 4.4 compares correlation coefficients between CBH and surface variables in summer daytime (a) weak-wind and (b) strong-wind conditions. Under weak-wind conditions, all models except GEMLAM have a stronger than observed coupling.

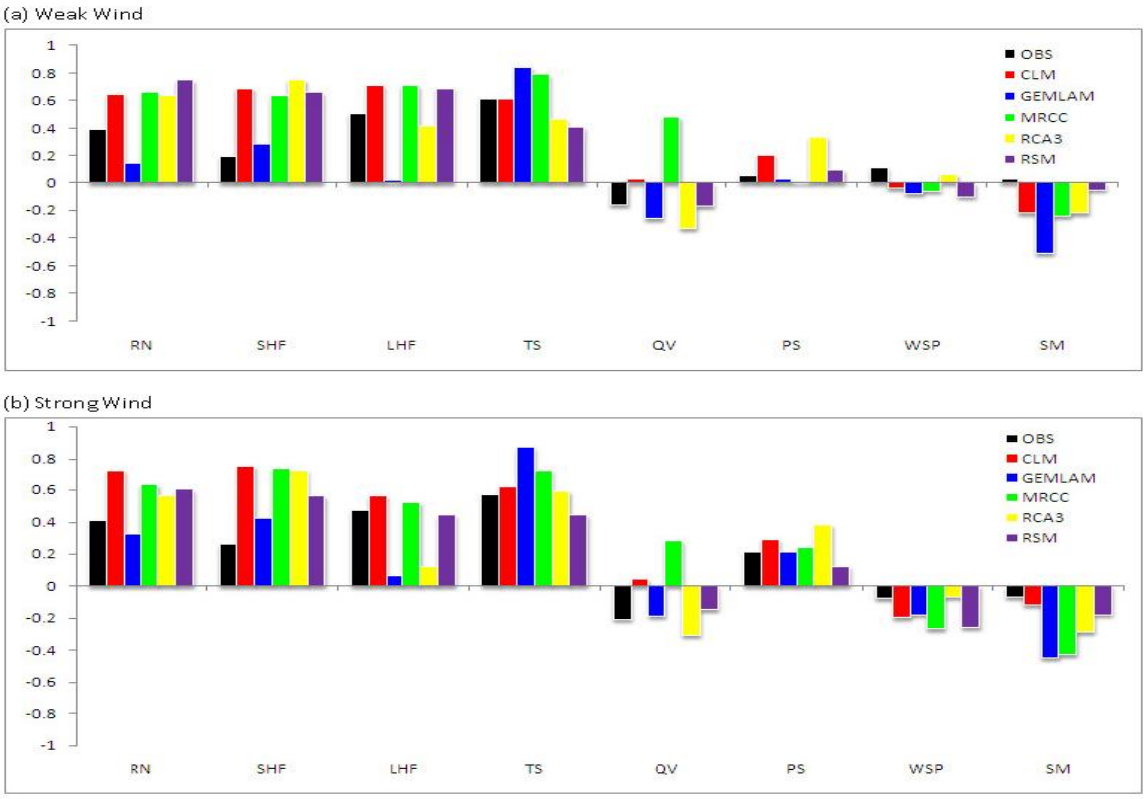

Figure 4.4: Correlation coefficients between the CBH and net surface total radiation (R_N), sensible heat flux, latent heat flux, surface temperature (T_S, 2m), surface specific moisture (QV, 2m), soil moisture (SI), surface pressure (P_S) and wind speed (WSP, 10 m) for summer daytime (a) weak wind (b) strong wind cases in observed (OBS) and models (CLM, GEMLAM, MRCC, RCA3 and RSM) data over Cabauw.

GEMLAM does poorly here, failing to reproduce the observed relationship although it does rather well under strong (WSP > 3 ms^{-2}) wind conditions. The observed SHF (LHF) is weakly (strongly) coupled to the CBH in weak-wind situations. All the models capture the sign of this relationship but with varying magnitudes; CLM and MRCC reproduce

high, nearly equal SHF-CBH and LHF-CBH couplings. SHF is seen to be more strongly coupled to CBH than LHF in both RCA3 and RSM while GEMLAM shows no coupling between LHF and CBH in windless conditions. Under strong-wind conditions, the coupling of CBH with the net surface radiation, surface heat fluxes and temperature slightly increase in observed and models.

4.4 Conclusions

In this chapter, we have used observed and model data to study the coupling of cloud base height with the surface fluxes and other variables over Cabauw. We set out to investigate how well the models reproduce observed processes, which we did in part by looking at the couplings among these processes. We looked at the models' ability in reproducing each of the variables over the stations and then used PCA analysis to see how the processes are coupled. The PCA helped to identify the processes that couple the variables and to compare the coupling strengths in observation and models. Thus our interest has been not only in how well the models simulate certain fields, but also how well they simulate the physical processes linking these fields.

The models give reliable simulations of CBH and surface variables, though with different skills. CLM and RCA3 give the best simulation of the variables (i.e. CBH, surface fluxes, temperature, moisture, and wind). We note that these are the only two European models in the suite of five models applied over this European reference site. All the models (except CLM) underestimate soil moisture. GEMLAM also underestimates specific humidity, but overestimates sensible heat flux, temperature and CBH. MRCC underestimates temperature and CBH, but overestimates specific humidity. RSM shows the least overall performance of the five-model suite, and overestimates the surface fluxes because it uses a wrong surface albedo value. Taylor diagrams of correlation and standard deviations show that the CLM simulation of surface fluxes is nearest to observation for

Cabauw and agrees with the slight 'home advantage' effect of RCMs as reported in the findings of Takle et al. (2007).

The principal component analysis identified three processes that couple CBH with surface variables in the observed and model data: surface energy balance (i.e. surface fluxes), thermodynamics (i.e. temperature and moisture), and dynamic (i.e. surface pressure and wind speed) processes. The coupling between CBH and the surface fluxes is stronger in summer than winter, and in summer daytime than summer nighttime. However, this study found that wind speed has no significant influence on the coupling of CBH with surface fluxes over Cabauw, possibly because of the surface homogeneity of the station or that the synoptic winds are not strong enough in summer. We find that the models (generally) give the right relationships between fields, i.e., they appear to be simulating the physical couplings correctly. RCMs are prone to two main types of systematic errors, those arising from errors in forcing from the lateral boundary conditions (LBCs) and those intrinsic to the internal formulation of a given model (Risbey and Stone, 1996; Noguer et al., 1998; Menéndez et al., 2001; Misra et al., 2003). A study by Christensen et al. (1998) indicates that increasing model resolution amplifies the influence the systematic errors in the LBC have on the evolution of the simulated regional climate. To facilitate focus on sources of internal error, we constrained all the models to use the same LBC and horizontal resolution. These internal errors, such as incorrect prescribed parameters (e.g. the albedo case in RSM) could be responsible for isolated cases where observed couplings between fields are not well reproduced.

With the physics of simulating CBH being well reproduced in the models as exhibited by the Cabauw analysis, this raises the question of how well the models will perform when placed in a different environment without recalibration or retuning, i.e., how well do they transfer? The next chapter attempts to answer this very question.

Chapter 5

Transferability intercomparison

5.1 Introduction

Clouds play essential roles in the climate system. They significantly affect the energy budget in the Earth-atmosphere system. Cloud base height (CBH), in particular, influences the longwave radiation budget at the surface, hence the surface energy balance (Kiehl and Trenberth, 1997). As a feedback, the surface energy balance modulates the spatial and temporal distribution of CBH. The interaction between surface processes and cloud properties, such as CBH, are complex and not well known; and that constitutes one of the largest uncertainties in simulating climate change, because most climate models struggle to adequately capture the feedback (Cess et al., 1989; Cess et al., 1996; Houghton et al., 2001; Randall et al., 2003; Arakawa, 2004). To improve our understanding of the interactions, and consequently reduce uncertainties in simulating future climate, there is need to assess how models (both GCM and RCMs) reproduce the interaction under various atmospheric and geographical conditions (Takle et al., 2007).

The present study is geared in that direction. In the previous chapter, we considered a guiding hypothesis that "for non-monsoonal domains experiencing weak large scale forcing, day time surface energy fluxes are correlated to the cloud base height". We used the transferability experiment data over Cabauw, a homogenous non-monsoon station, to study the relationship between CBH and surface fluxes under different atmospheric conditions, and found a good correlation between the CBH and surface energy fluxes in all the models as in the observation. However, the magnitude of the correlation varied from model to model and with season; but did not vary with wind speed as suggested by the hypothesis. We attributed that to the homogenous surface characteristic of Cabauw. In this chapter, we investigate whether this hypothesis holds over other domains experienc-

ing weak large-scale forcing but with different climate and geographical settings from Cabauw.

5.2 Observed and modeled variables

Simulated seasonal and diurnal cycles of surface meteorological variables are compared with observations at station level and their Taylor diagrams (Taylor, 2001) presented. Taylor diagrams provide a way of graphically summarizing how closely a pattern (or a set of patterns) matches observations. The similarities or differences between patterns are quantified in terms of their correlation, root-mean-square difference and the amplitude of their variations (represented by their standard deviations). Taylor diagrams are useful for investigating multiple aspects of complex models or in evaluating the relative skill of several different models. The Taylor diagrams (using three hourly summer daytime data) of correlations and standard deviations between observations and models are discussed along with the seasonal and diurnal variations.

Figures 5.1 to 5.8 show the seasonal and diurnal variations observed at twelve CEOP reference stations with those simulated by our suite of five regional models and with Taylor plots of the summer daytime period at each station.

5.2.1 Net radiation

The observed seasonal variation of R_{net} over the stations exhibits two distinct patterns (Figure 5.1). The first pattern shows a widely varying R_{net} (from about -20 Wm^{-2} in winter to 200 Wm^{-2} in summer) over the midlatitude stations (Lindenberg, Cabauw, Lamont, Bondville, BERMS, Mongolia and Tongyu). The second pattern shows a weakly varying R_{net} (from 120 Wm^{-2} in winter to 180 Wm^{-2} in summer) over the tropical stations (Manaus, Chao Praya River and N.E. Thailand). The models successfully simulate the two patterns of R_{net}, but show different amplitude of errors in reproducing the actual values over the stations. The errors are less than 35 Wm^{-2} over most stations, but up to 50 Wm^{-2} in CLM (over BERMS and Santarem), in GEMLAM (over Himalayas and Santarem), in

MRCC (over Chao Praya River and Santarem), in RCA3 (over Santarem and Himalayas), and in RSM (over all the stations). In reproducing the diurnal cycle, all the models overestimate summer daytime R_{net} over the Southern Hemisphere (SH) stations Manaus and Santarem, but underestimate (overestimate) it in the morning (late afternoon) hours over the remaining stations. Part of the errors in the diurnal cycle of net radiation (especially for the Southern Hemisphere stations) may be due to excessive downward shortwave flux which results from the models underestimating daytime cloud cover during tropical convection. Underestimation of surface albedo, as in the case of RSM would not seem to be a major factor here in a tropical forest with typical low albedo values (see Shuttleworth and Dickinson, 1989). More importantly, the fact that all models show a consistent pattern of error in the diurnal cycle, albeit to varying degrees, suggests a carried over error in the forcing fields whereby more moisture is made available for evaporation in the day and less at night. In general, the correlation between observed and simulated R_{net} is high, ranging between r = 0.7 and r = 0.9. All the models show the highest correlation with observation over Chao Praya River and the lowest over Santarem. In CLM, the normalized standard deviations (NSDs) over the stations are very close, ranging between 0.8 and 1.2; in GEMLAM Himalayas and Santarem are outliers (NSDs are 0.6 and 1.4, respectively); but in MRCC, RCA3 and RSM, only Santarem is an outlier. Hence, in simulating R_{net}, CLM and RCA3 show the best transferability over the stations, because the two models have the least errors in the seasonal and diurnal cycles and the stations cluster together best in the Taylor diagram of CLM and RCA3. In these regards, RSM performs worst.

5.2.2 Sensible and latent heat fluxes

The midlatitude and tropical seasonal patterns are present in the observed SHF and the models capture this with varying magnitudes of error (Figure 5.2). Errors in simulating the seasonal cycle of SHF are generally below 40 Wm^{-2} at most stations for all models but up to 80 Wm^{-2} over North America (BERMS) for CLM, MRCC and RSM, and up to 70 Wm^{-2} for RCA3 over South America stations (Manaus and Santarem). These errors are propagated probably because of errors in net radiation over the respective stations in

the affected models. CLM, MRCC and RCA3 all reproduce the seasonal cycle of SHF best over Europe (Cabauw and Lindenberg) while RSM gives its best result over South America (Manaus), all with errors below 20 Wm^{-2}. Model errors in the diurnal cycle of SHF generally reach peak values around mid afternoon for all stations. CLM keeps most station errors confined below 50 Wm^{-2} while the other models have station errors within a 100 Wm^{-2} range from the observed values. Most models however struggle with reproducing the diurnal SHF cycle over South America (Santarem and Manaus) with errors ranging from about 250 Wm^{-2} (in RCA3) to 480 Wm^{-2} (in MRCC) at Santarem. The Taylor diagrams show an alignment of stations along similar correlation bands in each model but with different range of NSD going from one model to the other. RSM exhibits the greatest scatter of stations with regards to NSD, indicating it as the least transferable of all the models when simulating SHF.

The seasonal cycle of LHF is well simulated by CLM where only two stations have errors reaching 40 Wm^{-2}. The models also struggle with reproducing the LHF seasonal cycle over South America domains with errors at Santarem ranging from 50 Wm^{-2} (MRCC) to 140 Wm^{-2} (RCA3). In the diurnal cycle of LHF, errors are even more pronounced in all models for the South American domains. Amplitude of errors in LHF at Manaus range from 250 Wm^{-2} (RCA3) to 450 Wm^{-2} (RSM) and at Santarem from 100 Wm^{-2} (GEMLAM) to 350 Wm^{-2} (CLM). Strangely, CLM, GEMLAM and RCA3 show distinct underestimation errors of between 100 Wm^{-2} to 150 Wm^{-2} over Lamont in the North American domain contrary to the general trend. There is a tendency for the models to underestimate LHF values in the morning and overestimate them in the afternoon. The Taylor diagram shows a clustering of stations in CLM (with a correlation of between 0.6 and 0.85). There is no distinct clustering of stations for the other models while RSM has the most scattered stations of all the models. Again, in simulating LHF, CLM transfers best across the four ICTS domains while RSM transfers worst.

5.2.3 Temperature

The seasonal and diurnal cycle of temperature across the stations show a clearer picture of the variations described above. The observed seasonal temperature profile, like the seasonal net radiation profile, shows distinctive patterns for stations based on their latitudes. But unlike net radiation, three patterns are evident: First, tropical stations with mean annual temperature range of 15 to 30 °C (Chao Praya River, N. E. Thailand, Manaus and Santarem); second, midlatitude stations with a mean annual temperature range of -5 to 25 °C (Lindenberg, Cabauw, Lamont, Bondville) and third, high altitude midlatitude stations having a mean annual temperature range of -20 to 25 °C (BERMS, Tongyu, Mongolia, Himalayas). The mean diurnal pattern is similar for all stations, with peak temperatures in the late afternoon.

All the models reproduce the observed seasonal and diurnal patterns but with different amplitudes of error over the stations. The models give a range of errors on the average of about -/+ 5 °C over the stations except for Santarem in CLM (20 °C) and MRCC (8 °C), Santarem and Manaus in RCA3 (10 °C) and Tongyu in RSM (10 °C). In the diurnal cycle, CLM shows high errors over high altitude stations (about 8 °C and 20 °C for Mongolia and Himalayas respectively) possibly because the corresponding model grid points are lower than the actual station heights. However, the model simulates both diurnal and seasonal variations well (within a +/- 2 °C error range) over the remaining stations. Diurnal cycle errors over all stations are within -2 and 8 °C in GEMLAM, -5 and 10 °C in MRCC, -1 and 6 °C in RCA3 and -/+ 5 °C in RSM.

The temperature Taylor diagrams for all models shows over half the stations clustering about NSD = 1 with high correlations ($r < 0.9$) while five stations (Santarem, Manaus, Himalayas, Chao Praya River and N. E. Thailand) remain scattered throughout with NSD and correlations varying from one model to the other.

5.2.4 Specific humidity

The observed seasonal cycle of specific humidity (Q_v) also separates the stations into three groups. The specific humidity varies between 16 and 20 gkg^{-1} in the first group (Santarem and Manaus), 8 and 20 gkg^{-1} in the second group (Chao Praya River and N. E. Thailand), but 0 and 16.0 gkg^{-1} in the third (other stations). In this case GEMLAM shows the best result. The maximum error (in diurnal and seasonal simulation over all the stations) is about 3 gkg^{-1} in GEMLAM (N. E. Thailand), 4 gkg^{-1} in RCA3 (N. E. Thailand), 5 gkg^{-1} in RSM (Lamont), 6 gkg^{-1} RCM (at Himalaya), and 10 gkg^{-1} in MRCC (Lamont). In the Taylor diagrams, all the models produce plots with larger errors for the South American stations; however, the plots are best clustered in GEMLAM. Hence, GEMLAM shows the best transferability in simulating specific humidity over the stations.

5.2.5 Surface Pressure (hPa)

The range of observed seasonal cycle of surface pressure (PS) varies from about 555 hPa at the high altitude station Himalayas to just under 1020 hPa at Cabauw. PS varies little over most stations all year round except for Tongyu where there is a drop of about 20 hPa in summer. The models capture both the seasonal and diurnal patterns well over most stations. However, all models except RSM have a problem with simulating PS over Himalayas. CLM overestimates the seasonal cycle of pressure over Himalayas by a peak error of 300 hPa, GEMLAM (50 hPa), MRCC (80 hPa) and RCA3 (75 hPa). These errors probably indicate the models' grid point elevations corresponding to the station coordinates are much lower than the actual station height. The diurnal cycle of pressure is constant over midlatitude stations Lindenberg, Cabauw and BERMS while a slight increase (< 4 hPa) is observed over tropical stations (Chao Praya River, N.E. Thailand, Manaus and Santarem) in the midafternoon. The diurnal cycles of pressure for all models reflect the biases already seen in their respective seasonal cycles. The Taylor diagrams for all models show a high correlation (average of r = 0.9) between observed and simulated pressure for most stations and also well reproduced normalized standard distributions.

Generally, lower correlations and overestimations of model NSD occur for the two South American stations Santarem and Manaus.

5.2.6 Wind speed

The observed seasonal cycle of wind speed at 10 m (WSP) varies from station to station with an average of 1 ms^{-1} all year round over the two South American sites Santarem and Manaus to a peak of above 8 ms^{-1} in May over Himalayas. The models reproduce this with errors within +/- 2 ms^{-1} for most stations; however, some models reproduce much higher errors in a few stations. The performance of CLM in simulating wind speed over Europe is very good all year round, especially at Lindenberg but poorer over the tropical station N.E. Thailand with peak error above 3 ms^{-1} in winter. GEMLAM wind speed peak error is also up to 4 ms^{-1} in winter over N. E. Thailand. In MRCC, errors over the Himalayas are in excess of 8 ms^{-2} in winter while in RCA3 and RSM, WSP is overestimated to a peak of about 4 ms^{-1} and 6 ms^{-1} at the same station in early summer. The diurnal cycle over all stations shows wind speeds picking up in the afternoon and dropping by nightfall. Diurnal WSP varies from 1 ms^{-1} over tropical Chao Praya River to 8 ms^{-1} over midlatitude Lamont. In the models, CLM's diurnal cycle of WSP ranges from a peak underestimation error of 1.5 ms^{-1} at Lamont to a peak overestimation error of 2.2 ms^{-1} over Chao Praya River. GEMLAM overestimates diurnal WSP the most over Santarem by just above 2 ms^{-1} and underestimates it most (2.2 ms^{-1}) at noon over Himalayas. MRCC, RCA3 and RSM all overestimate diurnal WSP over Himalayas with peak errors of 3.5 ms^{-1}, 4.0 ms^{-1} and 6.8 ms^{-1} respectively. They also underestimate diurnal WSP most over Lamont with peak errors of 1.0 ms^{-1}, 2.0 ms^{-1} and 4.0 ms^{-1} respectively. The Taylor diagrams show that WSP is generally not well captured by the models as most stations have a correlation of $r < 0.6$ in CLM, GEMLAM, MRCC, RCA3 and RSM. The stations also fail to cluster about a particular NSD in most models although CLM exhibits a minor cluster about NSD = 0.8 of observed.

5.2.7 Cloud base height (m)

The highest peaks (above 1600 m) in the observed seasonal cycle of CBH are found over the tropical (Chao Praya River and N. E. Thailand) and subtropical (Mongolia and Tongyu) stations of the Asian domain. The remaining stations fall within a peak CBH range of 400 m (at BERMS) to 1200 m (at Santarem). In the models, the seasonal cycle of CBH is reproduced with errors within 500 m at most stations. CLM reproduces the seasonal cycle of CBH over the European and North American midlatitude stations of Lamont, Lindenberg, Cabauw and Bondville and tropical station Manaus, with less than 500 m error. However CBH is overestimated by a peak error of 1800 m over Himalayas in April and by 1000 m all summer over Mongolia. GEMLAM over predicts CBH at most stations in summer with the highest errors of about 1500 m over Mongolia and Lamont. MRCC overestimates CBH over Mongolia throughout the seasonal cycle to a maximum of about 1200 m in summer. RCA3 poorly simulates the seasonal cycle of CBH at some Asian and tropical sites with peak errors over 2000 m (at Tongyu, Mongolia and Manaus). RSM appears to capture the seasonal cycle of CBH well over Europe and North America (Lindenberg, Cabauw, Bondville and Lamont); nowhere over these stations do errors exceed 200 m. However errors are much higher (up to 1000 m) for Himalayas and N. E. Thailand. In the diurnal cycle of CBH, CLM has highest station error of about 700 m over N. E. Thailand where CBH is underestimated in the afternoon. GEMLAM produces a good diurnal cycle over tropical stations N.E. Thailand and Chao Praya River but with peak errors ranging from 1000 m at BERMS and Tongyu to 2600 m at Santarem. MRCC reproduces a very good diurnal cycle over Bondville while its highest errors are over Mongolia (1000 m), Manaus (1250 m) and Santarem (2200 m). RCA3 grossly overestimates the diurnal cycle of CBH with peak errors of 2750 and 3500 m at the South American stations Manaus and Santarem respectively. It reproduces the diurnal cycle well (errors < 100 m) over Cabauw and BERMS. RSM overestimates the diurnal cycle of CBH over Manaus, Himalayas and Santarem with peak errors of 1000 m, 1300 m and 2250 m respectively.

Correlations between observed and simulated CBH fall mostly between r = 0.6 and r = 0.8 across most models. CLM performs worst over Himalayas (r = 0.25, NSD = 1.8) while its best performance is over Bondville (r = 0.6, NSD = 1.0). About half of GEMLAM stations cluster around r = 0.6 with NSD = 1.4 of observed while its worst performance is over Tongyu (r = 0.35, NSD = 2.0). MRCC underestimates NSD most at Lindenberg (r = 0.6, NSD = 0.42) and overestimates it most at Santarem (r = 0.7, NSD = 2.4). RCA3 has no station cluster whatsoever, underestimating NSD at BERMS (r = 0.6, NSD = 0.8) all the way to overestimating it at Santarem (r = 0.58, NSD = 2.8). RSM overestimates NSD for all Asian stations but underestimates for others. Its best performance is over Manaus (r = 0.6, NSD = 1.0).

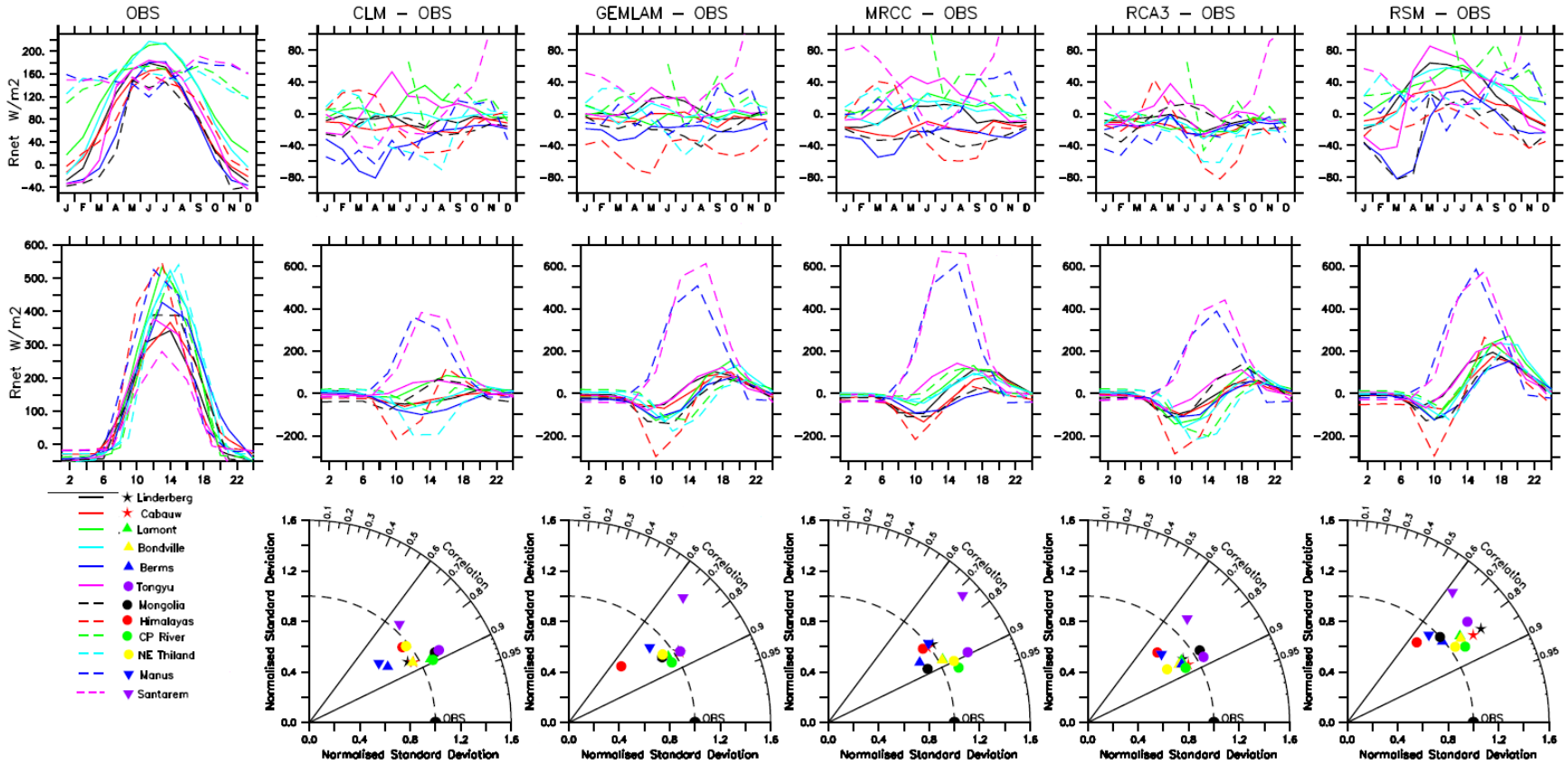

Figure 5.1: of simulated and observed seasonal (upper left panel) and diurnal (middle left panel) net total radiation (R_{net}) at 12 stations. Upper panels 2-6 show the difference between seasonal observed and model net radiation for CLM, GEMLAM, MRCC, RCA3 and RSM. Middle panels 2-6 show the difference between observed diurnal and model net radiation while Lower panels 2-6 show Taylor diagrams for the entire summer daytime period for each of the models

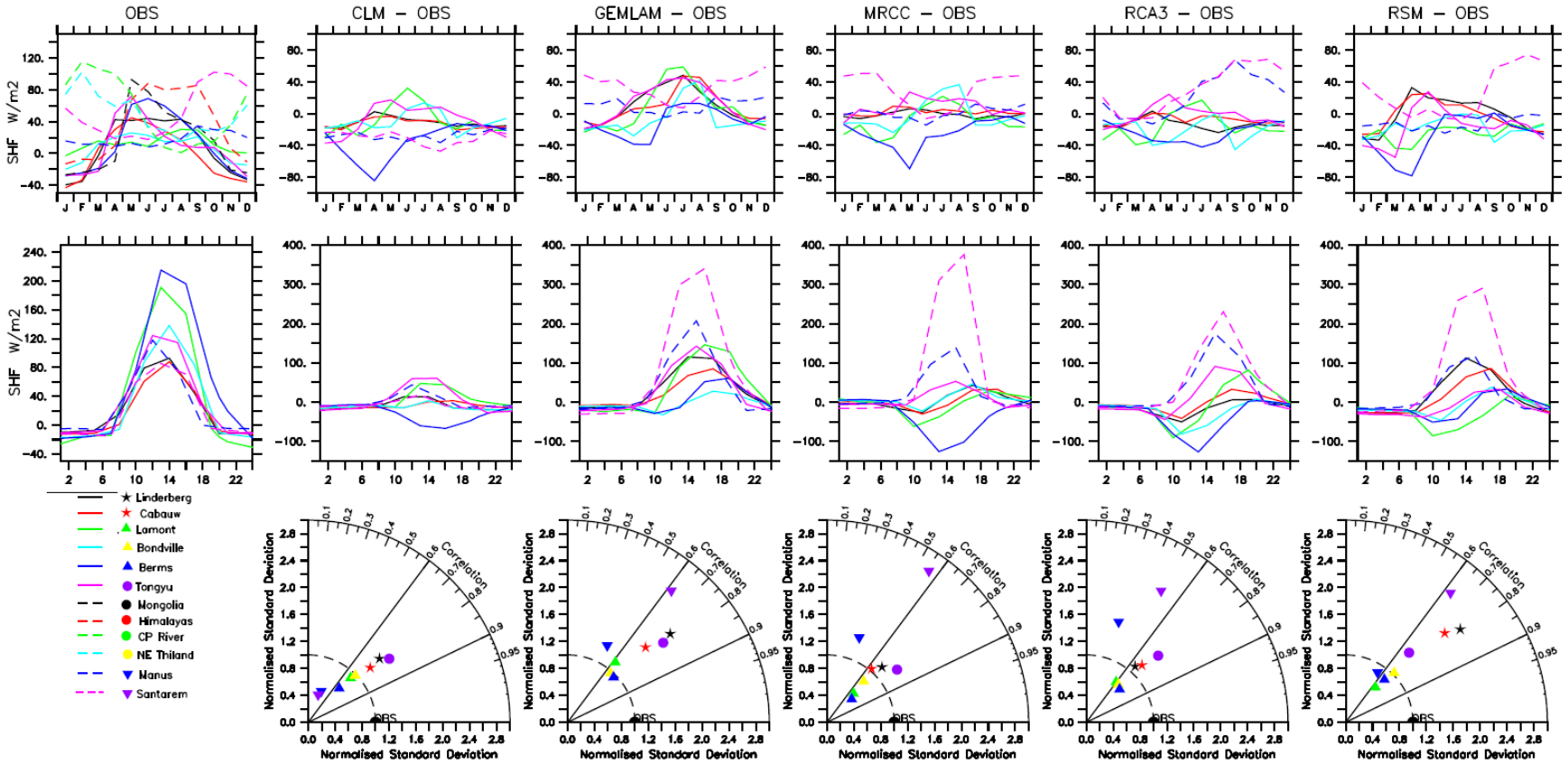

Figure 5. 2: Same as Figure 5.1 but for sensible heat flux (SHF)

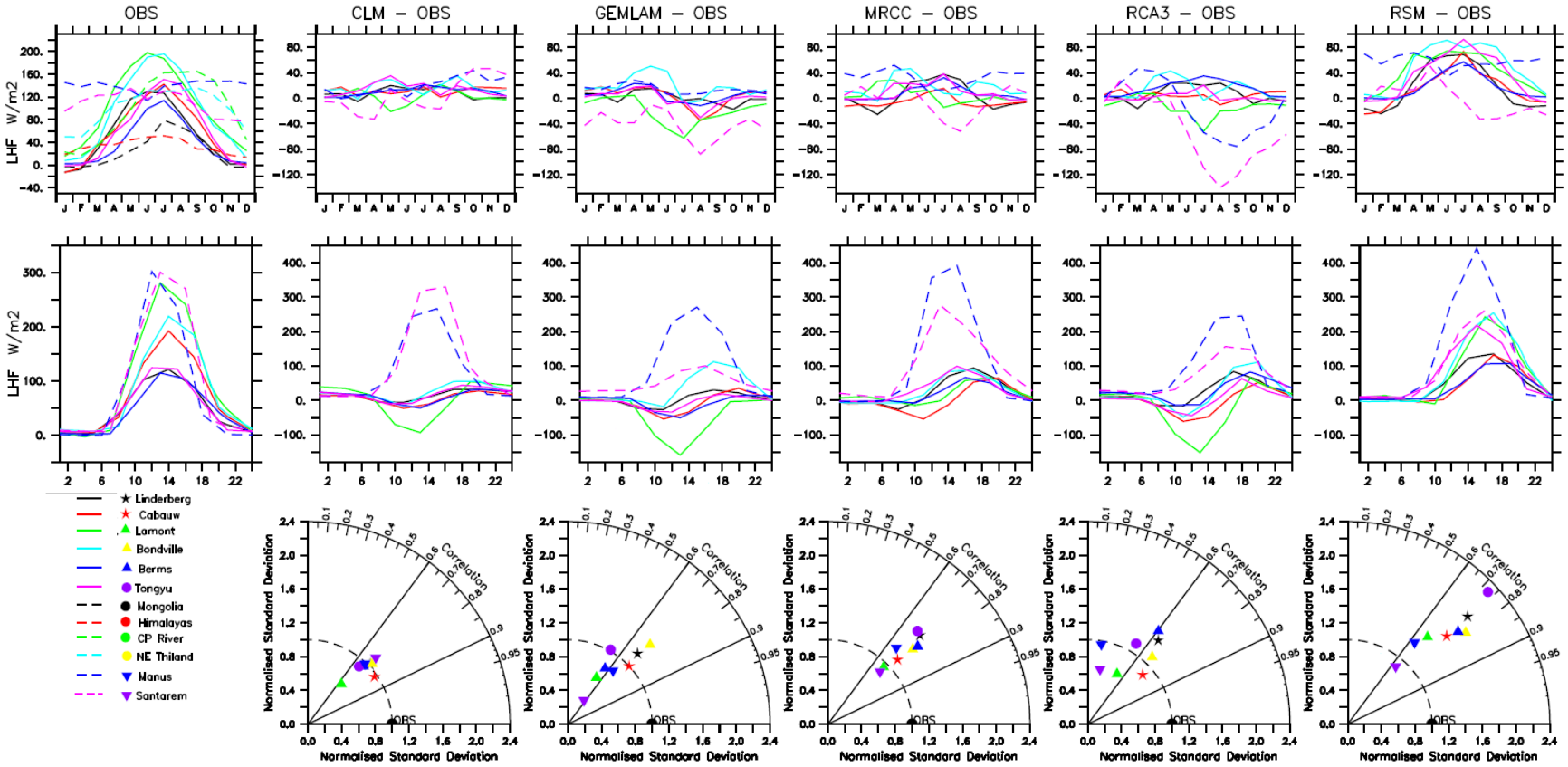

Figure 5.3: Same as Figure 5.1 but for latent heat flux (LHF)

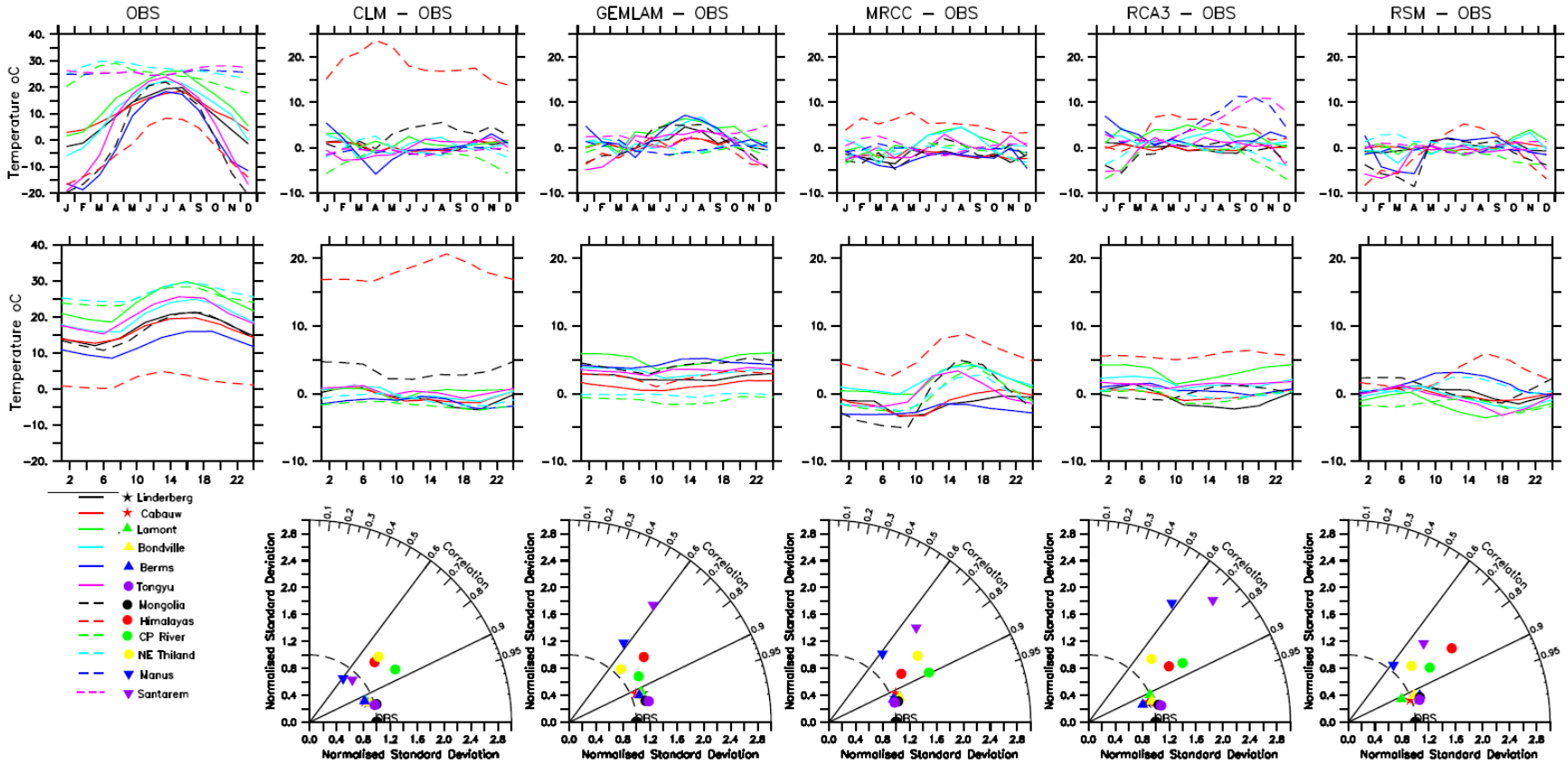

Figure 5.4: Same as Figure 5.1 but for temperature (T2M)

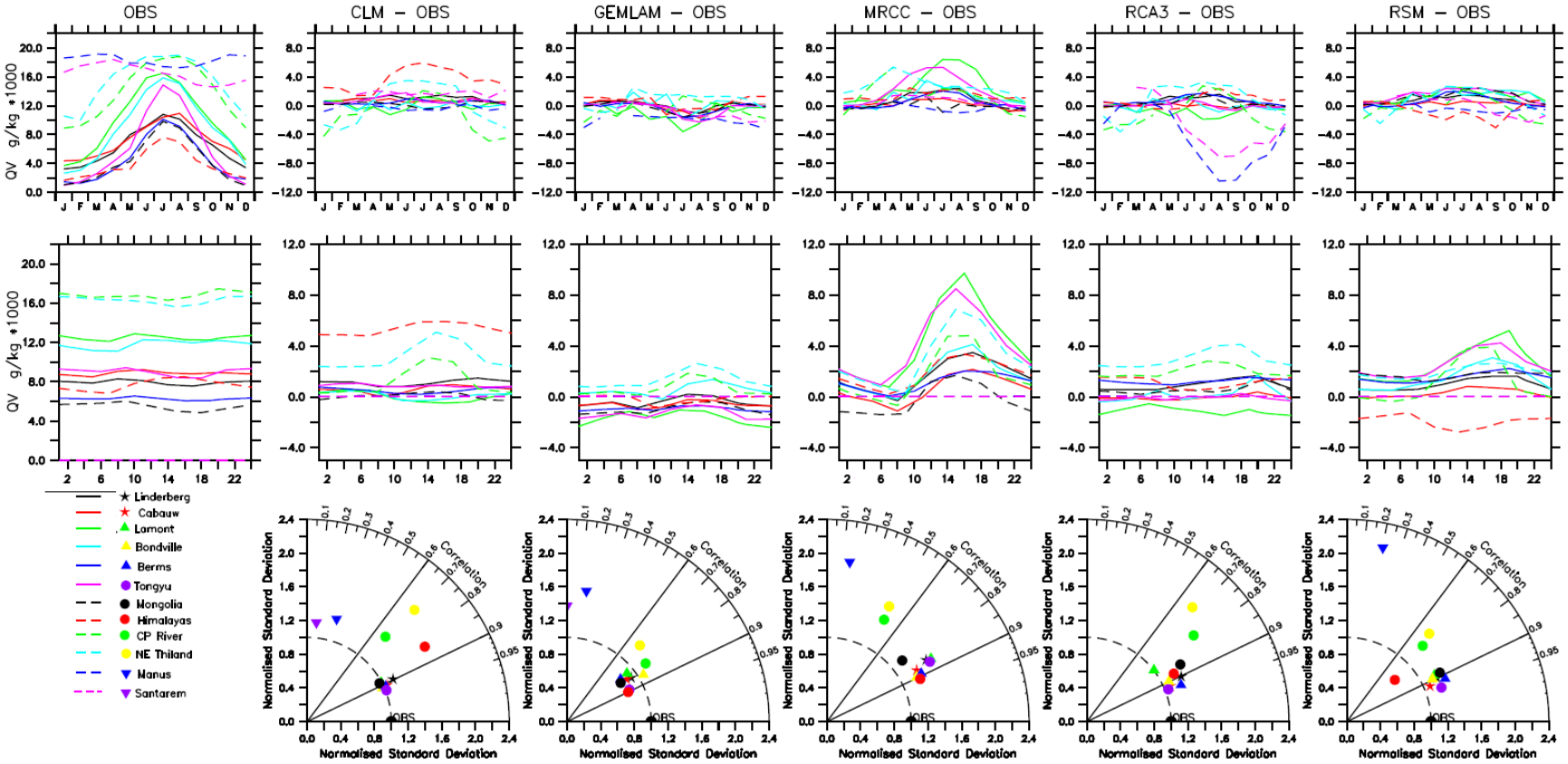

Figure 5. 5: Same as Figure 5.1 but for specific humidity (QV)

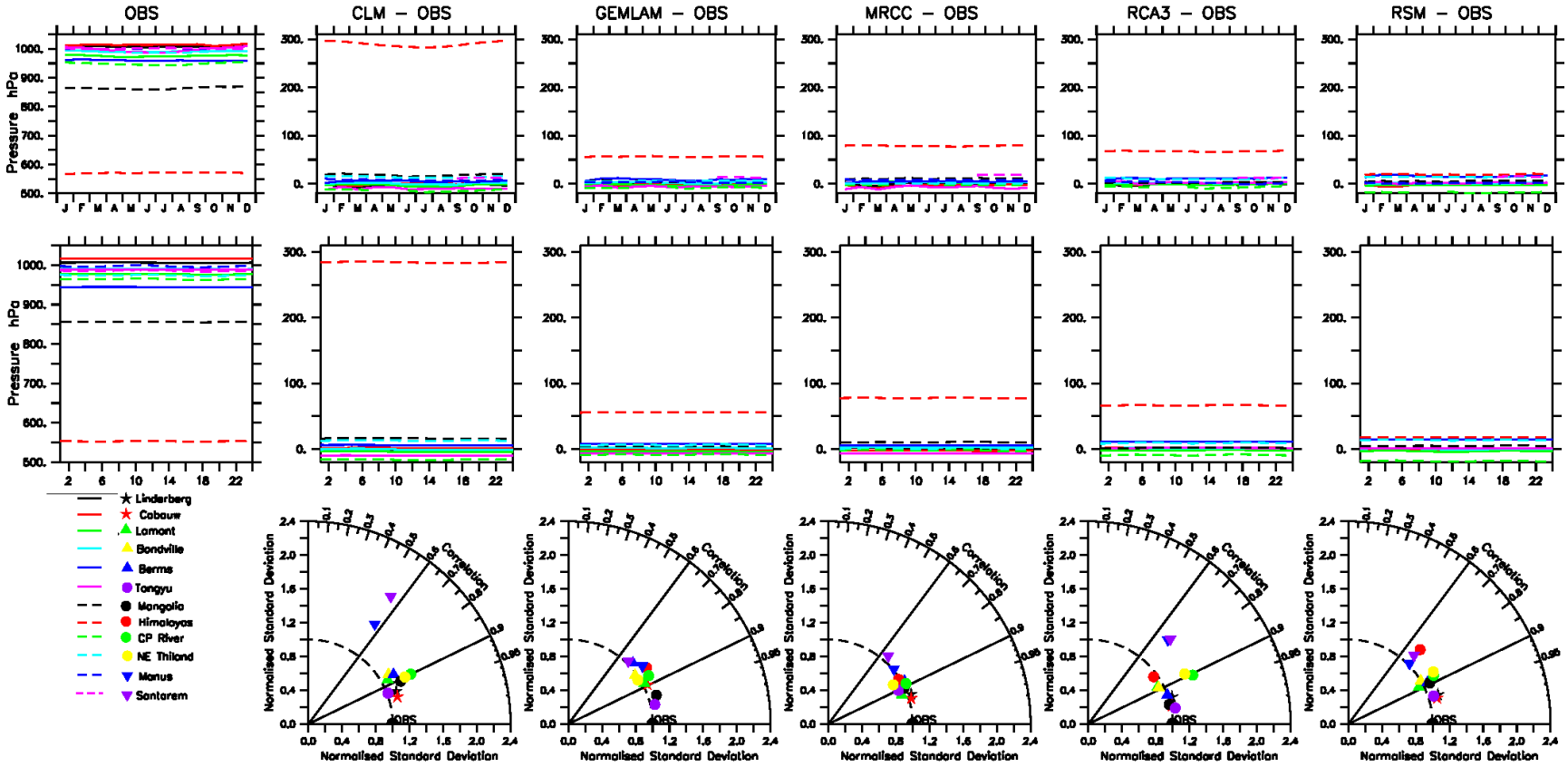

Figure 5.6: Same as Figure 5.1 but for surface pressure (PS)

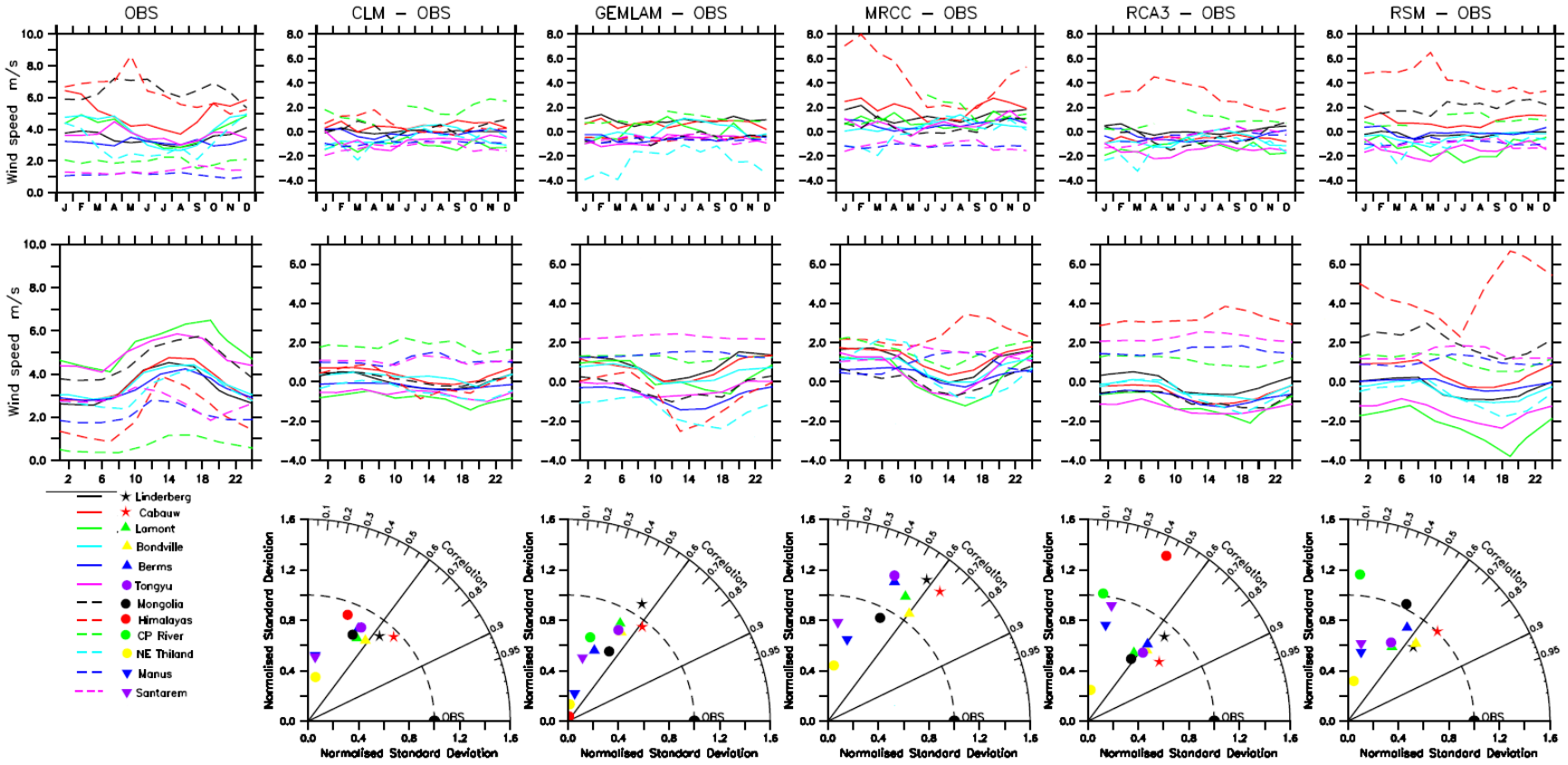

Figure 5. 7: Same as Figure 5.1 but for 10 m wind speed (WSP)

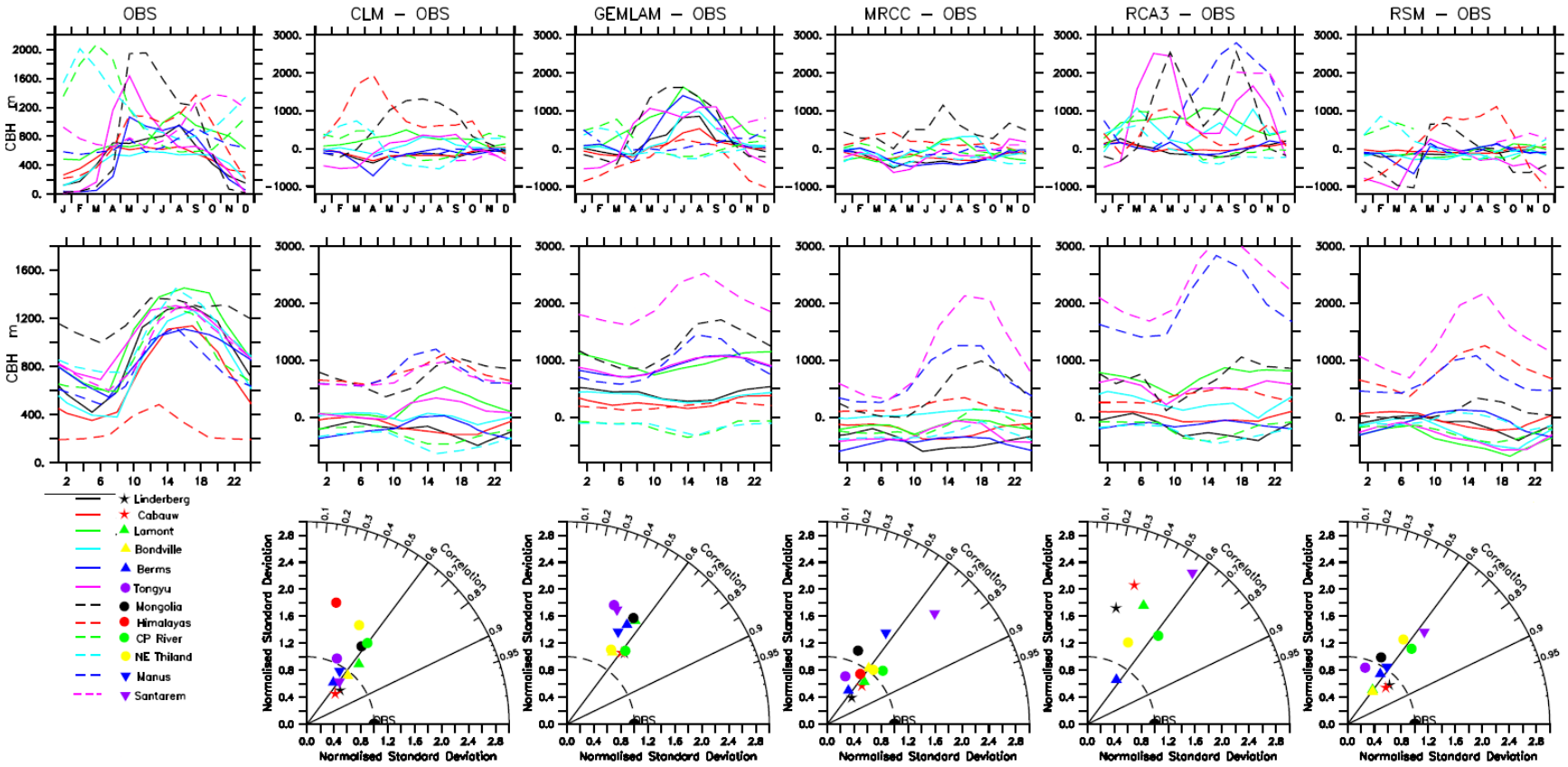

Figure 5.8: Same as Figure 1 but for cloud base height (CBH)

5.3 PCA loadings

5.3.1 Atmospheric patterns

Tables 5.1 and 5.2 represent the weak wind and strong wind summer daytime loadings of observed variables at six stations. in the weak-wind PCA loadings (Fig. 5.1),three of the six selected stations (Cabauw, Bondville and Lamont) returned two principal components and the other three (Lindenberg, BERMS and Tongyu) returned three principal components each (hereafter PF1, PF2 and PF3). In Lindenberg, PF1 explains about 35% of the total variance and has high loadings for net radiation, NTR (0.98), sensible heat flux, SHF (0.91) and latent heat flux, LHF (0.91). This loading pattern describes the surface energy process as identified in the previous chapter. PF2 explains 20.43% of the total variance and has moderately strong loadings in PS (-0.55), T2M (0.60) and a high QV loading (0.93). This possibly describes both dynamic and thermodynamic processes in the boundary layer. PF3 explains 19.20% of the total variance and has high loadings for CBH (0.95) and T2M (0.75). Unlike observations, CLM, MRCC and RSM all return only two principal components for Lindenberg, their respective PF1s effectively combining the surface energy process (PF1 in observed) with high loadings in CBH and T2M (PF3 in observed). However, PF2 of the three models is similar to observations. GEMLAM and RCA3, like the observed, extract three principal components for Lindenberg. In GEMLAM, PF1 reproduces the observed loadings well, but its PF2 gives high loadings for T2M and CBH (like PF3 in the observed) instead of describing the thermodynamic relationship. PF3 in GEMLAM shows high loadings for QV and PS. RCA3 reproduces the classic case identified in the previous chapter where PF1 describes a surface energy process accompanied by a high CBH loading, PF2 describes the thermodynamic (temperature-moisture) process while PF3 depicts the dynamic (pressure-wind speed) association.

PF1 for BERMS accounts for 38.81% of the total variance at that station and exhibits a similar loading pattern as Lindenberg, with very strong loadings for the surface energy process variables NTR (0.95), SHF (0.92), LHF (0.84). PF2 here has very strong loadings for QV and T2M which characterizes the temperature-moisture (thermodynamic) process. PF3 at BERMS, with strong negative loading for WSP (-0.81) and a

moderate loading for PS (0.56), describes the already established dynamic pressure-wind speed process. Unlike observations, CLM, MRCC, RCA3 and RSM all return two principal components for BERMS with PF1s describing the surface energy process associated with high CBH loadings and PF2s describing the classic thermodynamic (temperature-moisture) process. GEMLAM returns three principal components as observed but with different loadings. PF1 in GEMLAM describes the surface energy process as observed; PF2 has highest loadings for QV and PS while the highest loading in PF3 is for CBH, followed by WSP. At Tongyu, things change a bit. PF1 here, accounting for 30% of the total variance in the station data, describes a thermodynamic (temperature-moisture) process associated with a strong negative loading for surface pressure. PF2, which accounts for 27% of the total variance in the station data, describes the surface energy process and PF3 has a very strong loading for CBH (0.92) with a moderate loading for T2M (0.50), similar to what obtains at Lindenberg. Unlike the observed, CLM, GEMLAM and MRCC each return two principal components for Tongyu, their PF1s describing the energy process accompanied by moderate to strong loadings for CBH and T2M. For these models, the highest variable loadings for PF2 are for QV and PS. RCA3 and RSM both return three principal components for Tongyu as observed, both depicting the classic surface energy process in their PF1s, a QV-PS dominated PF2 for RCA3 and a T2M-QV dominated PF2 for RSM. PF3 in RCA3 simply explains the variance in WSP while in RSM, PF3 depicts the pressure-wind speed dynamic process.

The loadings for stations returning only two principal components in the observed data tell a similar story for the most part. PF1 accounts for about 40% of the total variance in the Cabauw station data. High loadings for NTR (0.96), SHF (0.87), and LHF (0.93) PF1 establish the surface energy process as the dominant atmospheric process over Cabauw. PF2 explains about 24% of the total variance and has high loadings in both T2M (0.87) and QV (0.81) which indicates surface thermodynamic processes as the next dominant factor at Cabauw. CLM, MRCC and RSM all, like observed, return two principal components for Cabauw and they also capture the observed loadings well with the exception that PF1 for CLM and RSM are much stronger than observed. GEMLAM and RCA3, unlike observed, both return three principal components for Cabauw. GEMLAM's most dominant process (PF1) being

that of surface energy and followed by a PF2 describing a CBH-T2M association and PF3 showing high loadings for QV and PS. RCA3 reproduces the classic PF1, PF2, PF3 case with a high CBH loading in PF1. Both Bondville and Lamont display the same general characteristics as Cabauw with PF1 representing the surface energy process and PF2 the thermodynamic process, but there are differences. For one, Bondville and Lamont both have a high loading for CBH in their PF1s (0.93 and 0.87 respectively) and two, the loadings of T2M in PF1 and PF2 is of comparable magnitude at both stations unlike Cabauw where the loadings of T2M is much less in PF1 than PF2. Another difference is that the loadings of PS is higher in PF2 at Bondville (-0.61) and Lamont (-0.76) than it is over Cabauw (-0.49) which translates to a higher dynamic influence on the thermodynamic process at both stations. All five models return two principal components over Bondville as in the observed, their PF1s depicting the surface energy process and high loadings for CBH and PF2s having moderate to strong loadings for T2M, QV and PS. The comparable contributions of T2M to PF1 and PF2 is reproduced in all models except MRCC where the loading for T2M in PF1 (0.92) is much higher than that in PF2 (-0.17). At Lamont, CLM, MRCC and RSM all return two principal components as observed, RSM and CLM replicate observed PF1 and PF2 relationships but MRCC, unlike observed, has low T2M and QV loadings in PF2. GEMLAM and RCA3 return three principal components for Lamont. GEMLAM reproduces the already identified PF1 and PF2 patterns but with a PF3 that has a high CBH loading along with moderate QV and PS loadings. In RCA3, PF1 describes the energy process along with high loadings in CBH and T2M, PF2 has high loadings for QV and an inverse, moderately high PS while PS3 mainly shows a high WSP loading.

5.3.2 Coupling of cloud base height and the surface fluxes

Under weak wind conditions, the coupling of CBH to the surface fluxes varies from station to station, from very weak at Lindenberg and Tongyu, to moderate at Cabauw and BERMS and very strong at Bondville and Lamont. A very weak coupling is observed between cloud base height and the surface energy process at Lindenberg where CBH has a loading of 0.16 on PF1. However, PF2 shows very high loadings for CBH and T2M (0.95 and 0.76 respectively) which indicates a coupling between cloud base height and the temperature profile over the station. CLM, RCA3 and RSM all exhibit

a strong coupling between CBH and the surface energy fluxes with CBH loadings of 0.89, 0.71, 0.84 and 0.86 respectively while MRCC gives a moderate but higher than observed coupling (0.50). Only GEMLAM reproduces a similar to observed weak CBH-surface flux coupling (0.16) on PF1 and a high coupling between CBH and T2M on PF2. At Cabauw, we observe a moderate CBH coupling (0.59) with the surface fluxes and a weak CBH coupling with PF2 (0.25). CLM, RCA3 and RSM all show a much stronger than observed coupling between CBH and the energy process, with CBH loadings of 0.84, 0.80 and 0.86 respectively under PF1. The situation is different in GEMLAM with an extremely weak CBH-surface energy process coupling (0.07 CBH loading). MRCC however reproduces a similar to observed, moderate CBH loading (0.66) for PF1. At Bondville, there is a very strong observed CBH coupling with the surface fluxes (0.93 CBH loading) but the loading of CBH is virtually nonexistent (0.06) in PF2. All models capture the strong coupling between CBH and the surface energy fluxes over Bondville with CBH loadings of 0.92, 0.80, 0.83, 0.87 and 0.91 respectively for CLM, GEMLAM, MRCC, RCA3 and RSM. At Lamont, observed CBH is strongly coupled to the surface fluxes (0.87) and weakly coupled to PF2 (0.20). CLM, MRCC, RCA3 and RSM all reproduce high loadings for CBH in PF1 (0.94, 0.90, 0.71 and 0.90 respectively).

GEMLAM fails to capture the strong coupling between CBH and the surface fluxes at Lamont, reproducing instead a moderate association with a CBH loading of 0.59 under PF1. At BERMS, we observe a moderately strong CBH coupling (0.64) with the surface fluxes (PF1), no perceivable coupling with PF2, and a moderate coupling (0.44) with PF3. CLM, MRCC, RCA3 and RSM all show a stronger than observed coupling between CBH and the surface fluxes with CBH loadings of 0.96, 0.91, 0.75 and 0.90 respectively in PF1. Over Tongyu, CBH shows an extremely weak coupling (0.12) with the surface fluxes in PF1, and a strong coupling (0.92) with WSP in FP3. CLM, GEMLAM and MRCC all show much stronger coupling between CBH and the surface fluxes than is observed, while RSM gives a moderate but still stronger than observed coupling. RCA3 gives the closest to observed coupling strength between CBH and the surface processes over Tongyu. Under strong wind conditions, the observed couplings slightly decrease at most stations except for Tongyu where there is a

very slight increase in CBH-surface flux coupling. The models generally depict this trend across the stations.

In weak wind conditions, observed CBH is weakly coupled with the surface fluxes at Lindenberg. It is however very strongly coupled with temperature. CBH is also weakly coupled with the surface fluxes at Tongyu. The coupling of CBH with surface fluxes is moderately strong at Cabauw and BERMS and very strong at Bondville and Lamont. The models also show a varying pattern of coupling between CBH and the surface fluxes going from one station to another. CLM reproduces a tightly coupled CBH with surface fluxes at all stations except Tongyu where the coupling is moderately strong. GEMLAM reproduces a weakly coupled CBH and surface fluxes at Lindenberg and BERMS with almost nonexistent coupling over Cabauw. However CBH is well coupled to temperature at these three stations. The CBH to surface fluxes coupling is very strong in Bondville and Tongyu and moderate over Lamont. MRCC, RCA3 and RSM strongly couple CBH to the surface fluxes at all stations except Cabauw (in MRCC where the coupling strength is moderate), Tongyu (in RCA3 and RSM where the coupling is weak and moderate respectively.)

The general patterns seen in the weak wind situation persist under strong wind conditions but with some differences. Observed CBH is weakly coupled with the surface fluxes at Lindenberg and Tongyu. It is however strongly coupled with temperature at Lindenberg and with wind speed at Tongyu. The coupling of CBH with surface fluxes is moderately strong at Cabauw but very strong at Bondville and Lamont and BERMS. The models also show a varying pattern of coupling between CBH and the surface fluxes going from one station to another. CLM reproduces a tightly coupled CBH-surface fluxes at all stations while in GEMLAM, CBH is weakly coupled with surface fluxes all stations. In RCA3, CBH is strongly coupled to the surface fluxes at Lindenberg, Cabauw and Bondville, moderately coupled at Lamont and weakly coupled at Tongyu and BERMS.

Table 5.1: PCA loadings for weak wind summer daytime at six stations for (a) observed (OBS) and models (b) CLM, (c) GEMLAM, (d) MRCC, (e) RCA3 and (f) RSM. Significant values from 0.70 and above in red

(a) OBS

Variable	Lindenberg			Cabauw			Bondville			Lamont			Berms			Tongyu		
	PF1	PF 2	PF 3	PF1	PF 2	PF 3	PF1	PF 2	PF 3	PF1	PF 2	PF 3	PF1	PF 2	PF 3	PF1	PF 2	PF 3
NTR	0.98	0.00	0.10	0.96	-0.01		0.95	0.14		0.95	0.13		0.95	0.08	-0.06	0.22	0.84	0.02
SHF	0.91	-0.13	0.13	0.87	-0.18		0.89	-0.07		0.72	-0.05		0.92	-0.08	0.01	0.04	0.72	-0.04
LHF	0.91	0.13	0.13	0.96	0.00		0.86	0.20		0.79	0.14		0.84	0.23	-0.09	0.11	0.90	0.01
CBH	0.16	-0.21	0.95	0.59	0.25		0.93	0.06		0.87	0.20		0.64	0.01	0.44	-0.22	0.12	0.92
T2M	0.19	0.60	0.76	0.34	0.87		0.64	0.72		0.60	0.73		0.37	0.85	0.20	0.78	0.19	0.50
QV	0.07	0.93	-0.02	-0.13	0.81		0.12	0.92		0.04	0.91		-0.04	0.94	-0.10	0.95	0.13	-0.11
PS	0.27	-0.55	0.11	0.17	-0.49		0.38	-0.61		0.10	-0.76		0.24	-0.41	0.56	-0.85	-0.15	0.00
WSP	0.09	-0.13	0.05	0.09	0.41		0.05	0.18		0.06	0.12		0.19	-0.16	-0.81	0.23	-0.14	0.42
Tot. Var(%)	34.64	20.43	19.20	38.91	23.89		48.34	22.83		39.41	25.50		38.81	23.47	15.29	29.84	26.65	16.22

(b) CLM

Variable	Lindenberg			Cabauw			Bondville			Lamont			Berms			Tongyu		
	PF1	PF 2	PF 3	PF1	PF 2	PF 3	PF1	PF 2	PF 3	PF1	PF 2	PF 3	PF1	PF 2	PF 3	PF1	PF 2	PF 3
NTR	0.94	-0.10		0.94	0.12		0.98	0.02		0.98	0.10		0.97	-0.03		0.89	0.18	
SHF	0.89	-0.23		0.92	0.02		0.97	-0.03		0.97	0.05		0.95	-0.11		0.79	0.10	
LHF	0.80	0.13		0.91	0.16		0.94	-0.02		0.96	0.14		0.91	0.14		0.93	-0.11	
CBH	0.89	-0.10		0.84	0.11		0.92	0.11		0.94	0.07		0.96	0.03		0.69	-0.52	
T2M	0.74	0.54		0.51	0.82		0.64	0.71		0.70	0.67		0.56	0.77		0.63	0.58	
QV	-0.05	0.89		0.01	0.96		0.06	0.92		-0.02	0.91		0.02	0.94		0.01	0.96	
PS	0.12	-0.68		0.33	-0.31		0.02	-0.76		-0.08	-0.77		0.12	-0.59		-0.22	-0.77	
WSP	0.03	0.31		-0.03	-0.26		-0.13	0.14		-0.06	-0.01		0.00	0.18		-0.02	0.11	
Tot. Var(%)	46.04	21.48		45.21	22.56		50.76	24.36		52.67	23.86		49.07	23.76		39.95	27.15	

(c) GEMLAM

Variable	Lindenberg			Cabauw			Bondville			Lamont			Berms			Tongyu		
	PF1	PF 2	PF 3	PF1	PF 2	PF 3	PF1	PF 2	PF 3	PF1	PF 2	PF 3	PF1	PF 2	PF3	PF1	PF 2	PF 3
NTR	0.98	0.07	0.03	0.98	0.08	0.00	0.94	0.06		0.98	0.03	0.08	0.97	-0.02	0.13	0.92	0.12	
SHF	0.85	0.24	0.17	0.77	0.29	-0.18	0.90	-0.09		0.90	-0.03	0.18	0.94	-0.07	0.10	0.84	0.02	
LHF	0.81	-0.13	-0.20	0.80	-0.10	0.24	0.78	0.14		0.82	0.11	-0.18	0.84	0.12	-0.01	0.77	0.13	
CBH	0.14	0.92	0.25	0.07	0.96	-0.15	0.80	-0.14		0.59	-0.02	0.72	0.34	0.13	0.86	0.70	-0.49	
T2M	0.23	0.95	-0.17	0.23	0.91	0.28	0.70	0.55		0.63	0.56	0.34	0.35	0.63	0.61	0.73	0.40	
QV	0.18	0.18	-0.81	0.25	-0.07	0.79	0.15	0.91		0.06	0.77	-0.55	0.10	0.87	-0.28	-0.08	0.95	
PS	0.14	0.08	0.77	0.21	-0.07	-0.73	0.18	-0.77		0.00	-0.80	-0.31	0.15	-0.80	-0.14	-0.23	-0.81	
WSP	0.10	-0.18	0.06	0.05	-0.21	0.18	0.29	0.01		-0.04	0.11	0.59	-0.11	-0.12	0.58	0.24	-0.14	
Tot. Var(%)	31.04	23.57	17.68	29.31	23.65	17.16	44.41	22.09		39.96	19.60	18.18	35.18	22.85	19.70	40.90	25.04	

(d) MRCC

Variable	Lindenberg			Cabauw			Bondville			Lamont			Berms			Tongyu		
	PF1	PF 2	PF 3	PF1	PF 2	PF 3	PF1	PF 2	PF 3	PF1	PF 2	PF 3	PF1	PF 2	PF 3	PF1	PF 2	PF 3
NTR	0.94	-0.10		0.93	0.24		0.95	0.08		0.94	0.24		0.94	0.23		0.92	0.24	
SHF	0.86	-0.16		0.91	0.07		0.91	0.20		0.91	0.25		0.93	0.15		0.82	-0.05	
LHF	0.81	0.05		0.84	0.42		0.90	0.01		0.88	0.21		0.87	0.35		0.84	0.24	
CBH	0.71	0.32		0.66	0.55		0.83	0.33		0.90	0.13		0.91	0.28		0.87	0.18	
T2M	0.72	0.61		0.44	0.87		0.92	-0.17		0.94	-0.18		0.34	0.92		0.55	0.80	
QV	0.52	0.70		0.15	0.91		0.68	-0.58		0.86	-0.34		0.05	0.98		0.14	0.93	
PS	0.13	-0.71		0.46	-0.50		-0.04	0.85		-0.15	0.91		0.38	-0.21		0.13	-0.91	
WSP	-0.01	0.32		-0.01	-0.04		0.18	0.26		0.19	0.39		0.24	0.03		0.14	0.22	
Tot. Var(%)	44.82	19.94		40.70	29.76		57.32	16.29		62.41	16.40		45.90	26.62		41.91	31.40	

(e) RCA3

Variable	Lindenberg			Cabauw			Bondville			Lamont			Berms			Tongyu		
	PF1	PF 2	PF 3	PF1	PF 2	PF 3	PF1	PF 2	PF 3	PF1	PF 2	PF 3	PF1	PF 2	PF 3	PF1	PF 2	PF 3
NTR	0.93	0.01	-0.03	0.92	-0.02	0.03	0.97	0.11		0.96	0.02	-0.03	0.96	-0.04		0.95	-0.03	-0.02
SHF	0.90	-0.19	0.01	0.91	-0.13	0.17	0.91	-0.02		0.92	-0.06	-0.05	0.87	-0.26		0.90	0.24	-0.13
LHF	0.80	0.33	-0.12	0.79	0.19	-0.36	0.91	0.19		0.77	0.20	-0.10	0.79	0.27		0.70	-0.21	0.14
CBH	0.84	-0.24	0.16	0.80	-0.04	0.40	0.87	-0.19		0.71	-0.30	0.47	0.75	-0.50		0.23	0.68	-0.39
T2M	0.49	0.74	0.21	0.53	0.77	-0.02	0.63	0.67		0.75	0.45	0.16	0.56	0.74		0.69	-0.50	0.03
QV	-0.29	0.91	0.06	-0.12	0.87	-0.36	0.02	0.93		0.04	0.87	-0.36	0.06	0.97		0.07	-0.92	-0.12
PS	0.16	-0.54	0.61	0.11	-0.01	0.87	0.16	-0.71		-0.07	-0.67	-0.41	0.16	-0.41		-0.21	0.75	0.05
WSP	0.09	-0.25	-0.82	0.16	-0.58	-0.29	-0.02	-0.14		-0.05	0.00	0.84	0.10	0.06		0.06	0.04	0.96
Tot. Var(%)	42.34	24.02	14.25	40.83	21.87	16.25	47.07	24.09		42.92	19.25	15.67	40.22	25.58		34.72	27.93	14.15

(f) RSM

Variable	Lindenberg			Cabauw			Bondville			Lamont			Berms			Tongyu		
	PF1	PF 2	PF 3	PF1	PF 2	PF 3	PF1	PF 2	PF 3	PF1	PF 2	PF 3	PF1	PF 2	PF 3	PF1	PF 2	PF 3
NTR	0.95	-0.14		0.97	0.11		0.96	0.22		0.97	0.15		0.98	0.01		0.94	0.22	0.00
SHF	0.85	-0.35		0.89	-0.16		0.96	0.01		0.96	-0.01		0.95	-0.11		0.87	-0.22	-0.09
LHF	0.86	0.10		0.88	0.28		0.91	0.28		0.95	0.20		0.93	0.10		0.81	0.34	0.02
CBH	0.86	-0.11		0.86	0.01		0.91	0.23		0.90	0.26		0.90	0.04		0.56	-0.63	0.37
T2M	0.74	0.57		0.40	0.89		0.52	0.79		0.62	0.72		0.58	0.76		0.49	0.73	0.28
QV	0.12	0.93		-0.11	0.96		0.23	0.91		0.30	0.87		0.13	0.93		0.06	0.98	0.07
PS	0.20	-0.50		0.20	-0.28		0.09	-0.72		0.05	-0.73		0.21	-0.62		-0.20	-0.20	-0.70
WSP	0.02	-0.24		-0.05	-0.26		-0.12	0.00		-0.05	-0.02		0.00	-0.17		-0.23	-0.08	0.72
Tot. Var(%)	46.61	20.79		43.27	24.66		48.18	26.88		50.72	24.28		49.08	23.43		36.98	26.89	15.48

Table 5.2: PCA loadings for strong wind summer daytime at six stations for (a) observed (OBS) and models (b) CLM, (c) GEMLAM, (d) MRCC, (e) RCA3 and (f) RSM. Significant values from 0.70 and above in red.

(a) OBS

Variable	Lindenberg			Cabauw			Bondville			Lamont			Berms			Tongyu		
	PF1	PF 2	PF 3	PF1	PF 2	PF 3	PF1	PF 2	PF 3	PF1	PF 2	PF 3	PF1	PF 2	PF 3	PF1	PF 2	PF 3
NTR	0.98	0.11	0.04	0.95	0.07	0.00	0.94	0.22	0.01	0.94	0.05		0.96	0.05	0.06	0.89	0.24	0.15
SHF	0.88	0.15	-0.08	0.88	-0.09	-0.04	0.88	-0.10	0.03	0.73	-0.12		0.94	-0.08	0.02	0.86	0.03	-0.14
LHF	0.86	0.10	0.09	0.92	0.09	-0.08	0.73	0.37	0.03	0.79	0.14		0.83	0.25	0.08	0.79	0.08	0.20
CBH	0.17	0.93	-0.29	0.56	0.22	0.45	0.90	0.02	-0.06	0.86	0.19		0.77	0.11	-0.28	0.20	-0.11	0.87
T2M	0.19	0.82	0.52	0.31	0.91	0.19	0.52	0.81	0.00	0.64	0.67		0.43	0.86	-0.11	0.22	0.77	0.44
QV	0.04	-0.03	0.96	-0.13	0.89	-0.18	-0.04	0.97	0.05	0.05	0.84		-0.05	0.95	0.08	0.09	0.93	-0.17
PS	0.14	0.13	-0.39	0.13	-0.27	0.77	0.27	-0.29	-0.77	0.20	-0.77		0.23	-0.34	-0.69	-0.08	-0.77	-0.13
WSP	0.13	0.02	-0.33	0.25	-0.18	-0.77	0.24	-0.18	0.84	0.24	0.58		0.16	-0.20	0.83	-0.05	0.26	0.69
Tot. Var(%)	32.05	20.01	19.41	37.75	22.20	18.22	42.55	23.88	16.37	41.13	26.74		41.82	23.40	15.78	28.16	27.55	19.39

(b) CLM

Variable	Lindenberg			Cabauw			Bondville			Lamont			Berms			Tongyu		
	PF1	PF 2	PF 3	PF1	PF 2	PF 3	PF1	PF 2	PF 3	PF1	PF 2	PF 3	PF1	PF 2	PF 3	PF1	PF 2	PF 3
NTR	0.95	0.00	0.04	0.96	0.11	0.06	0.98	0.08	0.03	0.98	-0.01		0.97	0.01	-0.01	0.90	0.19	
SHF	0.88	-0.16	-0.10	0.87	0.06	0.25	0.95	-0.09	-0.02	0.95	-0.10		0.95	-0.12	-0.03	0.71	0.07	
LHF	0.66	0.16	0.38	0.86	-0.01	-0.21	0.87	0.11	0.12	0.90	0.07		0.81	0.21	0.23	0.91	0.15	
CBH	0.86	-0.02	-0.22	0.81	0.19	0.27	0.92	0.09	-0.08	0.93	-0.08		0.94	0.11	-0.04	0.85	-0.24	
T2M	0.69	0.62	-0.19	0.44	0.86	0.16	0.53	0.82	-0.01	0.71	0.62		0.56	0.80	-0.03	0.58	0.66	
QV	-0.06	0.94	0.03	-0.06	0.97	-0.03	-0.11	0.96	0.08	-0.15	0.89		-0.06	0.97	0.00	-0.23	0.91	
PS	0.22	-0.32	-0.68	0.23	-0.16	0.77	0.12	-0.37	-0.76	-0.09	-0.77		0.24	-0.46	-0.69	-0.17	-0.72	
WSP	0.09	-0.35	0.78	0.07	-0.27	-0.82	0.13	-0.16	0.88	0.32	0.14		0.21	-0.21	0.86	0.24	0.17	
Tot. Var(%)	42.34	19.27	16.38	41.80	22.98	18.51	47.45	22.48	17.39	52.10	22.77		47.32	23.84	15.93	41.94	24.30	

(c) GEMLAM

Variable	Lindenberg			Cabauw			Bondville			Lamont			Berms			Tongyu		
	PF1	PF 2	PF 3	PF1	PF 2	PF 3	PF1	PF 2	PF 3	PF1	PF 2	PF 3	PF1	PF 2	PF 3	PF1	PF2	PF 3
NTR	0.97	0.17	0.07	0.27	0.94	0.14	0.96	0.12	0.22	0.97	-0.02	-0.01	0.97	0.18	-0.05	0.98	0.00	0.07
SHF	0.80	0.34	0.06	0.50	0.63	0.15	0.77	-0.18	0.40	0.89	0.14	-0.10	0.90	0.19	-0.17	0.88	-0.02	-0.03
LHF	0.80	-0.18	-0.01	-0.11	0.89	0.01	0.90	0.27	0.02	0.65	-0.37	0.16	0.73	-0.24	0.30	0.74	-0.03	0.10
CBH	0.08	0.94	0.12	0.94	0.08	0.11	0.19	-0.13	0.95	0.47	0.83	0.22	0.08	0.94	-0.14	0.22	0.87	0.38
T2M	0.11	0.96	0.11	0.93	0.11	0.12	0.28	0.55	0.75	0.67	0.39	0.32	0.08	0.95	0.23	0.46	0.18	0.68
QV	0.04	-0.03	-0.04	0.03	0.06	0.01	0.20	0.86	-0.02	0.18	-0.84	0.11	0.02	0.09	0.71	0.18	-0.92	0.16
PS	0.11	0.03	0.78	0.13	0.10	0.79	0.13	-0.77	0.04	0.02	-0.03	-0.88	0.19	-0.14	-0.77	-0.09	0.39	-0.78
WSP	0.01	-0.16	-0.84	-0.09	-0.07	-0.77	0.05	0.25	0.03	0.09	-0.01	0.80	0.15	-0.20	0.48	-0.11	0.19	0.61
Tot. Var(%)	28.21	25.02	16.93	26.43	26.37	16.17	31.23	23.11	20.85	35.94	21.37	20.08	29.35	24.78	19.10	32.36	22.79	20.39

(d) MRCC

Variable	Lindenberg			Cabauw			Bondville			Lamont			Berms			Tongyu		
	PF1	PF 2	PF 3	PF1	PF 2	PF 3	PF1	PF 2	PF 3	PF1	PF 2	PF 3	PF1	PF 2	PF 3	PF1	PF 2	PF 3
NTR	0.95	0.18	0.09	0.93	0.21	0.10	0.94	0.04		0.94	0.13		0.96	0.16	0.06	0.95	0.05	
SHF	0.86	0.12	0.18	0.92	0.04	0.20	0.87	0.22		0.92	0.19		0.95	0.05	0.14	0.81	-0.10	
LHF	0.81	0.24	0.00	0.82	0.31	0.01	0.83	-0.06		0.86	0.12		0.92	0.25	0.02	0.77	0.09	
CBH	0.50	0.54	0.19	0.75	0.25	0.22	0.81	0.22		0.93	-0.03		0.95	0.17	-0.01	0.90	0.14	
T2M	0.31	0.93	0.11	0.52	0.80	0.16	0.90	-0.11		0.92	-0.16		0.43	0.89	-0.01	0.74	0.58	
QV	0.11	0.93	0.00	0.17	0.95	0.03	0.67	-0.34		0.84	-0.22		0.09	0.98	0.00	0.46	0.76	
PS	0.17	-0.13	0.85	0.22	-0.14	0.82	-0.01	0.87		-0.11	0.85		0.19	-0.26	0.77	-0.06	-0.81	
WSP	-0.03	-0.33	-0.77	-0.05	-0.38	-0.75	-0.06	-0.76		-0.11	-0.71		0.07	-0.22	-0.85	-0.29	0.46	
Tot. Var(%)	33.73	28.08	17.56	41.12	23.93	16.88	53.21	19.58		61.29	17.12		47.69	24.76	16.80	47.40	22.79	

(e) RCA3

Variable	Lindenberg			Cabauw			Bondville			Lamont			Berms			Tongyu		
	PF1	PF 2	PF 3	PF1	PF 2	PF 3	PF1	PF 2	PF 3	PF1	PF 2	PF 3	PF1	PF 2	PF 3	PF1	PF2	PF 3
NTR	0.90	0.17	-0.01	0.91	0.10	0.18	0.94	0.20	0.05	0.96	-0.01	0.01	0.93	0.28	0.00	0.95	0.13	0.07
SHF	0.88	-0.19	0.12	0.92	-0.06	-0.10	0.90	-0.03	-0.04	0.92	-0.17	-0.03	0.93	0.06	-0.07	0.85	0.35	0.03
LHF	0.66	0.43	-0.28	0.52	0.17	0.60	0.88	0.26	0.15	0.68	0.44	0.04	0.36	0.60	0.25	0.71	-0.37	-0.09
CBH	0.81	-0.06	0.15	0.82	-0.04	-0.27	0.82	-0.13	-0.13	0.52	-0.78	0.26	0.88	-0.11	-0.04	0.34	0.85	0.17
T2M	0.51	0.75	0.13	0.52	0.76	-0.18	0.50	0.80	0.02	0.66	-0.20	0.43	0.21	0.90	-0.01	0.65	-0.13	0.41
QV	-0.20	0.94	0.00	-0.21	0.94	0.08	-0.12	0.97	0.13	0.09	0.85	0.18	-0.42	0.88	0.03	0.16	-0.92	0.13
PS	0.29	-0.25	0.76	0.41	-0.30	-0.63	0.21	-0.27	-0.79	0.13	0.02	-0.87	0.36	-0.18	-0.72	-0.13	0.42	-0.64
WSP	0.14	-0.32	-0.79	-0.05	-0.24	0.74	0.18	-0.07	0.87	0.21	0.11	0.73	0.16	-0.01	0.89	-0.01	0.23	0.81
Tot. Var(%)	38.49	23.26	16.79	38.60	20.78	18.15	43.47	22.22	17.94	37.64	20.17	19.82	37.60	25.87	17.27	33.82	26.03	16.20

(f) RSM

Variable	Lindenberg			Cabauw			Bondville			Lamont			Berms			Tongyu		
	PF1	PF 2	PF 3	PF1	PF 2	PF 3	PF1	PF 2	PF 3	PF1	PF 2	PF 3	PF1	PF 2	PF 3	PF1	PF 2	PF 3
NTR	0.96	-0.05	-0.02	0.97	0.04	0.03	0.96	0.19	0.10	0.96	0.22	0.06	0.97	0.05	-0.01	0.97	-0.02	0.06
SHF	0.86	-0.28	0.14	0.84	-0.17	0.33	0.95	-0.04	-0.09	0.90	0.06	-0.19	0.93	-0.08	-0.12	0.85	-0.22	-0.19
LHF	0.78	0.25	-0.25	0.83	0.26	-0.24	0.91	0.27	0.17	0.93	0.24	0.16	0.87	0.20	0.12	0.85	0.09	0.17
CBH	0.79	0.08	0.23	0.73	0.08	0.25	0.84	0.26	-0.02	0.83	0.13	0.10	0.78	0.16	0.13	0.43	-0.71	0.17
T2M	0.52	0.78	0.14	0.32	0.91	0.14	0.37	0.91	0.00	0.48	0.84	0.06	0.48	0.83	0.10	0.60	0.45	0.25
QV	-0.18	0.91	-0.07	-0.13	0.96	-0.02	0.09	0.98	0.02	0.10	0.96	0.03	-0.03	0.95	0.00	0.18	0.97	0.10
PS	0.22	-0.23	0.79	0.11	-0.13	0.75	0.04	-0.21	-0.81	0.03	-0.32	-0.79	0.22	-0.37	-0.74	-0.13	-0.17	-0.78
WSP	0.19	-0.41	-0.72	-0.06	-0.30	-0.81	0.10	-0.18	0.81	0.09	-0.18	0.85	0.27	-0.19	0.85	-0.04	-0.14	0.83
Tot. Var(%)	40.86	22.56	16.32	37.46	24.58	18.24	43.98	25.56	17.18	44.05	23.81	17.87	43.82	22.99	16.51	36.99	21.76	18.29

5.3.3 *Influence of wind speed on summer daytime correlations of CBH and other atmospheric variables*

Figures 5.9 and 5.10 show the correlation coefficients of CBH with the surface variables (NTR, SHF, LHF, T2M, QV, PS, WSP) over the stations, under weak wind and strong wind conditions, respectively. In the observed (for the weak wind condition), the correlation coefficients between CBH and R_{net} (r_{CR}) is strong ($r_{CR} > 0.5$) over three stations (Lamont, Bondville and BERMS), moderate ($0.4 < r_{CR} < 0.5$) in two stations (Lindenberg and Cabauw), and weak ($r_{CR} < 0.4$) in one station (Tongyu). The highest r_{CR} (0.7) is over Lamont. In the models, except GEMLAM, r_{CR} is strong over all the stations, but moderate over Tongyu (in CLM, RCA3 and RSM). In GEMLAM, r_{CR} is only strong over Lamont and Bondville, moderate over BERMS, Tongyu and Lindenberg, but weak over Cabauw. So, both observed and models (except GEMLAM) show that CBH is coupled with R_{net} in weak wind condition over all the stations (except Tongyu). With the increase in wind speed, there is no remarkable change in observed and simulated r_{CB}, except for the small increase in the observed r_{CB} over Tongyu, and in GEMLAM r_{CB} decreases over the stations. The observed and simulated correlation coefficients between CBH and SHF (hereafter, r_{CS}) exhibit similar patterns with that of r_{CR}.

The observed correlation between CBH and LHF (r_{CL}) is slightly different from that of r_{CS}. It is strong over 3 stations (Cabauw, Lamont and Bondville), moderate at BERMS and weak over Lindenberg and Tongyu. CLM reproduces a strong r_{CL} over all the stations; MRCC and RSM have strong r_{CL} over 4 stations with moderate r_{CL} at Lindenberg (MRCC) and weak r_{CL} at Tongyu (RSM). In RCA3, r_{CL} is strong at two stations (Lindenberg and Lamont), moderate over 3 (Cabauw, Bondville and BERMS) and very weak and negative over Tongyu. In GEMLAM, r_{CL} is very weak over all stations. With increased wind speed, r_{CL} is weak over all stations in observed, GEMLAM and RCA3.

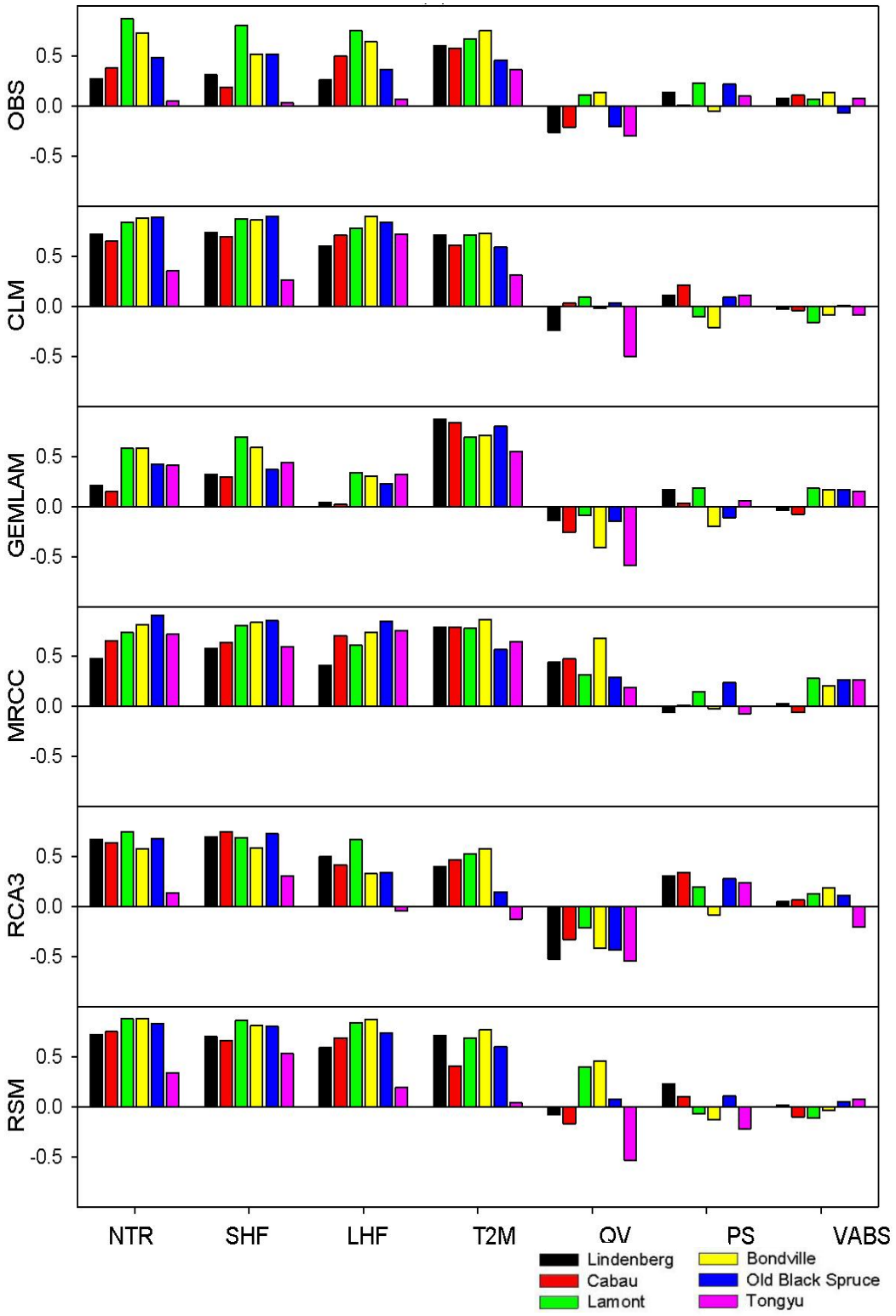

Figure 5.9: Correlation coefficients between the CBH and net surface total radiation (R_N), sensible heat flux, latent heat flux, surface temperature (T_S, 2m), surface specific moisture (QV, 2m), surface pressure (P_S) and wind speed (WSP, 10 m), respectively, for summer daytime weak wind case in observation (OBS) and models (CLM, GEMLAM, MRCC, RCA3 and RSM) data over CEOP stations Lindenberg, Cabauw, Bondville, Lamont, BERMS (Old Black Spruce) and Tongyu.

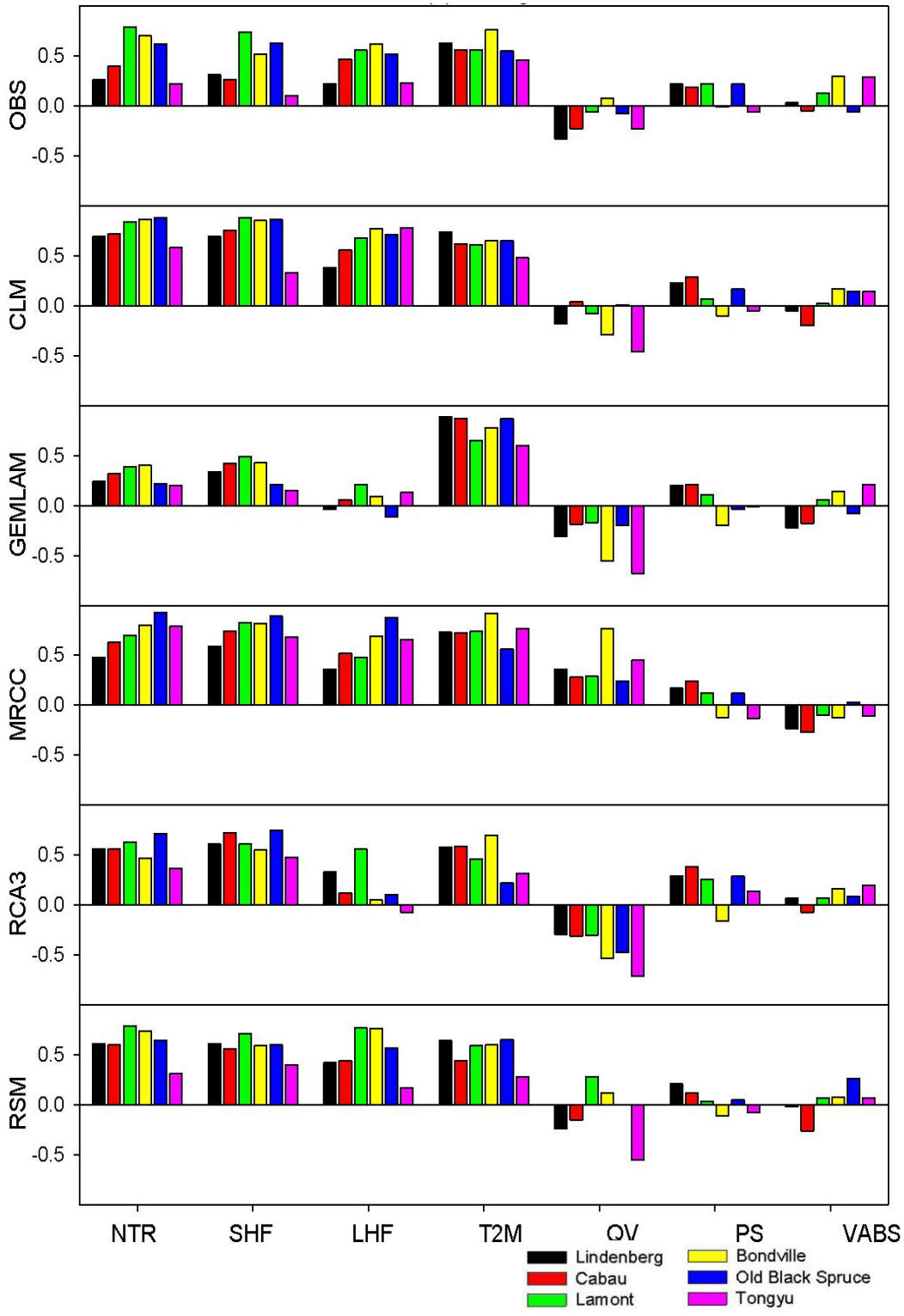

Figure 5.10: Same as Figure 5.9 but for strong wind conditions.

The observed correlation between CBH and temperature (r_{CT}) is strong over 4 stations (Lindenberg, Cabauw, Lamont and Bondville) and moderate over the remaining 2 stations (BERMS and Tongyu). In CLM, it is strong over the stations, but moderate over Tongyu. In GEMLAM and MRCC, r_{CT} is strong over all the stations, RSM reproduces strong r_{CT} over 4 stations (Lindenberg, Lamont, Bondville and BERMS) while r_{CT} is moderate over Cabauw and very weak over Tongyu. RCA3 reproduces a moderate r_{CT} over 3 stations (Lindenberg, Cabauw and Lamont), strong r_{CT} in Bondville, weak over BERMS, and weak and negative over Tongyu. In general, r_{CT} does not show any sensitivity to the increase in the wind speed.

The observed correlation coefficient between CBH and specific humidity (r_{CQ}) is weak in all six stations. CBH decreases with increasing QV at all stations except Bondville. There is no general agreement between the observed and simulated r_{CQ}. In CLM, r_{CQ} is positive over Cabauw but negative everywhere else, while in RSM, r_{CQ} is positive at Lamont and Bondville but nonexistent in BERMS. r_{CQ} is negative everywhere in GEMLAM and RCA3 and positive over all stations in MRCC. However, $r_{CQ} > 0.5$ over Tongyu for all models.

5.4 Conclusions

We investigated the skills of five regional climate models in reproducing the diurnal and seasonal cycles of surface energy fluxes, cloud base height and other surface parameters across twelve sites on four continents. We then used observed data as reference to study the coupling of cloud base height with the surface energy fluxes in the models at six midlatitude sites, Lindenberg (Europe), Cabauw (Europe), Lamont (North America), Bondville (North America), BERMS (North America) and Tongyu (Asia) by means of principal component analyses. Correlation coefficients between CBH and station surface variables then provided more understanding about the respective feedbacks between these variables and the CBH.

All models reproduced the stations' seasonal and diurnal patterns of the surface variables but with different biases. CLM and RCA3 gave the least errors in simulating diurnal and seasonal variation in the surface energy fluxes for all stations. All the models showed some difficulty with simulating the amplitudes of diurnal and season-

al temperature over tropical stations but gave a good reproduction over the midlatitude stations. Most models except GEMLAM however displayed a high over-overestimation of surface temperature at Himalayas, CLM errors being the highest at about 20 °C. This general error of the models in simulating temperature at the Himalayas station is most likely due to differences between actual station elevation and the corresponding grid points in the affected models. This is further verified by similar errors in magnitude occurring for pressure in these models. In simulating specific humidity, GEMLAM transferred very well across the validation stations however in RCA3, there is marked discrepancy between observed and simulated specific humidity over the two South American tropical stations Manaus and Santarem.

Regarding transferability of specific variables across domains for each model and taking net radiation as an example, it was found that CLM transferred best to home domains Lindenberg and Cabauw and to the midlatitude American domain of Lamont and Asian site Chao Praya. It transferred worst to high latitude American domain Bondville and the South American domains Manaus and Santarem. GEMLAM performs best in North American domain Lamont, Bondville and its Canadian home domain BERMS, with worst performance in the Himalayas and South American domain Santarem. MRCC transferred best to Bondville and also transferred better to the Asian domains of N. E. Thailand and the Himalayas than it does to its home domain BERMS. It transfers worst to the South American stations Manaus and Santarem. RCA3 transferred best to Tongyu and Mongolia, performed well for the midlatitude European and American domains as well as Chao Praya and worst to Himalayas and the South American stations. Interestingly, in separate RCM evaluation studies using the same set of models but focusing on precipitation, Meinke et al. (2007) and Rockel and Geyer (2008) found that the models gave the most erratic overestimation of precipitation in tropical and high altitude locations. RSM gives the poorest overall transferability for net radiation, showing no home advantage whatsoever, it does best over Chao Praya and N.E. Thailand, BERMS and Mongolia and worst over The South American and European stations.

The dominant factors coupling surface variables in the stations are the surface energy, thermodynamic and dynamic processes and usually in that order. All the models re-

produce these patterns except GEMLAM where the thermodynamic component is often undetectable over some stations. However GEMLAM shows a strong feedback between surface temperature and cloud base height at these stations and also strong connections between surface pressure and moisture. Observed summer daytime surface energy fluxes are well coupled to the cloud base height over most stations but poorly coupled over Lindenberg and Tongyu. All models except GEMLAM reproduce this coupling over all stations but usually with a stronger than observed magnitude. The sign of the coupling is however everywhere consistent with observations. The coupling between CBH and surface fluxes is slightly weaker over most stations under strong wind conditions (indicative of strong large scale forcing). This is reproduced in the models as well. In closing, the models generally transferred acceptably between domains and this is indicative of well adjusted combinations of parameterizations. Excellent transferability is expected of a model that is not tuned for a specific domain, one in which the underlying physics is general and thus applicable and recoverable in every respect. But such a model does not yet exist, (and some will argue would never exist). Where the transferability is bad, as in the case of RSM and GEMLAM, we see systematic errors at play or a less than ideal choice of parameterization for important processes. These are issues that can be addressed and corrected in models and this should be and is a continuing effort on the part of modelers.

Chapter 6

Synthesis

6.1 Summary

This thesis is an exploratory work which built on the preliminary results of the Transferability Working Group (TWG; Rockel, 2005; Takle et al., 2007). It focused on investigating the transferability of a suite of regional climate models from their respective domains of design and application to non-native domains across the globe. The primary aim was the investigation of the fourth transferability hypothesis which states "for non-monsoon regions experiencing weak synoptic scale forcing, the height of the cloud base is correlated with the daytime surface fluxes". The primary objectives of the thesis, in support of this aim are encapsulated in the following questions:

Do models couple cloud base with surface energy fluxes as seen in observations (Betts, 2004) and do they reproduce the observed diurnal and seasonal variations in the direction and magnitude of cloud base-surface energy flux couplings?

What influences do weak and strong synoptic forcings have on the coupling of cloud base height with surface fluxes in models?

What differences exist in the coupling of surface fluxes and cloud base height in monsoon versus non-monsoon domains?

Are there specific areas of commonalties or divergence in models, in other words, do the models in this study exhibit common weaknesses or strengths and on which aspects do they diverge?

Can we verify that regional models exhibit a 'home advantage' which gives them better predictive capabilities in their domain of development and application as suggested in the preliminary results of Takle et al. (2007)?

To investigate these issues, model output location time series from five regional climate models were compared with surface observations from three enhanced observing periods of the Coordinated Enhanced Observing Period programme of GEWEX, the Global Energy and Water Cycle Experiment. The models used in the study were CLM, the Climate version of the Lokal Modell (LM) run at the Geesthacht Institute for Coastal Research (GKSS), the Global Environmental Multiscale-Limited Area Model (GEM-LAM) of the University of Quebec at Montreal (Canada), Canadian Regional Climate Model (CRCM) of the Consortium on Regional Climatology and Adaptation to Climate Change (OURANOS) and the University of Quebec at Montreal, version 3 of the Rossby Centre Atmosphere model (RCA3) of the Swedish Meteorological and Hydrological Institute (SMHI) and RSM, the Regional Spectral Model of the United States Experimental Climate Prediction Centre.

By design, transferability studies are essentially anti-tuning experiments and therefore in the ICTS, each participating model used the same settings most suitable for its primary domain of design and application to simulate all the other domains of the study. To reduce all forms of variability that might occur due to external factors, all the models were forced at the lateral boundaries by the same reanalysis [National Centers for Environmental Prediction (NCEP2) reanalysis data].

In the first of two experiments, all five models are transferred to the European test bed station Cabauw, The Netherlands, in what was essentially a model intercomparison experiment. Cabauw's characteristic as homogeneous midlatitude grassland makes it a suitable site for model evaluation. Moreover at this site, deep soil remains saturated throughout the year ensuring that evapotranspiration is hardly hindered by water supply. Variability in water-storage time constants and variability in root-zone soil moisture across land surface schemes in RCMs are potential sources of model divergence (Shao, 1994; Yang et al., 1995) and these two features of Cabauw are expected to minimize this. We assessed the models' ability to correctly simulate the diurnal and seasonal cycles of surface state variables over the Cabauw test bed and subsequently gained a preliminary understanding of the relationship between surface fluxes and cloud base height as simulated by RCMs.

Having tested the models over Cabauw and armed with insight into how they performed, a second experiment involving multi-domain transferability intercomparison then followed, which focused on determining if and how the relationships identified over Cabauw change when the models are applied over different climate domains. The same models and model configuration as in the first experiment provided the dataset for this study. All five models were transferred across multiple domains, providing in essence, a comparison of several transferability experiments. The observed data is from the same time frame as the Cabauw experiment but this time for twelve stations across four continents, including the benchmark site Cabauw. Six of these stations, alongside Cabauw, were used in the principal component analysis. The other stations are Lindenberg (Germany, Europe), Lamont (USA, North America), BERMS (Canada, North America), Bondville (USA, North America) and Tongyu (China, Asia). The stations were chosen based on energy flux data availability for the period under investigation (October 2002 - December 2004). Soil moisture was excluded from the variables investigated to reduce the noise which might filter into the analyses from errors in soil moisture index values. The models were compared with observed data by means of analysis of bias of their diurnal and seasonal cycles. Statistical information on correlations and normalized standard deviations of modeled and observed data were evaluated for the summer daytime situation. A principal component analysis revealed information on the coupling structure of atmospheric variables in the various stations and finally correlations of cloud base height with other state variables are studied. This study revealed the controlling atmospheric processes which couple surface variables in these domains and the models' abilities to simulate the coupling between the surface energy fluxes and cloud base height at different stations. The key findings of these experiments are discussed in the following section.

6.2 Discussions

Results from model validations over Cabauw show that all five models are capable of reproducing well the diurnal and seasonal cycles of net radiation. RSM produces the largest bias, overestimating the annual cycle maximum by about 40 Wm^{-2}. This particular discrepancy is due to the choice of surface albedo constant in the model (0.06) which is much lower than observed (0.2). RSM is also the only spectral model in the

suite which, as suggested by Rockel and Geyer (2008), may explain the different structure in its results compared to the other models. Overall, in the partitioning of net radiation into the surface fluxes, the models made more energy available for latent heating than for sensible heating and this agrees with observations at Cabauw. The albedo error in RSM effectively transfers through partitioning to the surface fluxes of latent and sensible heat as reproduced by the model, giving it the poorest performance in the suite for these two variables. Taylor diagrams of correlation and standard deviations show that the CLM's simulation of surface fluxes is nearest to observation for Cabauw and agrees with the 'home advantage' effect of RCMs as reported in the findings of Takle et al. (2007).

Soil moisture is of major importance to land surface processes, since it controls the partitioning of available net radiation into sensible and latent heat flux, and of precipitation into infiltration and runoff. All the RCMs performed poorly in simulating soil moisture over Cabauw. While the observed diurnal cycle of soil moisture is invariant, the seasonal cycle reflected the effect of summer latent heating which depletes soil moisture by 0.3 m more than in winter. This winter-summer difference is not captured by any of the models. There are various reasons why soil moisture is one of the least known variables in climate simulations. Soil moisture is usually highly heterogeneous in space due to soil type variability and is not a routinely observed variable on scales larger than catchments (Pan et al., 2001). This variability severely reduces the representativeness of soil moisture measurement and complicates its parameterization in numerical models. In a study to investigate the causes of poor performance of RCMs at capturing soil moisture, Pan et al. (2001) compared soil moisture variations in 10-year regional climate simulations with observed soil moisture data for Illinois and Iowa and found that errors in soil moisture correspond both in space and time with precipitation errors indicating that much of the soil moisture error is attributable to a low bias of precipitation. Their results indicate that improvement of soil moisture simulation will depend mainly on improvement in predicting precipitation, and better representation of biophysical processes that control evapotranspiration.

Temperature is another key state variable in the evaluation of model performance. The poor performance of all five models in simulating soil moisture notwithstanding, they

reproduced the diurnal and seasonal cycles of surface temperature quite well, only GEMLAM overestimates summer surface temperature by up to 2 ^{o}C while MRCC underestimates it by the same value. According to the Fourth Assessment Report (IPCC: Solomon et al., 2007), studies have shown that RCMs capture the spatial variation of temperature and precipitation in Europe better than global models but tend to simulate warmer and drier conditions in summer, both when driven by analyzed boundary conditions (Hagemann et al., 2004) and when driven by GCM data (e.g. Jacob et al., 2007). Most but not all RCMs also overestimate the interannual variability of summer temperatures (Jacob et al., 2007; Lenderink et al., 2007; Vidale et al., 2007). The excessive temperature variability is linked with excessive interannual variability in either shortwave radiation or evaporation, or both (Lenderink et al., 2007). This implies a need for improvement in the modeling of soil, boundary layer and cloud processes. One of the key model parameters may be the depth of the hydrological soil reservoir, which appears to be too small in many RCMs (Van den Hurk et al., 2005) as the case is with GEMLAM.

The simulated diurnal and seasonal cycles of cloud base height agree with observations with maximum heights in summer and minimum in winter. The RCMs are thus consistent with ceilometer data in terms of variation while in terms of magnitude, the measured values are much higher. This is to be expected as the cloud base height used in the study is calculated by means of parcel theory which results in lifted condensation levels bordering on the lower bounds of actual measured cloud bases. GEMLAM produced the highest bias in CBH of all the models and this could well be related to the above concerns on model parameterizations.

The principal component analysis of surface fluxes, cloud base height and state variables revealed the controlling atmospheric processes that link variables over Cabauw. This study found that summer daytime loadings gave the strongest couplings of variables. Three major processes were identified over Cabauw. First and most dominant is the surface energy process which couples sensible and latent heat with net radiation. The second process is thermodynamic, coupling temperature and surface moisture (specific humidity) and the third is a dynamic process which couples pressure and wind speed. The findings of the study strongly support the hypothesis in that cloud

base height is well coupled to the surface fluxes over Cabauw in the models and that this coupling is stronger in summer than in winter. However we found that wind speed has no definite influence over the strength of this coupling. This is attributable to the homogeneous nature of the Cabauw pastor lands and therefore invited investigation over other domains with different climatic regimes. Will the effect of strong large scale forcing (represented by strong wind speed regimes in the models) affect the coupling of cloud base height and surface energy fluxes in these domains? The transferability intercomparison sought to answer this question and the findings are presented below.

The intercomparison across the six midlatitude domains confirmed the findings at Cabauw that the cloud base is correlated with surface energy fluxes as in observation and the sign of the correlations in the models is as observed. This finding is important for the modeling community as it establishes the fact that the models are actually simulating the direction of influence of surface fluxes and possibly, soil water variability, on cloud processes (Betts, 2004). This implies that the models are also able to reproduce the consequent feedbacks on surface radiation and resulting surface fluxes induced by cloud occurrences.

The simulation of the amplitude and phase of the diurnal cycle is an important metric for testing the representation of land surface-atmosphere interactions. It is also useful for verification of the physical parameterizations (land surface, planetary boundary layer, cloud processes etc.) of a model (Yang et al., 2002) . The models we tested clearly reproduce the diurnal and seasonal variations of the key surface variables although with amplitudes different from observed and markedly so in a few cases. These biases and errors in amplitude serve a useful purpose, being in essence pointers to those parameterizations which need improvement in the affected models. Examples of such errors revealed in our analysis include the location-specific grid point elevation error in CLM (over the Himalayas) and the incorrect prescribed surface albedo in RSM. Thus we see that a model transfers differently across various climatic domains and that while some model errors are systematic, others could be domain-specific. Overall CLM transfers best generally across the six domains while RSM transfers worst. It is worth noting here that apart from RSM being the only spectral model in

the lot, it is also the only one that employed a different convection scheme (Simplified Arakawa Schubert scheme, Pan and Wu, 1995) while the other models all used the Kain-Fritch mass flux scheme. However, accuracy in simulating specific variables was found not to be the sole purvey of any single model. For example CLM's simulation of temperature over Himalayas is very poor in comparison to the other models and this is attributed to the difference in actual station height and the model grid point elevation nearest to the station coordinates. It is thus useful to approach these model comparison efforts carefully, from a point of view of understanding the causes of inter-model deficiencies and/or strengths rather than seeking out the 'best' model for the job.

The dominant factors coupling surface variables, as identified over Cabauw, hold across the other domains for all the models except GEMLAM. GEMLAM stands apart from the remaining models in that the thermodynamic component is unidentifiable over some stations. In fact, while most models consistently simulate a stronger coupling between cloud base and the surface fluxes than observed, coupling in GEMLAM was found to be weaker. This issue may be due to the choice of parameterization the model employs for radiation scheme. The model also exhibits a strong feedback between surface temperature and cloud base height at these stations. GEMLAM's sister model MRCC performs more akin to the European models in how it couples the surface fluxes with the cloud base.

With regard to the influence of weak and strong synoptic forcing on the coupling of cloud base height with surface fluxes in models, we found that in homogeneous domains e.g. Cabauw, the presence or lack of synoptic forcing has a negligible impact on the strength of coupling. Upon transfer to other less homogenous domains of the study, a very slight decrease in the strength of coupling is seen in most of the models, under strong large scale forcing. This would suggest that the coupling between cloud base height and surface fluxes is possibly more influenced by radiative forcing than by synoptic controls.

On the issue commonalty, the models all struggle with simulating the tropical domains as evident in their performance over Manaus and Santarem which are both

quite close to the equator. This is a well known problem for regional models and it stresses the need for the development of model parameterizations with the major climate controls of the tropics taken well into account. This of course requires a better understanding of the physics of climate of the region and an extremely important factor, especially for tropical Africa, i.e. high temporal resolution observational data! All the models showed remarkable skill in simulating temperature more than any other variable. This is interesting given that there are significant differences in their simulation of radiative and non-radiative surface fluxes which influence temperature. An explanation could be that the different noises from the radiative fluxes cancel out quite well giving a mean temperature variation which is closer to observations. Studies by Meinke et al. (2007) and Rockel and Geyer (2008) also show these same suite of models as generally performing well in the simulation of precipitation. Temperature and precipitation are the two most important surface variables in climate and climate change and a lot of modeling groups take their models through rigorous testing and adaptation (tuning) processes to ensure these variables behave as expected before running actual simulations. A question that comes to mind in the light of this analysis is, are we arriving the right answers through the wrong routes?

Takle et al. (2007) found in their pioneering study on transferability that models exhibit a slight 'home advantage' which gives them better predictive capabilities in their domain of development. This home advantage was evident in our study over Cabauw, where the European models CLM and RCA3 performed better overall than the remaining models. Our multidomain transferability intercomparison however sheds an interesting light on the home advantage issue. While each model generally gave its best results over its own domain of development, it does not necessarily mean such a result is the best for all models applied over such a domain. An example of this is GEMLAM which, when its performance over all domains is evaluated, undoubtedly performed best over its North American home domain. But CLM performed better over North America than GEMLAM. In essence, we found that the home advantage issue is one of 'personal best' where regional models are concerned.

This thesis has provided a useful approach for the systematic intercomparison of models across domains to expose singular and collective biases in the modeling pro-

cess. Using a different approach to earlier intercomparisons, we made use of principal component analysis, a statistical tool; to bring out the underlying physical relationships between surface fluxes and the cloud base. We assessed models' skills in reproducing the diurnal and seasonal cycles. In general, amplitudes of biases were found to be higher over tropical stations than the midlatitudes. Our investigation confirms the transferability hypothesis which states that models do reproduce the observed coupling between cloud base height and the surface fluxes in summer daytime non-monsoon climates under weak large scale forcing. A weak coupling is not necessarily wrong or erroneous and in many cases coupling in models is much stronger than observed. The weak nature of these couplings in observations at Tongyu (and to a less extent, Lindenberg) could be due to observational accuracy issues (this would be especially true at locations with weaker diurnal cycles).

We have shown that there are strong couplings between the cloud base height and the surface energy budget and that models in their present formulation are able to simulate this to varying extents as allowed by their parameterizations. The implication of this for modelers of regional climate is that boundary layer processes, clouds and land surface components in models should be evaluated as a tightly coupled system, rather than as independent discrete components.

This entire analysis provides a robust framework for comparing models with each other, and for validating them against climate observations. This is a huge task which we are just beginning to scratch the surface of. In addition, the varied couplings and complex feedbacks of processes on the land surface presents a major validation challenge for models that employ interchangeable parameterization schemes for the different physical processes. Since these feedbacks are likely to change each time a module is changed, their combination needs careful evaluation.

6.2.1 Caveats

As with any model evaluation study, these studies are limited by a few caveats and assumptions and these should be taken into consideration when interpreting the results.

As discussed in earlier studies (e.g. Meinke et al., 2004; Meinke, 2006) there are two major sources of uncertainties in the evaluation of regional model simulations. First is the uncertainty in the observation data used in validating the model results. The second source of uncertainties stem from the lateral boundary conditions used to drive the RCM simulations (Palmer, 2000; Vidale et al., 2003). On the observation data aspect, only surface data was used in these analyses, there was no sounding data that could shed more light on the boundary layer properties e.g. boundary layer thickness and structure. In the same light, lifted condensation levels, calculated using the parcel theory assumption, were used as proxy for cloud base height. The observed data moreover are from high resolution CEOP measuring campaigns but there is no consideration of observation errors beyond the quality control carried out prior to the release of the data to the scientific community. Regarding the models, various uncertainties are introduced from the spatial representation of land surface heterogeneities. No attempt was made to unify the various land surface schemes employed by the models that participated in these experiments. Inter-model variability is a huge factor in model evaluation results and studies have shown that the same model could give widely differing results based on the choice of schemes it employs to parameterize key processes like convection and large scale condensation (Hagemann et al., 2004).

The focus of this work is on the surface energy fluxes and as such the errors from the models' internal physics will carry through to this. As mentioned earlier, RCM errors can also arise from errors carried over through the forcing reanalysis or GCM at the lateral boundaries. Although the effect of this has been minimized in this experiment by the use of the same forcing for all models, the inconsistencies between model solutions and lateral boundary forcings can still produce noise differently in the models based on their sponge zone implementations (Davies, 1976). This study has used the observed data as is and has not taken into account either class of uncertainties. It is worth metioning here that there are some emerging class of GCMs with adaptive variable grids (e.g. cubed-grid; icosahedral grid with ying-Yang descretizations) which could address some of the afore mentioned deficiencies of RCMs. For example, the ICOsahedral Non-hydrostatic General Circulation Model (ICON GCM) comes with a new dynamical core which solves the system of equations in grid point space on the icosahedral grid, allowing quasi-isotropic horizontal resolution on the sphere and re-

striction to regional domains. Another example is the still-in-development CAM-EULAG, which is an implementation of the EULAG non-hydrostatic, parallel computational model as a dynamical core in the Community Atmospheric Model (CAM). CAM-EULAG allows higher resolution in selected regions without causing anomalous behavior such as spurious wave reflection. (see Abiodun et. al. 2008).

6.3 Recommendations

It would be highly desireable to have an African domain included in such a study as this. Transferability is a major issue for simulations and climate change studies over the African continent because the models we employ for research and operational purposes come from and are primarily designed for non-native domains. More specifically, these models are usually from midlatitudes where the dominant controls on the climate are different. Transferability intercomparisons would definitely bring an increase in understanding in climate modeling in the tropical and sub tropical regions of the African continent. The ICTS realizes the importance of this and West African (AMMA) domain was an integral part of the coordinated simulations. However till date, no high resolution enhanced observation campaigns had been carried out over the continent and these measurements are much needed for such intercomparisons as were done in this study. Important diagnostic variables like relative humidity, cloud base, and cloud cover should be measured along with the radiation fields in climate measuring campaigns which traditionally usually measure temperature, precipitation, and solar radiation.

It needs be mentioned here that the single biggest scientific problem in dealing with climate change over Africa is the dearth of qualitative observations. Having said this, it is however hoped that the ongoing African Monsoon Multidisciplinary Analyses (AMMA) field campaign should provide some much needed high resolution data for future transferability studies over the West African region. The participation and use of more models will also provide a wider repertoire of model transferability knowledge to add to the global model intercomparison framework, in a region where the scientific community is dependent on models designed primarily with the midlatitude climates in mind.

To this end, the recently established COordinated Regional climate Downscaling Experiment (CORDEX) is a welcome development. CORDEX, already mentioned in the first chapter, is a World Climate Research Program (WPRC) sponsored effort to organize an international coordinated framework to produce an improved generation of regional climate change projections world-wide for input into impact and adaptation studies within the IPCC Fifth Assessment Report (AR5) timeline and beyond. With initial focus on Africa, multiple common domains covering all (or most) land areas in the World have been selected for CORDEX simulations to produce an ensemble of multiple dynamical and statistical downscaling models considering multiple forcing GCMs from the CMIP5 archive. Longer simulations will facilitate investigations of inter-annual variability in models while higher temporal resolutions will provide improved representation of their diurnal cycles. Such a coordinated global effort would undoubtedly provide a database of high resolution simulations over Africa which would benefit model evaluation, assessment and transferability initiatives. More importantly as a spin-off, it would also hopefully engender much needed high temporal resolution observation campaigns over the African region.

Acronyms

AIACC	Assessments of Inputs and Adaptations to Climate Change
AMIP	Atmospheric Model Intercomparison Project
AMIP2	Atmospheric Model Intercomparison Project version 2
AMMA	African Monsoon Multidisciplinary Analysis
AOGCM	Atmosphere-Ocean General Circulation Models
ArcMIP	Arctic Regional Climate Model Intercomparison Project
ARM	Atmospheric Radiation Measurement
BALTEX	Baltic Sea Experiment
BERMS	Boreal Ecosystem Research and Monitoring Sites
CMIP5	Coupled Model Intercomparison Project Phase 5
CEOP	Coordinated Energy and Water Cycle Observations Project (formerly Coordinated Enhanced Observing Period)
CLM	Climate version of the Lokal Model
CORDEX	COordinated Regional climate Downscaling Experiment
CRCM	Canadian Regional Climate Model
CSE	Continental Scale Experiment
ECMWF	European Centre for Medium-Range Weather Forecasts
ECPC	Experimental Climate Prediction Center
EOP	Enhanced Observing Period
GAME	GEWEX Asian Monsoon Experiment
GAPP	GEWEX Americas Prediction Project
GCSS	GEWEX Cloud System Study
GEMLAM	Global Environmental Multiscale-Limited Area Model

GEWEX	Global Energy and Water Cycle Experiment
GHP	GEWEX Hydrometeorology Panel
ICTS	Inter-CSE Transferability study
IRI/ARC	International Research Institute/Applied Research Centers
LAM	Limited Area Model
LBA	Large-Scale Biosphere–Atmosphere
LPB	La Plata Basin
LRGSCL	Large Scale Condensation Routine
LSM	(Noah) Land Surface Model
MAGS	Mackenzie GEWEX Study
MDB	Murray-Darling Basin
MIP	Model Intercomparison Projects
MRCC	(*see* CRCM)
NAMAP	North American Monsoon Model Assessment Project
NAME	North American Monsoon Experiment
NAMS	North American Monsoon System
NCEP2	National Centers for Environmental Prediction 2
NEWBALTIC	Numerical Studies of the Energy and Water Cycle in the Baltic region
OGCM	Ocean only Global Climate Models
PIRCS	Project to Intercompare Regional Climate Simulations
PRUDENCE	Prediction of Regional Scenarios and Uncertainties for Defining European Climate Change Risks and Effects
QUIRCS	Quantification of Uncertainties in Regional Climate Change and Climate Change Simulations
RCA3	Rossby Centre Atmospheric regional climate model v3
RCM	Regional Climate Model

RMIP	Regional Climate Model Intercomparison Project for Asia
RSM	Regional Spectral Model
SGMIP	Structured Grid Model Intercomparison Project
SGP	Southern Great Plains
SHEBA	Surface Heat Budget of the Arctic Ocean
TWG	Transferability Working Group
USGS	United States Geological Survey
WCRP	World Climate Research Programme

References

Abiodun, B. J., Prusa, J. M., and Gutowski, W. J. (2008). Implementation of a non-hydrostatic, adaptive-grid dynamics core in CAM3. Part I: Comparison of dynamics cores in aquaplanet simulations. *Clim. Dynamics*, 31, 795-810.

Abiodun, B., Pal, J., Afiesimama, E., Gutowski, W., & Adedoyin, A. (2008). Simulation of West African monsoon using RegCM3 Part II: impacts of de-forestation and desertification. *Theoretical and Applied Climatology, 93*(3), 245-261.

Albrecht, B. (1981). Parameterization of trade-cumulus cloud amounts. *Journal of the Atmospheric Sciences, 38*(1), 97-105.

Allen, M., & Ingram, W. (2002). Constraints on future changes in climate and the hydrologic cycle. *Nature, 419*(6903), 224-232.

Allmen, M. C., & Kegelmeyer, W. P. (1996). The computation of cloud-base height from paired whole-sky imaging cameras. *Journal of Atmospheric and Oceanic Technology, 13*(1), 97-113.

Arakawa, A. (2004). The cumulus parameterization problem: Past, present, and future. *Journal of Climate, 17*, 2493-2525.

Bard, E. (2002). Climate shock: Abrupt changes, over millennial time scales. *Physics Today, 55*(12), 32-38.

Barros, A., & Hwu, W. (2002). A study of land-atmosphere interactions during summertime rainfall using a mesoscale model. *Journal of Geophysical Research-Atmospheres, 107*(D14), 4227.

Bechtold, P., Bazile, E., Guichard, F., Mascart, P., & Richard, E. (2001). A mass-flux convection scheme for regional and global models. *Quarterly Journal of the Royal Meteorological Society, 127*(573), 869-886.

Bélair, S., Crevier, L., Mailhot, J., Bilodeau, B., & Delage, Y. (2003). Operational implementation of the ISBA land surface scheme in the Canadian regional weather forecast model. Part I: Warm season results. *Journal of hydrometeorology, 4*(2), 352-370.

Beljaars, A., & Bosveld, F. (1997). Cabauw data for the validation of land surface parameterization schemes. *Journal of Climate, 10*(6), 1172-1193.

Bengtsson, L. (1995). Baltic Sea Experiment BALTEX: Initial implementation plan. International Baltex Secretariat Publ. (Available from Max-Planck-Institute for Meteorology, Hamburg), 2, 84.

Beniston, M., Stephenson, D., Christensen, O., Ferro, C., Frei, C., Goyette, S., et al. (2007). Future extreme events in European climate: an exploration of regional climate model projections. *Climatic Change, 81*, 71-95.

Berger, A., & Loutre, M. (2004). Astronomical theory of climate change. *Journal of Physics IV France, 121*, 1-35.

Betts, A. K. (2004). Understanding hydrometeorology using global models. *Bulletin of the American Meteorological Society, 85*(11), 1673-1688. doi: 10.1175/bams-85-11-1673

Betts, A. K., Chen, F., Mitchell, K. E., & Janjić, Z. I. (1997). Assessment of the Land Surface and Boundary Layer Models in Two Operational Versions of the NCEP Eta Model Using FIFE Data. *Monthly Weather Review, 125*(11), 2896-2916. doi: doi:10.1175/1520-0493(1997)125<2896:AOTLSA>2.0.CO;2

Beyrich, F., & Adam, W. (2004). A note on the use of CEOP reference site data for comparison with the output of global models: The Lindenberg example. *CEOP Newsletter, 6*, 6–7.

Bigg, G., & Wadley, M. (2001). Millennial-scale variability in the oceans: an ocean modelling view. *Journal of Quaternary Science, 16*(4), 309-319.

Bjerknes, V. (1904). Das Problem der Wettervorhersage, betrachtet vom Standpunkte der Mechanik und der Physik. *Meteorologische Zeitschrift, 21*, 1–7.

Bond, G. C., & Lotti, R. (1995). Iceberg Discharges into the North-Atlantic on Millennial Time Scales during the Last Glaciation. *Science, 267*(5200), 1005-1010.

Bosilovich, M. G., & Lawford, R. (2002). Coordinated Enhanced Observing Period (CEOP) International Workshop (Vol. 83, pp. 1495-1499).

Cahalan, R., Ridgway, W., Wiscombe, W., Bell, T., & Snider, J. (1994). The albedo of fractal stratocumulus clouds. *Journal of the Atmospheric Sciences, 51*(16), 2434-2455.

Cattell, R. (1966). The scree test for the number of factors. *Multivariate behavioral research, 1*(2), 245-276.

Caya, D., & Laprise, R. (1999). A semi-implicit semi-Lagrangian regional climate model: The Canadian RCM. *Monthly Weather Review, 127*(3), 341-362.

Cess, R., Zhang, M., Ingram, W., Potter, G., Alekseev, V., Barker, H., et al. (1996). Cloud feedback in atmospheric general circulation models: An update. *Journal of Geophysical Research, 101*(D8), 12791.

Cess, R. D., Potter, G. L., Blanchet, J. P., Boer, G. J., Ghan, S. J., Kiehl, J. T., et al. (1989). Interpretation of Cloud-Climate Feedback as Produced by 14 Atmospheric General-Circulation Models. *Science, 245*(4917), 513-516.

Chen, T., Henderson-Sellers, A., Milly, P., Pitman, A., Beljaars, A., Polcher, J., et al. (1997). Cabauw experimental results from the project for intercomparison of land-surface parameterization schemes. *Journal of Climate, 10*(6), 1194-1215.

Chou, M. (1992). A solar radiation model for use in climate studies. *Journal of the Atmospheric Sciences, 49*(9), 762-772.

Chou, M., & Lee, K. (1996). Parameterizations for the absorption of solar radiation by water vapor and ozone. *Journal of Atmospheric Sciences, 53*, 1203-1208.

Chou, M., & Suarez, M. (1994). An efficient thermal infrared radiation parameterization for use in general circulation models. *NASA Tech. Memo, 104606*(3), 85.

Chou, M., & Suarez, M. (1996). A solar radiation parameterization (CLIRAD-SW) for atmospheric studies. . *NASA Technical Memorandum no. 104606., 15*, 40 pp.

Christensen, J. (2005). Prediction of Regional scenarios and Uncertainties for Defining EuropeaN climate change risks and Effects. PRUDENCE Final Report (pp. 269).

Christensen, J., Carter, T., Rummukainen, M., & Amanatidis, G. (2007). Evaluating the performance and utility of regional climate models: the PRUDENCE project. *Climatic Change, 81*, 1-6.

Christensen, J., Machenhauer, B., Jones, R., Schär, C., Ruti, P., Castro, M., et al. (1997). Validation of present-day regional climate simulations over Europe: LAM simulations with observed boundary conditions. *Climate Dynamics, 13*(7), 489-506.

Christensen, J. H., & Christensen, O. B. (2007). A summary of the PRUDENCE model projections of changes in European climate by the end of this century. *Climatic Change, 81*, 7-30. doi: DOI 10.1007/s10584-006-9210-7

Christensen, O., Christensen, J., Machenhauer, B., & Botzet, M. (1998). Very high-resolution regional climate simulations over Scandinavia—Present climate. *Journal of Climate, 11*, 3204-3229.

Collins, M., Osborn, T., Tett, S., Briffa, K., & Schweingruber, F. (2002). A comparison of the variability of a climate model with paleotemperature estimates from a network of tree-ring densities. *Journal of Climate, 15*, 1497–1515.

Côté, J. (1997). Variable resolution techniques for weather prediction. *Meteorology and Atmospheric Physics, 63*(1), 31-38.

Côté, J., Desmarais, J., Gravel, S., Méthot, A., Patoine, A., Roch, M., et al. (1998a). The operational CMC–MRB global environmental multiscale (GEM) model. Part II: Results. *Monthly Weather Review, 126*(6), 1397-1418.

Côté, J., Gravel, S., Méthot, A., Patoine, A., Roch, M., & Staniforth, A. (1998b). The operational CMC–MRB global environmental multiscale (GEM) model. Part I: Design considerations and formulation. *Monthly Weather Review, 126*(6), 1397-1418.

Cubasch, U., Meehl, G., Boer, G., Stouffer, R., Dix, M., Noda, A., et al. (2001). Projections of future climate change: PNNL-SA-39649, JT Houghton, et al; Cambridge University Press, New York, NY, United States (US).

Cubasch, U., Voss, R., Hegerl, G., Waszkewitz, J., & Crowley, T. (1997). Simulation of the influence of solar radiation variations on the global climate with an ocean-atmosphere general circulation model. *Climate Dynamics, 13*(11), 757-767.

Cuxart, J., Bougeault, P., & Redelsperger, J. (2000). A turbulence scheme allowing for mesoscale and large-eddy simulations. *Quarterly Journal of the Royal Meteorological Society, 126*(562), 1-30.

Dai, A., & Trenberth, K. E. (2004). The Diurnal Cycle and Its Depiction in the Community Climate System Model. *Journal of Climate, 17*(5), 930-951. doi: doi:10.1175/1520-0442(2004)017<0930:TDCAID>2.0.CO;2

Davies, H. C. (1976). Lateral Boundary Formulation for Multilevel Prediction Models. *Quarterly Journal of the Royal Meteorological Society, 102*(432), 405-418.

Déqué, M., Jones, R. G., Wild, M., Giorgi, F., Christensen, J. H., Hassell, D. C., et al. (2005). Global high resolution versus Limited Area Model climate change projections over Europe: quantifying confidence level from PRUDENCE results. *Climate Dynamics, 25*(6), 653-670. doi: DOI 10.1007/s00382-005-0052-1

Déqué, M., Rowell, D., Lüthi, D., Giorgi, F., Christensen, J., Rockel, B., et al. (2007). An intercomparison of regional climate simulations for Europe: assessing uncertainties in model projections. *Climatic Change, 81*, 53-70.

Dickinson, R. (1986). How will climate change? The climate system and modelling of future climate. In B. Bolin, Döos, B.R., Jäger, J. and Warrick, R.A (Ed.), *The Greenhouse Effect, Climatic Change, and Ecosystems (SCOPE 29)* (pp. 206-270).

Dickinson, R. (2000). How coupling of the atmosphere to ocean and land helps determine the timescales of interannual variability of climate. *Journal of Geophysical Research, 105*(D15), 20115-20119.

Dickinson, R., Errico, R., Giorgi, F., & Bates, G. (1989). A regional climate model for the western United States. *Climatic Change, 15*(3), 383-422.

Dudek, M., Liang, X., & Wang, W. (1996). A regional climate model study of the scale dependence of cloud-radiation interactions. *Journal of Climate, 9*(6), 1221-1234.

Eva, H., Belward, A., De Miranda, E., Di Bella, C., Gond, V., Huber, O., et al. (2004). A land cover map of South America. *Global Change Biology, 10*(5), 731-744.

Fu, C. B., Wang, S. Y., Xiong, Z., Gutowski, W. J., Lee, D. K., McGregor, J. L., et al. (2005). Regional climate model intercomparison project for Asia. *Bulletin of the American Meteorological Society, 86*(2), 257-266. doi: 10.1175/bams-86-2-257

Gal-Chen, T., & Somerville, R. (1975). On the use of a coordinate transformation for the solution of the Navier-Stokes equations. *Journal of Computational Physics, 17*, 209-228.

Gates, W. L. (1992). Amip - the Atmospheric Model Intercomparison Project. *Bulletin of the American Meteorological Society, 73*(12), 1962-1970.

Giorgi, F. (1989). Two-dimensional simulations of possible mesoscale effects of nuclear war fires 1. Model description. *Journal of Geophysical Research, 94*(D1).

Giorgi, F. (1990). Simulation of regional climate using a limited area model nested in a general circulation model. *Journal of Climate, 3*(9), 941-963.

Giorgi, F. (2006). Regional climate modeling: Status and perspectives. *J. Phys. IV France, 139*, 101-118.

Graham, L. P., & Bergström, S. (2000). Land surface modelling in hydrology and meteorology - lessons learned from the Baltic Basin. *Hydrology and Earth System Sciences, 4*(1), 13-22.

Graham, L. P., & Bergström, S. (2001). Water balance modelling in the Baltic Sea drainage basin - analysis of meteorological and hydrological approaches. *Meteorology and Atmospheric Physics, 77*(1-4), 45-60.

Graves, C. E., Valdes, J. B., Shen, S. S. P., & North, G. R. (1993). Evaluation of Sampling Errors of Precipitation from Spaceborne and Ground Sensors. *Journal of Applied Meteorology, 32*(2), 374-385.

Grell, G. (1993). Prognostic evaluation of assumptions used by cumulus parameterizations. *Monthly Weather Review, 121*(3), 764-787.

Gutowski, W., Takle, E., & Arritt, R. (1998). Project to Intercompare Regional Climate Simulations, Workshop II, 5-6 June 1997. *Bulletin of the American Meteorological Society, 79*(4), 657-659.

Gutzler, D. S., Kim, H. K., Higgins, R. W., Juang, H. M. H., Kanamitsu, M., Mitchell, K., et al. (2005). The North American Monsoon Model Assessment Project - Integrating numerical modeling into a field-based process study. *Bulletin of the American Meteorological Society, 86*(10), 1423-1429. doi: Doi 10.1175/Bams-86-10-1423

Hagemann, S., Machenhauer, B., Jones, R., Christensen, O., Déqué, M., Jacob, D., et al. (2004). Evaluation of water and energy budgets in regional climate models applied over Europe. *Climate Dynamics, 23*(5), 547-567.

Hair, J., Anderson, R., Tatham, R., & Black, W. (1998). *Multivariate data analysis* (5th ed.): Prentice-Hall, Englewood Cliffs, NJ.

Hall, N., & Valdes, P. (1997). A GCM simulation of the climate 6000 years ago. *Journal of Climate, 10*(1), 3-17.

Haltiner, G., & Williams, R. (1980). *Numerical prediction and dynamic meteorology*: John Wiley and Sons, New York.

Hamelbeck, F., Haimberger, L., & Hantel, M. (2001). Convection in PIDCAP part I: Evaluating LAM convection. *Meteorology and Atmospheric Physics, 77*(1-4), 85-98.

Hansen, J., Sato, M., Lacis, A., Ruedy, R., Tegen, I., & Matthews, E. (1998). Climate forcings in the industrial era. *Proceedings of the National Academy of Sciences, 95*(22), 12753-12758.

Hansen, J., Sato, M., & Ruedy, R. (1997a). Radiative forcing and climate response. *Journal of Geophysical Research, 102*(D6), 6831–6864.

Hansen, J., Sato, M., Ruedy, R., Lacis, A., Asamoah, K., Beckford, K., et al. (1997b). Forcings and chaos in interannual to decadal climate change. *Journal of Geophysical Research-Atmospheres, 102*(D22), 25679-25720.

Hansen, J., Sato, M., Ruedy, R., Nazarenko, L., Lacis, A., Schmidt, G., et al. (2005). Efficacy of climate forcings. *Journal of Geophysical Research, 110*(D18), D18104.

Harvey, L. (2000). Climate and global environmental change: Prentice Hall.

Harvey, L., Gregory, J., Hoffert, M., Jain, A., Lal, M., Leemans, R., et al. (1997). An introduction to simple climate models used in the IPCC Second Assessment Report. *IPCC Technical Paper II*, 26-27.

Henderson-Sellers, A., & McGuffie, K. (1987). *A climate modelling primer*: Wiley. Chichester. GB.

Henderson-Sellers, A., Pitman, A., Love, P., Irannejad, P., & Chen, T. (1995). The project for intercomparison of land surface parameterization schemes (PILPS): Phases 2 and 3. *Bulletin of the American Meteorological Society, 76*(4), 489-503.

Hewitson, B. C., & Crane, R. G. (1996). Climate downscaling: techniques and application. *Climate Research, 07*(2), 85-95.

Hong, S., & Pan, H. (1996). Nonlocal boundary layer vertical diffusion in a medium-range forecast model. *Monthly Weather Review, 124*(10), 2322-2339.

Hotelling, H. (1933). Analysis of a complex of statistical variables into principal components. *Journal of educational psychology, 24*(6), 417-441.

Houghton, J., Ding, Y., Griggs, D., Noguer, M., van der Linden, P., Dai, X., et al. (2001). Climate change 2001: the scientific basis. Contributions ofWorking

Group I to the Third Assessment Report of the Intergovernmental Panel on Climate Change: Cambridge University Press Cambridge.

Jacob, D., Bärring, L., Christensen, O., Christensen, J., de Castro, M., Déqué, M., et al. (2007). An inter-comparison of regional climate models for Europe: model performance in present-day climate. *Climatic Change, 81*, 31-52.

Jacob, D., Van den Hurk, B. J. J. M., Andrae, U., Elgered, G., Fortelius, C., Graham, L. P., et al. (2001). A comprehensive model inter-comparison study investigating the water budget during the BALTEX-PIDCAP period. *Meteorology and Atmospheric Physics, 77*(1-4), 19-43.

Jacobsen, I., & Heise, E. (1982). A new economic method for the computation of the surface temperature in numerical models. *Beitraege zur Physik der Atmosphaere, 55*(2), 128-141.

James, I. (1994). *Introduction to circulating atmospheres*: Cambridge University Press.

Janeiro, F. M., Wagner, F., Ramos, P. M., & Silva, A. M. (2009). *Cloud base height estimation using a low-cost digital camera*. Paper presented at the XIX IMEKO World Congress Fundamental and Applied Metrology, Lisbon, Portugal.

Jiao, Y., & Caya, D. (2006). An investigation of summer precipitation simulated by the Canadian Regional Climate Model. *Monthly Weather Review, 134*(3), 919-932.

Jolliffe, I. T. (1990). Principal component analysis: A beginner's guide- Introduction and application. *Weather, 45*, 375-382.

Jones, C., & Sanchez, E. (2002). The representation of shallow cumulus convection ans associated cloud fields in the Rossby Centre Atmospheric Model. *Hirlam Newsletter, 41*, 91–106.

Jones, C., Ullerstig, A., Willén, U., & Hansson, U. (2004a). The Rossby Centre regional atmospheric climate model (RCA). Part I: Model climatology and performance characteristics for present climate over Europe. *Ambio, 33*(4-5), 199-210.

Jones, C., Wyser, K., Ullerstig, A., & Willén, U. (2004b). The Rossby Centre Regional Atmospheric Climate Model Part II: Application to the Arctic Climate. *AMBIO: A Journal of the Human Environment, 33*(4), 211-220.

Jones, P., & Mann, M. (2004). Climate over past millennia. *Rev. Geophys, 42*(2), 1–42.

Jones, R., Murphy, J., & Noguer, M. (1995). Simulation of climate change over Europe using a nested regional-climate model: I: assessment of control climate, including sensitivity to location of lateral boundaries. *Quarterly Journal of the Royal Meteorological Society, 121*(526), 1413-1450.

Juang, H.-M. H., Hong, S.-Y., & Kanamitsu, M. (1997). The NCEP Regional Spectral Model: An Update. *Bulletin of the American Meteorological Society, 78*(10), 2125-2143.

Juang, H. M. H., & Kanamitsu, M. (1994). The NMC Nested Regional Spectral Model. *Monthly Weather Review, 122*(1), 3-26.

Kain, J., & Fritsch, J. (1993). The representation of cumulus convection in numerical models. *Meteor. Monger, 46*, 165-177.

Kain, J. S., & Fritsch, J. M. (1990). A One-Dimensional Entraining Detraining Plume Model and Its Application in Convective Parameterization. *Journal of the Atmospheric Sciences, 47*(23), 2784-2802.

Kaiser, H. (1958). The varimax criterion for analytic rotation in factor analysis. *Psychometrika, 23*(3), 187-200.

Källén, E. (1996). HIRLAM documentation manual *System* (Vol. 2, pp. 178 pp.).

Kalnay, E., & Cai, M. (2003). Impact of urbanization and land-use change on climate (vol 423, pg 528, 2003). *Nature, 425*(6953), 102-102. doi: Doi 10.1038/Nature01952

Kanamitsu, M., Ebisuzaki, W., Woollen, J., Yang, S., Hnilo, J., Fiorino, M., et al. (2002). NCEP–DOE AMIP-II Reanalysis (R-2). *Bulletin of the American Meteorological Society, 83*(11), 1631-1643.

Kattenberg, A., Giorgi, F., Grassl, H., Meehl, G., Mitchell, J., Stouffer, R., et al. (1996). Climate models—projections of future climate *Climate change 1995: The science of climate change* (pp. 285-357): Cambridge University Press.

Kattsov, V. M., Walsh, J. E., Chapman, W. L., Govorkova, V. A., Pavlova, T. V., & Zhang, X. (2007). Simulation and Projection of Arctic Freshwater Budget Components by the IPCC AR4 Global Climate Models. *Journal of Hydrometeorology, 8*(3), 571-589. doi: doi:10.1175/JHM575.1

Kessler, E. (1969). On the distribution and continuity of water substance in atmosferic circulations. *Meteorological Monographs, 32*(10).

Kiehl, J., & Ramanathan, V. (2006). *Frontiers of climate modeling*. Camebridge: Cambridge University Press.

Kiehl, J., & Trenberth, K. (1997). Earth's annual mean global energy budget. *Bulletin of the Meteorological Society, 78*(2), 197-208.

Kjellström, E., Bärring, L., Gollvik, S., Hansson, U., Jones, C., Samuelsson, P., Rummukainen, M., Ullerstig, A., Willén, U. and K. Wyser. (2005). A 140-year simulation of European climate with the new version of the Rossby Centre regional atmospheric climate model (RCA3). *Reports Meteorology and Climatology,SMHI, SE-60176 Norrköping, Sweden*(108), 54 pp.

Knutti, R. (2009). The end of model democracy? *Climatic Change*, 1-10. doi: 10.1007/s10584-010-9800-2

Knutti, R., Cermak, J., Furrer, R., Tebaldi, C., & Meehl, G. (2010). Challenges in combining projections from multiple climate models. *Journal of Climate*(23), 2739-2758.

Knutti, R., Stocker, T. F., Joos, F., & Plattner, G. K. (2002). Constraints on radiative forcing and future climate change from observations and climate model ensembles. *Nature, 416*(6882), 719-723.

Køltzow, M., Eastwood, S., & Haugen, J. (2003). Parameterization of snow and sea ice albedo in climate models *Research Report* (Vol. 149).

Kong, F., & Yau, M. (1997). An explicit approach to microphysics in MC2. *Atmosphere Ocean, 35*, 257-291.

Koster, R., Dirmeyer, P., Guo, Z., Bonan, G., Chan, E., Cox, P., et al. (2004). Regions of strong coupling between soil moisture and precipitation. *Science, 305*(5687), 1138-1140.

Koster, R., Suarez, M., & Heiser, M. (2000). Variance and predictability of precipitation at seasonal-to-interannual timescales. *Journal of hydrometeorology, 1*(1), 26-46.

Laprise, R., Caya, D., Bergeron, G., & Giguère, M. (1997). The formulation of the André Robert MC2 (mesoscale compressible community) model. *Numerical Methods in Atmospheric and Oceanic Modelling, The André J. Robert Memorial Volume*, 195–220.

Laprise, R., Caya, D., Giguere, M., Bergeron, G., Côté, H., Blanchet, J., et al. (1998). Climate and climate change in western Canada as simulated by the Canadian Regional Climate Model. *Atmosphere- ocean, 36*(2), 119-167.

Lenderink, G., & De Rooy, W. (2000). A robust mixing length formulation for a TKE-l turbulence scheme. *Hirlam Newsletter, 36*, 25-29.

Lenderink, G., & Holtslag, A. (2004). An updated length-scale formulation for turbulent mixing in clear and cloudy boundary layers. *Quarterly Journal of the Royal Meteorological Society, 130*(604), 3405-3428.

Lenderink, G., van Ulden, A., van den Hurk, B., & van Meijgaard, E. (2007). Summertime inter-annual temperature variability in an ensemble of regional model simulations: analysis of the surface energy budget. *Climatic Change, 81*, 233-247. doi: DOI 10.1007/s10584-006-9229-9

Leung, L., Wigmosta, M., Ghan, S., Epstein, D., & Vail, L. (1996). Application of a subgrid orographic precipitation/surface hydrology scheme to a mountain watershed. *Journal of Geophysical Research-Atmospheres, 101*(D8).

Li, J., & Barker, H. (2005). A radiation algorithm with correlated-k distribution. Part I: Local thermal equilibrium. *Journal of the Atmospheric Sciences, 62*(2), 286-309.

Lian, M., & Cess, R. (1977). Energy balance climate models- A reappraisal of ice-albedo feedback. *Journal of the Atmospheric Sciences, 34*(7), 1058–1062.

Lorant, V., McFarlane, N., & Laprise, R. (2002). A numerical study using the Canadian Regional Climate Model for the PIDCAP period. *Boreal environment research, 7*(3), 203-210.

Lorenz, S., Grieger, B., Helbig, P., & Herterich, K. (1996). Investigating the sensitivity of the atmospheric general circulation model ECHAM 3 to paleoclimatic boundary conditions. *Geologische Rundschau, 85*(3), 513-524.

Lott, F., & Miller, M. (1997). A new subgrid scale orographic drag parameterization; its testing in the ECMWF model. *Quarterly Journal of the Royal Meteeorological Society, 123*, 101-127.

Louis, J., Tiedtke, M., & Geleyn, J. (1981). A short history of the operational PBL-parameterization at ECMWF.

Mann, M., & Jones, P. (2003). Global surface temperatures over the past two millennia. *Geophysical Research Letters, 30*(15), 1820. doi: 10.1029/2003GL017814

Manzato, A., & Morgan, G. (2003). Evaluating the sounding instability with the lifted parcel theory. *Atmospheric Research, 67-8*, 455-473. doi: 10.1016/s0169-8095(03)00059-0

Mayaux, P., Bartholomé, E., Fritz, S., & Belward, A. (2004). A new land-cover map of Africa for the year 2000. *Journal of Biogeography, 31*(6), 861-877.

McFarlane, N. (1987). The effect of orographically excited gravity wave drag on the general circulation of the lower stratosphere and troposphere. *Journal of the Atmospheric Sciences, 44*(14), 1775-1800.

McGregor, J. (1997). Regional climate modelling. *Meteorology and Atmospheric Physics, 63*(1), 105-117.

McGuffie, K., & Henderson-Sellers, A. (2001). Forty years of numerical climate modelling. *International Journal of Climatology, 21*(9), 1067-1109.

Meehl, G. (1984). Modeling the earth's climate. *Climatic Change, 6*(3), 259-286.

Meehl, G., Washington, W., Wigley, T., Arblaster, J., & Dai, A. (2003). Solar and greenhouse gas forcing and climate response in the twentieth century. *Journal of Climate, 16*(3), 426-444.

Meinke, I. (2006). A comparison of simulated clouds to ISCCP data. *Monthly Weather Review, 134*(6), 1669-1681.

Meinke, I., Roads, J., & Kanamitsu, M. (2007). Evaluation of RSM-simulated precipitation during CEOP. *J. Meteor. Soc. Japan, 85*(0), 145-166.

Meinke, I., Von Storch, H., & Feser, F. (2004). A validation of the cloud parameterization in the regional model SN-REMO. *Journal of Geophysical Research, 109*, D13205. doi: 10.1029/2004JD004520

Menéndez, C., Saulo, A., & Li, Z. (2001). Simulation of South American wintertime climate with a nesting system. *Climate Dynamics, 17*(2), 219-231.

Miller, N., & Kim, J. (1996). Numerical prediction of precipitation and river flow over the Russian River watershed during the January 1995 California storms. *Bulletin of the American Meteorological Society, 77*(1), 101-105.

Misra, V., Dirmeyer, P., & Kirtman, B. (2003). Dynamic downscaling of seasonal simulations over South America. *Journal of Climate, 16*, 103-117.

Mitchell, J. F. B., Karoly, D. J., Hegerl, G. C., Zwiers, F. W., Allen, M. R., & Marengo, J. (2001). The Scientific Basis. Contribution of Working Group I to the Third Assessment Report of the Intergovernmental Panel on Climate Change, chap. 12: Detection of Climate Change and Attribution of Causes. In Y. D. J. T. Houghton, D. J. Griggs, M. Noguer, P. J. van der & X. D. Linden, K. Maskell, and C. A. Johnsen. (Eds.), (pp. 525–582).

Mitchell, K., Lohmann, D., Houser, P., Wood, E., Schaake, J., Robock, A., et al. (2004). The multi-institution North American Land Data Assimilation System (NLDAS): Utilizing multiple GCIP products and partners in a continental distributed hydrological modeling system. *Journal of Geophysical Research, 109*.

Montoya, M., von Storch, H., & Crowley, T. (2000). Climate simulation for 125 kyr BP with a coupled ocean–atmosphere general circulation model. *Journal of Climate, 13*(6).

Morcrette, J. (1984). *Sur la paramétrisation du rayonnement dans les modèles de circulation générale atmosphérique.* PhD thesis, Université des Sciences et Techniques de Lille, Villeneuve d'Asq Cedex, France.

Muller. (1981). 1981: Internal waves and small scale processes. Scientific Surveys in Honor of H. Stommel, B. A. Warren and C. Wunsch, Eds., . *The MIT Press, 264–291*.

Noguer, M., Jones, R., & Murphy, J. (1998). Sources of systematic errors in the climatology of a regional climate model over Europe. *Climate Dynamics, 14*(10), 691-712.

North, G., & Cahalan, R. (1981). Predictability in a solvable stochastic climate model. *Journal of the Atmospheric Sciences, 38*(3), 504-513.

North, G., Short, D., & Mengel, J. (1983). Simple energy balance model resolving the seasons and the continents- Application to the astronomical theory of the ice ages. *Journal of Geophysical Research, 88*, 6576-6586.

Paegle, J., Mo, K., & Nogués-Paegle, J. (1996). Dependence of simulated precipitation on surface evaporation during the 1993 United States summer floods. *Monthly Weather Review, 124*(3), 345-361.

Palmer, T. (2000). Predicting uncertainty in forecasts of weather and climate. *Reports on Progress in Physics, 63*, 71-116.

Pan, H.-L., & Wu, W.-S. (1995). Implementing a mass flux convective parameterization package for the NMC medium-range forecast model *NMC Office Note 409* (pp. 40).

Pan, Z. T., Arritt, R. W., Gutowski, W. J., & Takle, E. S. (2001). Soil moisture in a regional climate model: simulation and projection. *Geophysical Research Letters, 28*(15), 2947-2950.

Pavlov, A., Toon, O., Pavlov, A., Bally, J., & Pollard, D. (2005). Passing through a giant molecular cloud:“Snowball” glaciations produced by interstellar dust. *Geophysical Research Letters, 32*(3), L03705.

Pearson, K. (1901). On lines and planes of closest fit to systems of points in space. *Philosophical Magazine Series 6, 2*(11), 559-572.

Philander, S. (1990). El Nino, La Nina, and the Southern Oscillation: Academic Press.

Pielke, R., & Avissar, R. (1990). Influence of landscape structure on local and regional climate. *Landscape Ecology, 4*(2), 133-155.

Plummer, D., Caya, D., Frigon, A., Côté, H., Giguère, M., Paquin, D., et al. (2006). Climate and climate change over North America as simulated by the Canadian RCM. *Journal of Climate, 19*(13), 3112-3132.

Puckrin, E., Evans, W., Li, J., & Lavoie, H. (2004). Comparison of clear-sky surface radiative fluxes simulated with radiative transfer models. *Canadian Journal of Remote Sensing, 30*(6), 903.

Räisänen, P., Rummukainen, M., & Räisänen, J. (2000). Modification of the HIRLAM radiation scheme for use in the Rossby Centre Regional Atmosphere Climate Model. *University of Helsinki Reports.* (Vol. 49, pp. 71).

Ramanathan, V., & Coakley, J. (1978). Climate modeling through radiative-convective models. *Reviews of Geophysics and Space Physics, 16*(4), 465–489.

Ramaswamy, V., Boucher, O., Haigh, J., Hauglustaine, D., Haywood, J., Myhre, G., et al. (2001). Radiative forcing of climate change. In J. T. H. e. al. (Ed.), *Climate Change 2001: The Scientific Basis* (pp. 349–416). New York: Cambridge University Press.

Randall, D., Khairoutdinov, M., Arakawa, A., & Grabowski, W. (2003). Breaking the cloud parameterization deadlock. *Bulletin of the American Meteorological Society, 84*(11), 1547-1564.

Randall, D., Xu, K., Somerville, R., & Iacobellis, S. (1996). Single-column models and cloud ensemble models as links between observations and climate models. *Journal of Climate, 9*(8), 1683-1697.

Rasch, P., & Kristjánsson, J. (1998a). A comparison of the CCM3 model climate using diagnosed and predicted condensate parameterizations. *Journal of Climate, 11*(7), 587-1614.

Rasch, P., & Kristjánsson, J. (1998b). A comparison of the CCM3 model climate using diagnosed and predicted condensate parameterizations. *Journal of Climate, 11*, 1587-1614.

Rial, J. A., Pielke, R. A., Beniston, M., Claussen, M., Canadell, J., Cox, P., et al. (2004). Nonlinearities, feedbacks and critical thresholds within the Earth's climate system. *Climatic Change, 65*(1-2), 11-38.

Richman, M. B. (1986). Rotation of Principal Components. *Journal of Climatology, 6*(3), 293-335.

Rinke, A., Dethloff, K., Cassano, J., Christensen, J., Curry, J., Du, P., et al. (2006). Evaluation of an ensemble of Arctic regional climate models: spatiotemporal fields during the SHEBA year. *Climate Dynamics, 26*(5), 459-472.

Risbey, J., & Stone, P. (1996). A case study of the adequacy of GCM simulations for input to regional climate change assessments. *Journal of Climate, 9*(7), 1441-1467.

Ritter, B., & Geleyn, J. (1992). A comprehensive radiation scheme for numerical weather prediction models with potential applications in climate simulations. *Monthly Weather Review, 120*(2), 303-325.

Roads, J., Chen, S., Cocke, S., Druyan, L., Fulakeza, M., LaRow, T., et al. (2003). International Research Institute/Applied Research Centers

(IRI/ARCs) regional model intercomparison over South America. *Journal of Geophysical Research, 108*(D14), 4425.

Robertson, A., Overpeck, J., Rind, D., Mosley-Thompson, E., Zielinski, G., Lean, J., et al. (2001). Hypothesized climate forcing time series for the last 500 years. *Journal of Geophysical Research, 106*(D14), 14783-14803.

Rockel, B., & Geyer, B. (2008). The performance of the regional climate model CLM in different climate regions, based on the example of precipitation. *Meteorologische Zeitschrift, 17*(4), 487-498.

Rockel, B., Roads, J. Meinke, I., Gutowski, W. J., Arritt, R. W., Takle, E.,. (2005). *ICTS (Inter-CSE Transferability Study): An Application of CEOP Data. Proceedings.* Paper presented at the 85th Annual AMS meeting San Diego, CA, January 11-15, 2005.

Rockel, B., Will, A., & Hense, A. (2008). The Regional Climate Model COSMO-CLM (CCLM). *Meteorologische Zeitschrift, 17*(4), 347-348.

Rogers, C. (1977). Radiative Processes in the Atmosphere. ECMWF Seminars. *Reading*, 5-66.

Ruddiman, W. (2003). The anthropogenic greenhouse era began thousands of years ago. *Climatic Change, 61*(3), 261-293.

Ryan, B., Katzfey, J., Abbs, D., Jakob, C., Lohmann, U., Rockel, B., et al. (2000). Simulations of a cold front by cloud-resolving, limited-area, and large-scale models, and a model evaluation using in situ and satellite observations. *Monthly Weather Review, 128*(9), 3218-3235.

Samuelsson, P., Gollvik, S., & Ullerstig, A. (2006). The land-surface scheme of the Rossby Centre regional atmospheric climate model (RCA3). *SMHI Reports Meteorology, 122*(76).

Sanderson, B. M., Knutti, R., Aina, T., Christensen, C., Faull, N., Frame, D. J., et al. (2008). Constraints on Model Response to Greenhouse Gas Forcing and the Role of Subgrid-Scale Processes. *Journal of Climate, 21*(11), 2384-2400. doi: doi:10.1175/2008JCLI1869.1

Sass, B. H., Rontu, L., Räisänen, P. (1994). HIRLAM-2 radiation scheme: documentation and tests. *HIRLAM technical report* (Vol. 16, pp. 43).

Savijärvi, H. (1990). Fast radiation parameterization schemes for mesoscale and short-range forecast models. *Journal of Applied Meteorology 29*(6), 437-447.

Schär, C., Lüthi, D., Beyerle, U., & Heise, E. (1999). The soil–precipitation feedback: A process study with a regional climate model. *Journal of Climate, 12*(3), 722-741.

Schrodin, R., & Heise, E. (2001). The multi-layer-version of the DWD soil model TERRA/LM. *Consortium for Small-Scale Modelling (COSMO) Tech. Rep, 2*, 16.

Sen, O., Wang, B., & Wang, Y. (2004a). Impacts of re-greening the desertified lands in northwestern China: Implications from a regional climate model experiment. *Journal of the Meteorological Society of Japan, 82*(6), 1679-1693.

Sen, O., Wang, Y., & Wang, B. (2004b). Impact of Indochina deforestation on the East Asian summer monsoon. *Journal of Climate, 17*(6), 1366-1380.

Shao, Y., R.D. Anne, A. Henderson-Sellers, P. Irannejad, P. Thornton, X. Liang, T.H. Chen, C. Ciret, C. Desborough, O. Balachova, A. Haxeltine and A. Ducharne. (1994). Soil moisture simulation. A report of the RICE and PILPS Workshop *GEWEX/GAIM Tech. Report* (pp. 179).

Shuttleworth, W., & Dickinson, R. (1989). Comments on "Modelling tropical deforestation: A study of GCM land-surface parameterizations.". *Quart. J. Roy. Meteor. Soc, 115*(489), 1177-1179.

Slingo, J. (1987). The development and verification of a cloud prediction scheme for the ECMWF model. *Quarterly Journal of the Royal Meteeorological Society, 113*, 899–927.

Sloan, L. C. (2006). A framework for regional modeling of past climates. *Theoretical and Applied Climatology, 86*(1-4), 271-279. doi: DOI 10.1007/s00704-005-0207-3

Solomon, S., Qin, D., Manning, M., Chen, Z., Marquis, M., Averyt, K., et al. (2007). IPCC 2007. Climate Change 2007: the Physical Science Basis Contribution of Working Group I to the Fourth Assessment Report of the Intergovernmental Panel on Climate Change: New York: Cambridge University Press.

Stephens, G. (1984). The parameterization of radiation for numerical weather prediction and climate models. *Mon. Wea. Rev.*, (112), 826-867.

Steppeler, J., Doms, G., Schättler, U., Bitzer, H., Gassmann, A., Damrath, U., et al. (2003). Meso-gamma scale forecasts using the nonhydrostatic model LM. *Meteorology and Atmospheric Physics, 82*(1), 75-96.

Sundqvist, H., Berge, E., & Kristjánsson, J. (1989). Condensation and cloud parameterization studies with a mesoscale numerical weather prediction model. *Monthly Weather Review, 117*(8), 1641-1657.

Tadross, M., Gutowski, W., Hewitson, B., Jack, C., & New, M. (2006). MM5 simulations of interannual change and the diurnal cycle of southern African regional climate. *Theoretical and Applied Climatology, 86*(1), 63-80.

Takle, E. S., Gutowski, W. J., Arritt, R. W., Pan, Z. T., Anderson, C. J., da Silva, R. R., et al. (1999). Project to Intercompare Regional Climate Simulations

(PIRCS): Description and initial results. *Journal of Geophysical Research-Atmospheres, 104*(D16), 19443-19461.

Takle, E. S., Roads, J., Rockel, B., Gutowski, W. J., Arritt, R. W., Meinke, I., et al. (2007). Transferability intercomparison - An opportunity for new insight on the global water cycle and energy budget. *Bulletin of the American Meteorological Society, 88*(3), 375-384. doi: 10.1175/bams-88-3-375.

Taylor K (2001) Summarizing multiple aspects of model performance in a single diagram. *Journal of Geophysical Research, 106*(D7), 7183-7192.

Tebaldi, C., & Knutti, R. (2010). Climate Models and Their Projections of Future Changes. *Climate Change and Food Security*, 31-56.

Tiedtke, M. (1989). A comprehensive mass flux scheme for cumulus parameterization in large-scale models. *Monthly Weather Review, 117*(8), 1779-1800.

Timmermann, A., Oberhuber, J., Bacher, A., Esch, M., Latif, M., & Roeckner, E. (1999). Increased El NinÄo frequency in a climate model forced by future greenhouse warming. *Nature, 398*, 694-697.

Tjernström, M., Zagar, M., Svensson, G., Cassano, J., Pfeifer, S., Rinke, A., et al. (2005). Modeling the Arctic boundary layer: An evaluation of six ARCMIP regional-scale models with data from the SHEBA project. *Boundary-Layer Meteorology, 117*, 337-381.

Trenberth, K. E., & Fasullo, J. T. (2010). Simulation of Present-Day and Twenty-First-Century Energy Budgets of the Southern Oceans. *Journal of Climate, 23*(2), 440-454. doi: doi:10.1175/2009JCLI3152.1

Troen, I., & Mahrt, L. (1986). A simple model of the atmospheric boundary layer; sensitivity to surface evaporation. *Boundary-layer meteorology, 37*(1), 129-148.

Tziperman, E., Stone, L., Cane, M., & Jarosh, H. (1994). El Nino Chaos: Overlapping of Resonances Between the Seasonal Cycle and the Pacific Ocean-Atmosphere Oscillator. *Science, 264*, 72-74.

Undén, P., Rontu, L., Järvinen, H., Lynch, P., & Calvo, J. (2002). HIRLAM-5 scientific documentation. *Swedish Meteorological and Hydrological Institute (SMHI), Norrköping, Sweden*.

Van den Hurk, B., Hirschi, M., Schär, C., Lenderink, G., van Meijgaard, E., van Ulden, A., et al. (2005). Soil control on runoff response to climate change in regional climate model simulations. *Journal of Climate, 18*(17), 3536-3551.

Van Meijgaard, E., Andrae, U., & Rockel, B. (2001). Comparison of model predicted cloud parameters and surface radiative fluxes with observations on the 100 km scale. *Meteorology and Atmospheric Physics, 77*(1-4), 109-130.

Verseghy, D. (1991). CLASS-A Canadian land surface scheme for GCMs. I. Soil model. *International Journal of Climatology, 11*(2), 111-133.

Verseghy, D., McFarlane, N., & Lazare, M. (1993). CLASS-A Canadian land surface scheme for GCMS, II. Vegetation model and coupled runs. *International Journal of Climatology, 13*(4), 347-370.

Vettoretti, G., & Peltier, W. (2004). Sensitivity of glacial inception to orbital and greenhouse gas climate forcing. *Quaternary Science Reviews, 23*(3-4), 499-519.

Vidale, P., Lüthi, D., Frei, C., Seneviratne, S., & Schär, C. (2003). Predictability and uncertainty in a regional climate model. *Journal of Geophysical Research, 108*, 4586.

Vidale, P. L., Luthi, D., Wegmann, R., & Schar, C. (2007). European summer climate variability in a heterogeneous multi-model ensemble. *Climatic Change, 81*, 209-232. doi: DOI 10.1007/s10584-006-9218-z

Von Storch, H., Langenberg, H., & Feser, F. (2000). A spectral nudging technique for dynamical downscaling purposes. *Monthly Weather Review, 128*(10), 3664-3673.

Vukicevic, T., & Paegle, J. (1989). The influence of one-way interacting lateral boundary conditions upon predictability of flow in bounded numerical models. *Monthly Weather Review, 117*(2), 340-350.

Walsh, K., & McGregor, J. (1995). January and July climate simulations over the Australian region using a limited-area model. *Journal of Climate, 8*(10), 2387-2403.

Wang, W., Gong, W., & Wei, H. (2000). A regional model simulation of the 1991 severe precipitation event over the Yangtze–Huai River Valley. Part I: Precipitation and circulation statistics. *Journal of Climate, 13*(1), 74-92.

Wang, Y., Leung, L., McGREGOR, J., Lee, D., Wang, W., Ding, Y., et al. (2004). Regional climate modeling: progress, challenges, and prospects. *Journal of the Meteorological Society of Japan, 82*(6), 1599-1628.

Wyser, K., & Jones, C. G. (2005). Modeled and observed clouds during Surface Heat Budget of the Arctic Ocean (SHEBA). *Journal of Geophysical Research-Atmospheres, 110*(D9), D09207. doi: 10.1029/2004JD004751

Yakimiw, E., & Robert, A. (1990). Validation experiments for a nested grid-point regional forecast model. *Atmosphere-Ocean, 28*, 466-472.

Yang, K., Koike, T., Fujii, H., Tamagawa, K., & Hirose, N. (2002). Improvement of surface flux parametrizations with a turbulence-related length. *Quarterly Journal of the Royal Meteorological Society, 128*(584), 2073-2087. doi: 10.1256/003590002320603548

Yang, K., Rasmy, M., Rauniyar, S., Koike, T., Taniguchi, K., Tamagawa, K., et al. (2007). Initial CEOP-based review of the prediction skill of operational

general circulation models and land surface models. *Journal of the Meteorological Society of Japan, 85A*, 99-116.

Yang, Z., Dickinson, R., Henderson-Sellers, A., & Pitman, A. (1995). Preliminary study of spin-up processes in land surface models with the first stage data of Project for Intercomparison of Land Surface Parameterization Schemes Phase 1 (a). *Journal of Geophysical Research-Atmospheres, 100D*(8). doi: 16 553–16 578

Zorita, E., von Storch, H., Gonzalez-Rouco, F., Cubasch, U., Luterbacher, J., Legutke, S., et al. (2004). Climate evolution in the last five centuries simulated by an atmosphere-ocean model: global temperatures, the North Atlantic Oscillation and the Late Maunder Minimum. *Meteorologische Zeitschrift, 13*(4), 271-290.